Aus dem Max-Delbrück-Centrum für Molekulare Medizin und
Charité – Universitätsmedizin Berlin

DISSERTATION

Acute optogenetic stimulation of serotonergic neurons in raphe nuclei reduces cell proliferation in the dentate gyrus of the mouse

Akute optogenetische Stimulation von serotonergen Neuronen in Raphe-Kernen reduziert Zellproliferation im Gyrus dentatus der Maus

zur Erlangung des akademischen Grades
Doctor medicinae (Dr. med.)

vorgelegt der Medizinischen Fakultät
Charité – Universitätsmedizin Berlin

von

Dr. rer. nat. Naozumi Araragi

Datum der Promotion: .....23.03.2024.....

Preface

Parts of the results of this dissertation have been published in: Araragi N, Alenina N, Bader M (2022) Carbon-mixed dental cement for fixing fiber optic ferrules prevents visually triggered locomotive enhancement in mice upon optogenetic stimulation. Heliyon 8. 1:e08692/ January 1, 2022.

Table of Contents

List of Figures and Tables

List of Abbreviations

Note: only frequently used abbreviations are listed here.

5-HIAA	5-hydroxyindoleacetic acid
5-HT	5-hydroxy-tryptamine = serotonin
5-HTP	5-hydroxy-L-tryptophan
5-HTT	serotonin transporter of humans and in general
5-Htt	murine serotonin transporter
AADC	aromatic L-amino acid decarboxylase
ACG	autocorrelogram
ACSF	artificial cerebrospinal fluid
AP	anterior-posterior
BI	burst index
BrdU	bromodeoxyuridine
CA1	cornu ammonis 1 of the hippocampus
CA3	cornu ammonis 3 of the hippocampus
CCK	cholecystokinin
ChR2 (*ChR2*)	channelrhodopsin 2 (*gene*)
CNS	central nervous system
Ctrl	control mice = mice without optogenetic stimulation
ddH_2O	double-distilled water
DG	dentate gyrus
DRN	dorsal raphe nucleus
DV	dorsoventral
EC	entorhinal cortex
EDTA	ethylenediaminetetraacetic acid
EPSP	excitatory postsynaptic potential
EYFP	enhanced yellow fluorescent protein
GABA	gamma-aminobutyric acid
GC	granule cell
GCL	granule cell layer
HHW	half-height width
HPLC	high-performance liquid chromatography
IML	inner molecular layer
KO	knockout (−/−)
LEC	lateral entorhinal cortex
LED	light-emitting diode
LPP	lateral perforant path
MAO	monoamine oxidase
MC	mossy cell
MCF	mossy cell fiber
MEC	medial entorhinal cortex
ML	molecular layer or mediolateral
MPP	medial perforant path
MRN	median raphe nucleus
NA	numerical aperture
NSC	neural stem cell
NSPC	neural stem and progenitor cell
OML	outer molecular layer
PBS	phosphate-buffered saline

PCR	polymerase chain reaction
PFA	paraformaldehyde
PP	perforant path
PV	parvalbumin
RZC	rated zone crossing
SD	standard deviation
SEM	standard error of the mean
SERT	serotonin transporter
SGZ	subgranular zone
SNR	signal-to-noise ratio
SSRI	selective serotonin reuptake inhibitor
Stim	mice with optogenetic stimulation
SVZ	subventricular zone
TBS	Tris-buffered saline
TCA	tricyclic antidepressant
TPH2	tryptophan hydroxylase 2 of humans and in general
Tph2	murine tryptophan hydroxylase 2
Trp	(L-)tryptophan
VT	volume transmission
WT	wiring transmission or wild type
ZC	zone crossing

Abstract

The subgranular zone of the hippocampal dentate gyrus (DG) is known to be replenished with new-born neurons even after fetal and early postnatal development has completed, a phenomenon called adult neurogenesis. Functions of these new-born neurons and regulatory mechanisms of adult neurogenesis are not fully understood. The DG receives various synaptic inputs including those from serotonergic neurons in the brain stem raphe nuclei. Previous studies in mice have suggested that physical activities enhance neurogenesis via serotonergic neurotransmission. In the present study, the influence of serotonin (5-HT) on adult neurogenesis was investigated by directly activating serotonergic neurons in the dorsal and median raphe nucleus (DRN, MRN) using optogenetics.

Specifically, cell proliferation was examined by bromodeoxyuridine (BrdU) labeling in the DG after overnight and one-week optogenetic activation of serotonergic neurons in the raphe nuclei in freely behaving tryptophan hydroxylase 2-channelrhodopsin 2 (Tph2-ChR2) transgenic mice. These mice express photo-excitable cation channels, ChR2, under the control of the Tph2 promoter, allowing specific activation of serotonergic neurons.

First, specific activation of serotonergic neurons in the DRN or MRN was electrophysiologically confirmed in brain slices and in anesthetized mice. In consequence of the optogenetic activation of serotonergic neurons in the DRN or MRN, a reduction in firing rates was observed in the DG in the anesthetized mice. After overnight stimulation of serotonergic neurons in the freely behaving animals, BrdU-positive cells in the DG were significantly reduced in number compared to non-stimulated control mice. The total distances traveled did not differ significantly between stimulated and non-stimulated mice, indicating that the reduced cell proliferation in the DG was not due to reduced physical movement. Further, as revealed by high-performance liquid chromatography (HPLC), reduced cell proliferation in the DG was accompanied by reduced 5-HT concentrations in both the raphe nuclei and the hippocampus, which may reflect autoinhibitory regulation of 5-HT release. When optogenetic stimulation of serotonergic neurons was extended for 6 nights, reduction in cell proliferation was absent without affecting total distances traveled, although interhemispheric differences in the number of BrdU-positive cells were observed. In sum, acute optogenetic stimulation of serotonergic neurons temporarily decreases cell proliferation in the DG, with the effect disappearing if the stimulation continues over days. This effect could be mediated by an electrophysiologically measured inhibitory influence of 5-HT on the DG and adaptive changes subsequent to long-term optogenetic stimulation.

Zusammenfassung

Die subgranuläre Zone des Gyrus dentatus (DG) im Hippocampus wird auch nach Ende der fetalen und frühen postnatalen Entwicklung mit neugeborenen Neuronen aufgefüllt, ein Phänomen, das als adulte Neurogenese bezeichnet wird. Die Funktionen dieser neugeborenen Neuronen und die Regulationsmechanismen der adulten Neurogenese sind nicht völlig verstanden. Der DG erhält verschiedene synaptische Inputs, einschließlich derer von serotonergen Neuronen in den Raphe-Kernen des Hirnstamms. Frühere Studien an Mäusen zeigten, dass körperliche Aktivitäten die Neurogenese mittels serotonerger Neurotransmission verbessern. In der vorliegenden Studie wurde der Einfluss von Serotonin (5-HT) auf adulte Neurogenese durch direkte Aktivierung serotonerger Neuronen im dorsalen und medianen Raphe-Kern (DRN, MRN) mittels Optogenetik untersucht.

Konkret wurde die Zellproliferation durch Bromdesoxyuridin (BrdU)-Markierung im DG nach über Nacht und einwöchiger optogenetischer Aktivierung von serotonergen Neuronen in den Raphe-Kernen in sich frei bewegenden transgenen Tryptophan Hydroxylase 2-Channelrhodopsin 2 (Tph2-ChR2)-Mäusen untersucht. Diese Mäuse exprimieren photoanregbare Kationenkanäle, ChR2, unter der Kontrolle des Tph2-Promotors, was eine spezifische Aktivierung von serotonergen Neuronen ermöglicht.

Zuerst wurde die spezifische Aktivierung von serotonergen Neuronen im DRN oder MRN in Gehirnschnitten und in anästhesierten Mäusen mit elektrophysiologischen Methoden bestätigt. In Folge der optogenetischen Aktivierung von serotonergen Neuronen im DRN oder MRN wurde eine Senkung der Feuerraten im DG in anästhesierten Mäusen beobachtet. Nach Stimulation von serotonergen Neuronen über Nacht in frei beweglichen Tieren war die Zahl der BrdU-positiven Zellen im DG im Vergleich zu nicht-stimulierten Kontrollen signifikant reduziert. Die reduzierte Zellproliferation war nicht auf reduzierte körperliche Bewegung zurückzuführen, da sich die zurückgelegte Gesamtstrecke zwischen stimulierten und nicht-stimulierten Mäusen nicht unterschied. Hochleistungs-Flüssigkeitschromatographie (HPLC) zeigte, dass die reduzierte Zellproliferation im DG von reduzierten 5-HT-Konzentrationen in den Raphe-Kernen und im Hippocampus begleitet wurde, was eine autoinhibitorische Regulierung der 5-HT-Freisetzung widerspiegeln könnte. Wenn die optogenetische Stimulation serotonerger Neuronen auf 6 Nächte verlängert wurde, wurden zwar interhemisphärische Unterschiede in der Anzahl von BrdU-positiven Zellen beobachtet, doch weder die Zellproliferation noch die zurückgelegte Gesamtstrecke waren beeinflusst. Kurz gefasst verringert die akute optogenetische Stimulation serotonerger Neuronen die Zellproliferation im DG vorübergehend, aber dieser Effekt

verschwindet, wenn die Stimulation über Tage andauert. Elektrophysiologisch gemessen könnte dieser Effekt durch den inhibitorischen Einfluss von 5-HT auf den DG und nachfolgende adaptive Veränderungen nach langfristiger optogenetischer Stimulation vermittelt sein.

1. Introduction

1.1. Optogenetics

Optogenetics is a tool in biology which uses methods both from the fields of optics and genetics. With optogenetics, the activities of excitable cells can be controlled using light at a spatial and temporal resolution that is unmatched by other conventional methods such as electrical stimulation, pharmacology, or lesions. Logically, it is therefore applicable in scientific fields dealing with excitable cells, mainly but not limited to the field of neuroscience. This technique allows the functional study of individual cells in isolation or in living tissues, as well as in behaving animals.

1.1.1. History of optogenetics

In his book, "Man on his Nature" (1940), Charles S. Sherrington rather poetically described neuronal activities at different stages of sleep-to-wake transition as points of light (Mohan, 2017). Much later, Francis Crick, a discoverer of the DNA structure who later turned to neuroscience, suggested in a series of lectures at the University of California in San Diego in 1999 that it should be possible to use light to precisely control the activity of individual neuronal subtypes (Lyon, 2013). The inspiration for such an idea comes from the working mechanism of mammalian eyes. Photoreceptors in the retina convert photon energy into chemical signals which in turn modify neuronal activities. Photoreceptors contain a pigment called rhodopsin, which consists of opsin and retinal. Opsin is a G-protein-coupled 7-transmembrane helix protein and retinal, a vitamin A aldehyde, is a chromophore cofactor which binds to a specific lysine residue in the 7^{th} helix. Photon absorption induces isomerization of retinal, changing its form from 11-cis-retinal to all-trans-retinal. This causes a conformational change in the opsin, known as "bleaching", leading to the activation of a G-protein-coupled signaling cascade (Lyon, 2013). One of the first artificial constructs using these optical properties of rhodopsin was created by Boris Yemelman and Gero Miesenbock at Sloan-Kettering Cancer Center in New York and termed "chARGe", and consisted of three Drosophila proteins: the blue light-sensitive rhodopsin, arrestin-2, and the α-subunit of the cognate heterotrimeric G-protein (Zemelman et al., 2002). When expressed in mammalian hippocampal neurons, the signaling cascade nonspecifically opened cation channels to produce action potentials. However, chARGe showed slow kinetics and high variability in latency (from several 100 milliseconds to tens of seconds), and was relatively complex to manipulate (reviewed in Lyon, 2013; Repina et al., 2017).

Since the 1970s, on the other hand, it has been known that a type of unicellular alga, *Halobacterium salinarum*, possesses a microbial opsin called bacteriorhodopsin and uses light to control ionic flows across its plasma membranes. Bacteriorhodopsin is a light-driven H^+ pump, which converts light energy into a H^+ gradient, and the energy stored in the H^+ gradient is used for generation of ATP. In addition to bacteriorhodopsin, *H. salinarum* contains other retinal proteins such as halorhodopsin. Halorhodopsin is a light-driven Cl^- pump which allows *H. salinarum* to maintain high intracellular salt concentrations upon growth. Organisms expressing halorhodopsins typically live in highly saline environments (e.g., >4 M salt). Okuno and colleagues, however, demonstrated that halorhodopsin from another alga, *Natronomonas pharaonis* (Halo/NpHR), works in a physiological chloride concentration (Okuno et al., 1999). Despite its potential suitability for controlling neuronal activities, use of halorhodopsins in neurons was not attempted for almost a decade (Mohanty and Lakshminarayananan, 2015).

In 2003, Nagel and colleagues identified another protein responsible for light-driven activities in *Chlamydomonas reinhardtii*. This protein called channelrhodopsin 2 (ChR2) was artificially expressed in *Xenopus* oocytes, human embryonic kidney (HEK) cells, or baby hamster kidney (BHK) cells and was shown to be directly gated by blue light, conducting cations non-selectively (Nagel et al., 2003). In 2005, Ed Boyden, Karl Deisseroth, and their colleagues at Stanford University introduced ChR2 into mammalian hippocampal neuronal cultures using lentiviral vectors and demonstrated that pulses of blue light triggered neuronal spiking, as well as excitatory and inhibitory synaptic transmission, with a latency of a few milliseconds, providing a reliable tool to control neuronal activity (Boyden et al., 2005).

In 2007, almost a decade after the first demonstration that Halo/NpHR works in a physiological chloride concentration, this molecule was successfully introduced in neurons and was shown to rapidly and reversibly inhibit neuronal activities by gating Cl^- influx when activated by yellow light (Zhang et al., 2007; Han and Boyden, 2007). So far, single-photon excitation via blue-light illumination had been used to trigger action potentials in ChR2-expressing neurons. In 2009, it was demonstrated that two-photon excitation can be used to stimulate action potentials in ChR2-expressing neurons *in vitro*, conferring an unprecedented spatial resolution in optogenetics (Rickgauer and Tank, 2009). In the same year, ChR2 was successfully introduced into neurons in the macaque frontal cortex using lentivirus under the calcium/calmodulin-dependent protein kinase II (CaMKII) promoter. Using optical stimulation and electrophysiological recordings, it was demonstrated that neuronal activities of pyramidal neurons were controlled with millisecond temporal resolution, thus verifying

applicability of optogenetic methods in non-human primates (Han et al., 2009). Although ChR2 had rapidly gained popularity in neuroscience research, its detailed molecular structure was long time unknown. It was not until 2012 that the crystal structure of ChR (a C1C2 chimaera between ChR1 and ChR2 from *C. reinhardtii*) at 2.3 Å resolution was first reported (Kato et al., 2012). Similar to vertebrate rhodopsin, ChR2 consists of the light-responsive protein opsin and the chromophore cofactor retinal, which is bound to opsin. Unlike rhodopsin, however, the function of ChR2 is not mediated by G-proteins. Rather, ChR2 includes a cation conduction pathway and works directly as an ion channel. This allows ChR2 to respond much faster to light than G-protein coupled receptors. Understanding the molecular basis of ChR2 then facilitated the development of channelrhodopsin variants in the coming years (reviewed in Lyon, 2013; Mohanty and Lakshminarayananan, 2015; Wang et al., 2017).

1.1.2. Practical aspects of optogenetics

The optogenetic approach typically involves five major steps in its experimental design: I) selection of opsin, II) selection of opsin delivery methods, III) selection of light delivery methods, IV) selection of light stimulation parameters, V) validation of optogenetic manipulation (Tye and Deisseroth, 2012; Mohan, 2017).

I) Selection of opsin

Optogenetics utilizes genetically encoded light-reactive membrane proteins called opsins to control activities of targeted neurons with light. They can be categorized into ion channels, G-protein coupled receptors, and pumps based on their biophysical properties. Further, depending on their microbial or animal origin, they can be categorized into type I or type II, respectively (Montagni et al., 2019). Microbial opsins like channelrhodopsins (ChR1, ChR2, VChR1 and SFOs) activate neurons. On the other hand, other microbial opsins like archaerhodopsin 3 (Arch) from *Halorubrum sodomense*, *Leptosphaeria maculans* fungal opsins (Mac), bacteriorhodopsin (BR and eBR [enhanced BR]) from *Halobacterium salinarum*, halorhodopsin (HsHR and NpHR), or genetically engineered chloride-conducting ChR2 (ChloC and iChloC, improved ChloC; Wietek et al., 2014; 2015) inhibit neurons (reviewed in Mohan, 2017; Deubner et al., 2019).

Both ChR1 and ChR2 derive from a green alga, *Chlamydomonas reinhardtii*, and can be activated by blue light, but they functionally differ in that ChR1 is selective for protons, whereas ChR2 is additionally conductive for monovalent and divalent cations. VChR1 is another cation-conducting channelrhodopsin isolated from a multicellular organism, *Volvox*

carteri, with an absorption maximum at a higher wavelength (589 nm, yellow light) than that of ChR1 or ChR2. Neuronal expression of VChR1, however, is about three times lower than that of ChR2 and its photocurrents (= currents induced by light) are normally very small. Nevertheless, its ability to be activated by yellow light could be useful and adds further diversity to the family of excitatory opsins (Zhang et al., 2008). One of the newer opsin variants, the step function opsin (SFO), induces prolonged, bi-stable, subthreshold depolarization of membrane potential.

Opsins like Arch, Mac, and (e)BR extrude protons from the cytoplasm to generate hyperpolarizing photocurrents and inhibit neuronal activities when illuminated with yellow light (Arch, 575 nm), blue-green light (Mac, 470–500 nm) and green light (eBR, 560 nm; Gradinaru et al., 2010; Chow et al., 2010; Pastrana, 2011).

On the other hand, halorhodopsin found in the cell membranes of halobacteria, is a bacteriorhodopsin-like retinal protein. When illuminated with yellow light, it works as an inward-directed Cl^- pump instead of as an outward-directed proton pump like Arch, Mac, or BR (Lanyi, 2012). Two versions of halorhodopsins have been reported, one from *Halobacterium salinarum* (HsHR) and the other from *Natronobacterium pharaonis* (= *Natronomonas pharaonis*; NpHR) with somewhat different characteristics. An engineered "enhanced" eNpHR has also often been used, modified later to eNpHR2.0 with enhanced membrane trafficking properties, and eNpHR3.0 with stable and repeatable large hyperpolarizing photocurrents, allowing for highly reactive neuronal silencing (Pedersen and Gross, 2018).

II) Selection of opsin delivery methods

There are three major ways to deliver opsins to the brain: A) injection of viral vectors, B) transgenic modification of animals, or C) *in utero* electroporation (Deubner et al., 2019).

A) Injection of viral vectors

Normally, an adeno-associated virus (AAV) or a lentivirus is used to package the opsin construct. To convert a virus into an apathogenic viral vector, the native genome first needs to be completely removed. Viral vectors carrying the genes encoding ChR2 can be stereotactically and intracranially injected into targeted brain regions. Lentiviral vectors are integrated into the genome of the host cell and thus enable permanent gene expression. AAV-

mediated expression, on the other hand, may be less stable because a much smaller percentage of the virus leads to actual gene expression (Mohanty and Lakshminarayananan, 2015).

In the case of *in vitro* experiments, the opsin construct is integrated into a bacterial plasmid, which can then be delivered into the cell via transfection, i.e., penetrating the cell membrane using, for example, electroporation or calcium phosphate. Alternatively, the construct is placed inside liposomes, which will then fuse with the cell membrane, leading to the release of the construct into the cell interior. Plasmid-based methods have advantages over viral vectors in that they permit the use of relatively large promoters to drive opsin expression. Moreover, electroporation can be used *in utero* to introduce opsin constructs, although it is technically challenging (Lyon, 2013).

Despite the variability in transduction efficiency and the limited packaging capacity, viral vectors are widely used to induce a local transfection in targeted brain regions with two main advantages: 1) the number of transfected neurons can be adjusted based on the volume and concentration of virus injected into the tissue, 2) the afferent or efferent projections from a region can be specifically transfected and stimulated, preventing unintended excitation of collateral regions (Montagni et al., 2019).

Cell type specificity of viral vectors can be achieved by selecting appropriate promotors, enhancers, viral serotypes, or spatial targeting methods (Mohanty and Lakshminarayananan, 2015; Deubner et al., 2019). With promoter-based methods, only cells with the necessary expression machinery for a specific promoter can initiate the expression process. Ubiquitous promoters, such as elongation factor 1α (ELF-1α), cytomegalovirus (CMV), synapsin (hSyn), or CAG, drive robust opsin expression in almost any cell type in which the construct is present. Contrarily, promoters expressed in certain cell types can induce opsin expression only in specific cell types, for example, α-CaMKII in excitatory neurons. Opsin expression initiated by cell-type specific promoters, however, can be relatively weak compared to that by ubiquitous promoters (Lyon, 2013). To overcome this problem, a strong ubiquitous promoter can be combined with a Cre recombinase driver mouse. Briefly, an opsin gene is placed downstream of a strong ubiquitous promoter but separated from it by a stop cassette flanked by two loxP sites. Cell type- or brain region-specific expression of the gene construct can be achieved by injecting the gene construct into the brain of Cre driver mice, which express Cre recombinase only in specific cell types or brain regions. Coexistence of the Cre recombinase and loxP causes excision of the stop cassette and thus expression of the opsin (Lyon, 2013).

Given the limited packaging capacity of viral vectors, an attractive alternative to larger promoters are small enhancers, such as binding sites for transcription factors, for example, constructs with dlx enhancers that specifically target GABAergic neurons (Deubner et al., 2019).

B) Transgenic modification of animals

A variety of genetic modification methods have been developed to produce transgenic mouse lines for optogenetic research. These can be categorized into three groups i) knock-in approaches, ii) plasmid transgenic approaches, iii) bacterial artificial chromosome (BAC) transgenic approaches (Ting and Feng, 2013).

i) Knock-in approaches

In this method, homologous recombination is used to introduce a transgene expression cassette into the mouse genome in embryonic stem cells. Several opsin expressing mouse and rat lines exist, some of which are commercially available. For example, it has become possible to purchase mice which express opsins under the control of promoters such as ChAT (cholinergic neurons) or VGAT (GABAergic interneurons) in the whole brain (Lyon, 2013). Alternatively, mouse or rat lines expressing the Cre recombinase in a specific subset of cells can be crossed with strains carrying a Cre-dependent opsin gene flanked by two pairs of incompatible Lox-sites, which prevent reversal of the Cre-induced DNA inversion, thus allowing a stable opsin expression (Deubner et al., 2019).

ii) Plasmid transgenic approaches

A plasmid is a small, double-stranded, often circular DNA which is separate from a cell's chromosomal DNA. Plasmids can be found in bacteria and some eukaryotes. They normally carry only a small number of genes which provide bacteria with some genetic advantages, such as antibiotic resistance. Plasmids vary in size and replicate independent of chromosomal DNA. Plasmids can be used as vectors to clone, transfer, and manipulate genes. Injection of fragmented linear plasmid DNA thus is one of the most straightforward and common methods to create a transgenic line. Well-defined, relatively short promotors to realize cell-type specific transgene expression are not always available, limiting creation of plasmid transgenic lines.

Even a single pronuclear injection often leads to broad transgene expression in multiple brain regions in plasmid transgenic lines or variable gene expression across multiple founder lines.

Although these features can be used to establish several transgene lines with unique characteristics, limiting transgene expression to small subtypes of cells in selected neural regions remains a challenge (Ting and Feng, 2013).

iii) BAC transgenic approaches

BACs are large (typically 100–300 Kb) DNA constructs consisting of a small cloning vector and large fragments of restriction-digested genomic DNA. The constructs can be stably propagated and manipulated in bacterial host cells (Ting and Feng, 2013, 2014). They typically span the entire genes and include substantial amounts of flanking sequences which are required to realize reliable expression of a particular gene *in vivo*. Using BACs, several transgene mouse lines with Cre drivers and GFP reporter genes have been developed, offering opportunities to choose appropriate mouse BAC lines to direct transgene expression in specific neuronal domains.

In addition to well-established BAC recombineering (= recombination-mediated genetic engineering) protocols, BAC clone libraries covering the mouse, rat, and human genome are available. One of the drawbacks of BAC methods is, however, that many BAC clone libraries contain undesirable extra genes which may lead to confounds due to overexpression of such extra genes, although a method to eliminate extra genes has been proposed (Ting and Feng, 2014).

C) In utero electroporation

In utero electroporation (IUE) is an alternative to viral-based methods and enables introduction of optogenetic proteins into specific brain regions, layers, or cell types, typically in the neocortex or hippocampus. For IUE, a solution containing opsin-carrying plasmids is injected into the brains of embryos and a current applied to the skull at specific angles and at distinct time points during development. Since IUE can target neurons in the very early phase of development, IUE is particularly suitable in delivering optogenetic constructs for experiments addressing developmental questions. Besides, an important advantage of IUE is the large genetic payload provided by plasmids in comparison to viral vectors. Moreover, a combination of IUE and optogenetics has emerged as an advantageous strategy to answer questions related to the early organization of neural circuits and the activity-dependent neural development (Martínez-Garay et al., 2016; Bitzenhofer et al., 2017; Deubner et al., 2019).

III) Selection of light source and light delivery methods

A) Light source

Two most common light sources for optogenetic applications are: i) light-emitting diodes (LEDs) and ii) lasers. Each of them has its own advantages and disadvantages and experimenters choose whichever method is more suitable for their experimental needs (**Table 1.1**).

	LED	Laser
Advantages	• Low cost • Safer for the eyes • Long lifetime • A wide range of wavelengths, i.e., diverse color options, available (from UV to NIR) • Low operating temperature	• High intensity • Tightly focused • Narrow spectral bandwidth, which enables selective illumination of multiple opsins • Highly efficient optical coupling
Disadvantages	• Light not focused (= high divergence) • A wider spectral bandwidth • Lower intensity	• Expensive • Limited availability of wavelengths • High operating temperature • Require eye safety measures

Table 1.1. Advantages and disadvantages of light-emitting diode (LED) and laser. Two major light sources used for optogenetic experiments are listed here. Each light source has advantages and disadvantages in terms of physical properties of light, mechanical aspects, economic factors, safety, and compatibilities with optogenetic opsins. Experimenters can choose suitable light sources based on their experimental needs. UV: ultraviolet. NIR: near infrared.

i) LED

High divergence of light makes fiber coupling less efficient by losing much of the light with each connection. Nonetheless, the LED is suitable for a wide range of optogenetic experiments, as long as the end light intensity is strong enough for intended experiments. Their small size and low driving power requirements make LEDs very useful for portable wireless optogenetic devices and multisite illumination (Guru et al., 2015). LEDs, however, are not suitable for applications where light needs to be tightly focused onto a tiny spot as in the laser-scanning system. The spatial resolution can be improved by changing the light

source to laser, as will be mentioned later, or to micro-LED (µLED), which both allow selective illumination of a limited region of interest (Montagni et al., 2019).

ii) Laser

Like LEDs, lasers are suitable for most optogenetic applications. Diode-pumped solid-state lasers (DPSSLs) with a maximum output power of 100 mW are an adequate choice in optogenetics (Guru et al., 2015). Since lasers can provide highly focused high-intensity light at longer wavelengths, they are particularly suitable for laser-scanning and two-photon microscopy optogenetic experiments (https://www.mightexbio.com/optogenetic-stimulation/).

B) Light delivery

Visible light is significantly scattered and absorbed in tissue, including the brain, leading to significant phase shifts and attenuation of light. For this reason, delivery of optogenetic light to deep brain locations requires use of waveguides or insertion of µLED sources into the brain (Mohanty and Lakshminarayananan, 2015). In the former case, the most common method to deliver light into targeted intracranial regions and permit optical control of deep brain structures is the use of optical fibers. Small diameter optical fibers (generally a multimode fiber with a core diameter of 50–200 µm) can be inserted into the brain to minimize tissue damage and can be coupled to light sources. Standard optical fibers are cleaved flat-face fibers (FFs), which convey light only within a small and fixed tissue volume in close vicinity of the tip of the fiber. Recently developed tapered optical fibers (TFs), on the other hand, allow excitation of a larger volume due to the cylinder-shaped homogeneous light emitted from the entire tapered fiber. In addition, TFs enable adjustment of light input angles to select the light-emitting portions. This allows simultaneous illumination of two different regions in the brain which are located along the same fiber (Montagni et al., 2019).

The waveguide/fiber can be held by a stereotaxic apparatus to keep it in place inside the brain during *in vivo* experiments with anesthetized animals. For *in vivo* experiments with freely moving animals, the optical fiber is inserted and fixed through a cannula guide. This, in turn, is pre-fixed to the skull of the animal using dental cement and screws, which work as anchors to stabilize the dental cement. Alternatively, optic fiber ferrules can be fixed to the skull with optical patch cables connected using sleeves, a so-called butt-coupling method. Use of cannulas facilitates, for example, simultaneous pharmacological manipulations. Finally, an optic commutator or rotary joint, which connects two optical cables, one from the light source and the other to the animal, is used to allow free movement of animals without twisting and

breakage of the optical fibers during experiments (Mohanty and Lakshminarayananan, 2015; Guru et al., 2015). Optionally, optic fibers can be coupled to recording electrodes for simultaneous electrophysiological recording and photostimulation. This construct is called optrode (= optic fiber + electrode) and takes advantage of both electrophysiology and optogenetics in the same experimental setup (Montagni et al., 2019).

IV) Selection of light stimulation parameters

Light stimulation patterns are determined in terms of: A) light intensity, B) waveform, C) frequency, and D) pulse width. The choice of appropriate stimulation parameters is important because each opsin has suitable stimulation patterns based on its optophysiological properties. Moreover, changing stimulation parameters can change the experimental outcomes even when the same neuronal subtypes are stimulated. Selection of appropriate stimulation parameters, such as light intensity, pulse duration, and frequency, is also important to prevent phototoxicity and heat damage in biological tissues (Montagni et al., 2019).

A) Light intensity

Previous *in vivo* and *in vitro* studies have shown that the minimal light intensity needed to activate ChR2-expressing neurons is in the order of 1 mW/mm^2 (Wang et al., 2012). Typical optogenetic activation of neurons, however, requires relatively high light intensity of at least 10 mW/mm^2 or higher over the targeted region. Care must be taken when using very strong light because it may damage the tissue due to the heat generated by light absorption. Generally, a safe range for *in vivo* experiments is up to ~75 mW/mm^2 at the target region for short pulses (~0.5 to 50 ms; Cardin et al., 2010). It should be noted that light absorption is stronger at a short wavelength (e.g., blue) than at a longer wavelength (e.g., red). For example, when using blue light (473 nm), half of the light intensity is lost due to the absorption in the brain tissue within 0.1 mm distance from the fiber tip (http://www.optogenetics-at-doric.com/). On the other hand, the optical fiber tip is intentionally placed several hundred micrometers up to mm away from the target region or the electrophysiological recording electrode to prevent mechanical damage on target tissues or electrodes caused by insertion of optic fibers. Moreover, in electrophysiological recording combined with optogenetic stimulation, the optical fiber tip is placed several hundred micrometers away from the recording electrode to prevent optically induced electrical artifacts (Cardin et al., 2010). For those reasons mentioned above, light intensity much higher than the required intensity is commonly emitted from the optical fiber tip so that the target

region receives enough light illumination even after absorption in tissues or emission in the free space.

B) Waveform

Two major waveforms used in optogenetics are pulses and sine waves. Padilla-Coreano and colleagues demonstrated that sine-wave, but not pulsatile, stimulation of the ventral hippocampus-medial prefrontal cortex (vHPC-mPFC) pathway increased avoidance behavior in mice (Padilla-Coreano et al., 2019). Sine-wave stimulation imitates neuronal oscillation, which can be naturally observed in certain brain areas such as the cortex and hippocampus. Neuronal oscillations can be used as indicators of specific neurological phenomena, e.g., sleep, perception, memory, motor control, pattern generation, and neuropsychiatric diseases such as epilepsy. Sine-wave stimulation, thus, has substantial relevance when investigating such neural oscillatory functions. Pulsed illumination, on the other hand, mimics the behavior of an on-off switch, allowing for fast depolarization-repolarization cycles. Compared to continuous light stimulation, pulsed stimulation has an advantage in that it causes less temperature increase in the illuminated tissue. Since heat may cause tissue damage, minimizing temperature increase is an important factor to be considered in optogenetic stimulation.

C) Frequency

The maximum evoked firing frequency varies depending on the targeted cell type. For example, light stimulation can drive ChR2-positive pyramidal cells in the neocortex to fire up to 30 Hz, whereas fast-spiking interneurons reach up to 100 Hz or more. In general, at lower frequencies (1–5 Hz), most ChR2-positive cells reliably generate action potentials in response to each pulsed light stimulation (Cardin et al., 2010; Zhang et al., 2010; Erofeev et al., 2019). Even when the same neuronal subtypes are stimulated, changing stimulation frequency may result in different experimental outcomes. For example, oscillatory stimulation of the vHPC-mPFC pathway has been shown to increase avoidance behavior and neural transmission in mice when stimulated at 8 Hz, but not at 2, 4, or 20 Hz (Padilla-Coreano et al., 2019). Moreover, optogenetic stimulation of the median raphe nucleus led to the release of serotonin and glutamate when stimulated at 20 Hz, but not at 50 Hz (Gölöncsér et al., 2017). The dependence of neuronal response on stimulation frequency is partly attributable to the fact that neuronal systems have their own rhythms at which they function. In the case of the vHPC-mPFC pathway, neural activities in these two brain regions were known to synchronize

at the theta-frequency range (4–12 Hz) in avoidance behaviors. Thus, optogenetically stimulating this pathway at a frequency that corresponds to the one observed in naturally occurring behaviors is most effective in artificially inducing certain behaviors in question (Padilla-Coreano et al., 2019).

D) Pulse width

Erofeev and colleagues investigated the dependency of photocurrents on light pulse duration, measured by whole-cell patch clamp in a hippocampal pyramidal cell primary culture transfected with ChR2 (Erofeev et al., 2019). They demonstrated that at least a 10 ms duration was necessary to induce full response. Interestingly, the photocurrent amplitude gradually decreased at longer pulse duration (30–500 ms). Based on the kinetic models of ChR2 activation, the authors assumed that photocurrents decreased after 30 ms because ChR2 went into its inactivation state. In sum, it can be concluded that the pulse durations between 10–30 ms are optimal for activating ChR2.

V) Validation of optogenetic manipulation: Readout

This is a step to verify that, with the previous steps (i.e., opsin choice, gene delivery method, illumination parameters) cells have been manipulated with the strength and specificity intended. Diverse approaches can be taken in this step, such as electrophysiology (e.g., field potential and whole-cell patch clamp recordings), imaging, immunohistochemistry (e.g., c-Fos staining), pharmacology, and behavior (e.g., movement; Tye and Deisseroth, 2012; Mohan, 2017.)

Combining electrophysiological recording with opsins targeted to specific neuronal subtypes enables the identification of these specific cell types. This way of identifying specific neuronal populations assisted by photostimulation is termed “phototagging” or “optotagging”. To be precise, targeted neurons can be identified as those neurons which respond to a given optogenetic illumination. Thus, phototagging combined with cell-type-specific expression of opsin allows the identification, characterization, and quantification of neurons. As long as enough opsin expression is realized, not only in the soma but also in the projection fibers, optical stimulation in the projection areas can be paired with electrophysiological recordings, allowing identification of projection profiles and pathway-specific subpopulations of neurons (Deubner et al., 2019).

One of the advantages of using optogenetics in behavioral research is that it enables within-subject and within-session controls in light-stimulated and non-stimulated experiments by temporarily and reversibly altering neuronal activities. This stands in contrast to lesions, which are irreversible, and pharmacological manipulations, for which sometimes minutes, hours, or even days may be required to have the drugs washed out of the brain (Lyon, 2013; Deubner et al., 2019).

Combining optogenetics with Ca^{2+} (genetically encoded Ca^{2+} indicator, GECI) or voltage indicators (GEVI) in particular appears attractive since both imaging ("read") and perturbing ("write") neuronal activities can be done in all-optical systems *in vivo*. Fiber photometry, miniaturized microscopes (miniscopes), and optical fiber scopes allow employing this technique in freely behaving animals. Among these, the fiber scope is the most advanced method, as it enables cellular-resolution imaging and optogenetic stimulation in behaving animals (Deubner et al., 2019).

Optogenetics can also be combined with functional magnetic resonance imaging (fMRI). Optogenetic fMRI (ofMRI) offers a non-invasive and indirect way of monitoring neuronal activities in response to optogenetic stimulation by measuring the blood-oxygenation-level-dependent (BOLD) signals. In comparison to electrophysiological measurement of neuronal activities, ofMRI is advantageous because it provides an overview of entire brain activities at high spatial resolution, even when distant from the optogenetic stimulation site. Use of optogenetic stimulation overcomes problems associated with the electrodes for electrical stimulation and the current running through them, namely as electromagnetic artifacts in fMRI signals. However, the heat generated by light stimulation is known to produce pseudoactivation in fMRI signals due to changes in relaxation times, although this problem can be addressed by selecting proper setups and controls. The relatively low temporal resolution of fMRI signals inherent in hemodynamic responses can also be a limiting factor for certain experiments (Lee et al., 2010; Lin et al., 2016).

1.2. Serotonergic system

1.2.1. Serotonin synthesis

Serotonin (5-hydroxytryptamine, 5-HT) is a biogenic monoamine, classified as indoleamine, and as a neurotransmitter plays diverse roles in the regulation of neurocognitive functions such as sensory processing, pain perception, motor activity, memory, cognition, sleep,

aggression, social and sexual behaviors, irritable bowel syndrome, and mood. Correspondingly, the dysregulation of 5-HT homeostasis manifests itself as diverse neurocognitive disfunctions such as mood disorders, anxiety, depression, panic disorders, cognitive deficits, sexual dysfunction, or compulsivity (Beecher et al., 2019). Moreover, 5-HT plays diverse physiological roles in the peripheral and central nervous system (CNS) including appetite and eating, digestion and gastrointestinal motility, emesis, peripheral and cerebral vascular tone, platelet function, migraine, systemic and pulmonary hypertension (reviewed in Mohammad-Zadeh et al., 2008).

The plethora of 5-HT functions arises from various factors, including the large number of receptor genes (14 in mice and 17 in humans), alternative splicing of gene transcripts, mRNA editing, different combinations of receptor subunits, and heterodimerization with non-5-HT receptors (Wyler et al., 2017 and references therein). In mice, 5-HT receptors are first classified into seven classes (5-$HT_{1–7}$), which are further divided into subtypes such as 5-HT_{1A}, 5-HT_{1B}, etc., comprising at least 14 different receptor subtypes (Barnes and Sharp, 1999). Among the seven receptor classes, the 5-HT_3 receptor is the only ionotropic receptor, which serves as a pentameric, ligand-gated Na^+/K^+ ion channel. Other six receptor classes are metabotropic (= G-protein-coupled) receptors. 5-HT_1 and 5-HT_5 receptors are negatively coupled with adenylyl cyclase, and thus activation of these receptors leads to reduction of cyclic AMP (cAMP). 5-HT_4 and 5-HT_7 receptors, on the other hand, are positively coupled with adenylyl cyclase, leading to increase of cAMP. 5-HT_2 receptor upregulates the inositol triphosphate (IP_3) and diacylglycerol (DAG) pathways, resulting in intracellular Ca^{2+} release. The influx of Na^+/K^+ ions associated with 5-HT_3 receptors depolarizes plasma membrane potential (reviewed in Mohammad-Zadeh et al., 2008).

5-HT is stored in three main cell types, in i) serotonergic neurons in the CNS and in the intestinal myenteric plexus, ii) enterochromaffin cells in the mucosa of the gastrointestinal tract, iii) blood platelets. Among them, only serotonergic neurons and enterochromaffin cells can produce 5-HT themselves, while platelets uptake and store externally synthesized 5-HT (Watling, 2006).

5-HT is synthesized from the essential amino acid L-tryptophan (Trp), which can be found in such foods as eggs, fish, milk, cheese, meats, sesame, soybeans, banana, and oats. Synthesis of 5-HT occurs in a two-step process — hydroxylation followed by decarboxylation. Trp is first converted into 5-hydroxytryptophan (5-HTP) by tryptophan hydroxylase (TPH), requiring O_2 and tetrahydrobiopterin (BH4) as cofactors. TPH is the rate-limiting enzyme of

the 5-HT synthesis and in normal situations is not saturated, rendering brain 5-HT sensitive to changes in dietary Trp levels (Daroff and Aminoff, 2003). Synthesized 5-HTP is then converted to 5-HT by aromatic L-amino acid decarboxylase (AADC; Carlsson et al., 1972) with pyridoxal phosphate as a cofactor (**Fig. 1.1**). There have been two isoforms of TPH reported: TPH1 in the periphery and the pineal gland; TPH2 in the CNS. TPH1 in the pineal gland produces 5-HT as a precursor for the subsequent enzymatic pathway leading to the formation of the pineal hormone, melatonin. Since 5-HT cannot cross the blood-brain barrier, central 5-HT produced by TPH2 and peripheral 5-HT produced by TPH1 constitute two distinct 5-HT pools (Wyler et al., 2017 and references therein).

1.2.2. Serotonin release

Synthesized 5-HT is stored in synaptic vesicles, which prevents 5-HT from being degraded by monoamine oxidase (MAO) and keeps it ready for release from axon terminals. In the nervous system, 5-HT has three different modes of action: i) locally at synaptic boutons as a neurotransmitter, ii) at a distance from its synaptic release sites upon diffusion as a neurotransmitter, producing volume effects, iii) circulating in the blood stream, producing hormonal effects (De-Miguel and Trueta, 2005). The first type of action is called wiring transmission (WT) since it occurs in a spatially constrained cellular chain (wire), whereas the second type has been termed volume (also called paracrine, parasynaptic, or diffusion) transmission (VT; Zoli et al., 1998; Kiss, 2008). It has been demonstrated that more than 80% of monoaminergic varicosities make no synaptic contacts but are able to release neurotransmitters directly into the extrasynaptic space, suggesting that the monoaminergic neurotransmission is predominantly of the VT type in nature. The VT of 5-HT can occur from vesicles in neuronal cell bodies, axonal varicosities, and dendrites, and can be induced by neuronal depolarization, by activation of glutamatergic receptors, by the stimulation of L-type calcium channels, and/or by activation of 5-HT_2 receptors (De-Miguel et al., 2015; Quentin et al., 2018). The resulting 5-HT release shows a slow kinetic and a large diffusion, i.e., the time scale of VT spans in the order of seconds/minutes and its spatial scale covers hundreds of micrometers, allowing released neurotransmitter to reach its target at a distance in the extracellular space (Kiss, 2008; Quentin et al., 2018). Firing patterns of serotonergic neurons are also associated with modes of 5-HT release. Serotonergic neurons by default display regular tonic, or “clock-like”, firing patterns, whereas in specific behaviors, they display phasic firing in bursts. Tonic firing of serotonergic neurons seems to be related to the tonic 5-HT levels in the extrasynaptic space and burst firing to the high-amplitude, rapid, and phasic 5-HT release in the intrasynaptic space. Although tonic and phasic firing of serotonergic

neurons and the resultant different modes of 5-HT release have been suggested to have opposite functions, their respective contributions to behavior remains unclear (Quentin et al., 2018).

Diffusedly released 5-HT then exerts neuromodulatory effects on excitatory and inhibitory synapses. For example, serotonergic neurons contact glutamatergic or GABAergic/glycinergic synapses to form synaptic triads that modulate the activity of excitatory or inhibitory synapses, respectively (Belmer et al., 2017). Histologically, 5-HT boutons opposed to excitatory synapses are characterized by their symmetrical configuration, whereas those opposed to inhibitory synapses assume asymmetrical configurations (Belmer et al., 2016). Further in accordance with the VT concept, the DRN is known to display little synaptic specialization and 5-HT uptake sites are not synaptically localized but rather are distributed widely on the serotonergic neurons, enabling an optimal control of 5-HT levels in the extracellular space (Bunin and Wightman, 1998). In sum, VT allows 5-HT to interact with many extrasynaptic elements through its three-dimensional diffusion of neurotransmitters in the extracellular fluid beyond the realm of synaptic contacts (Zoli et al., 1998).

1.2.3. Serotonin metabolism

5-HT action at synapses is terminated by reuptake into presynaptic terminals mediated by a membrane protein, the serotonin transporter (5-HTT or SERT). 5-HTT is a solute carrier family 6 member 4 protein which is expressed in the epithelial cells of the intestines and the blood platelets (Liu et al., 2021). In the brain, 5-HTT is specifically expressed by serotonergic neurons and thus used as a marker for this type of neurons (Nichols and Sanders-Bush, 2003; Beecher et al., 2019). Extra 5-HT is then first converted to 5-hydroxyindole acetaldehyde by MAO, for which two molecular subtypes are known, namely MAO-A and MAO-B. MAO-A has higher affinity for 5-HT and norepinephrine (NE), whereas MAO-B preferentially metabolizes phenylethylamine (PEA). Dopamine (DA) and other monoamines, e.g., tryptamine and tyramine, are metabolized by both MAO isoforms, although DA metabolism is mainly mediated by MAO-A in the rodent brain, while MAO-B plays a substantial role in DA metabolism in primates including humans (Bortolato et al., 2008). Counterintuitively, in human brains, MAO-A is found in catecholaminergic neurons, whereas MAO-B is found in serotonergic neurons and astrocytes. In other human tissues, MAO-A and MAO-B are mostly co-expressed and most abundant in the intestine. 5-HT taken up from the diet essentially undergoes complete first-pass metabolism by MAO-A in the gut wall and liver (Waller and Sampson, 2018). Fibroblasts and placenta, however, express only MAO-A, while platelets

and lymphocytes express only MAO-B (Shih and Chen, 2004). Blood platelets do not synthesize 5-HT but can accumulate high concentrations of 5-HT from the blood circulation. 5-HT is then released when platelets aggregate, and during migraine episodes (Waller and Sampson, 2018).

5-hydroxyindole acetaldehyde, produced from 5-HT by MAO, is in turn metabolized by aldehyde dehydrogenase (ALDH) with a cofactor of NADH to 5-hydroxyindoleacetic acid (5-HIAA), which then is excreted into the urine (**Fig. 1.1**; Bortolato et al., 2008). 5-HIAA is often used as an indicator for 5-HT levels in the brain because 5-HT is highly labile. Although non-neuronal cells such as gastrointestinal cells, produce more than 98% of the total 5-HT in the body, this 5-HT does not penetrate the blood-brain barrier. Therefore, concentrations of 5-HIAA in the cerebrospinal fluid reflect 5-HT activity in the CNS. Further other enzymes metabolize 5-HT to melatonin in the pineal gland (Nichols and Sanders-Bush, 2003; Kaufman and Milstein, 2013).

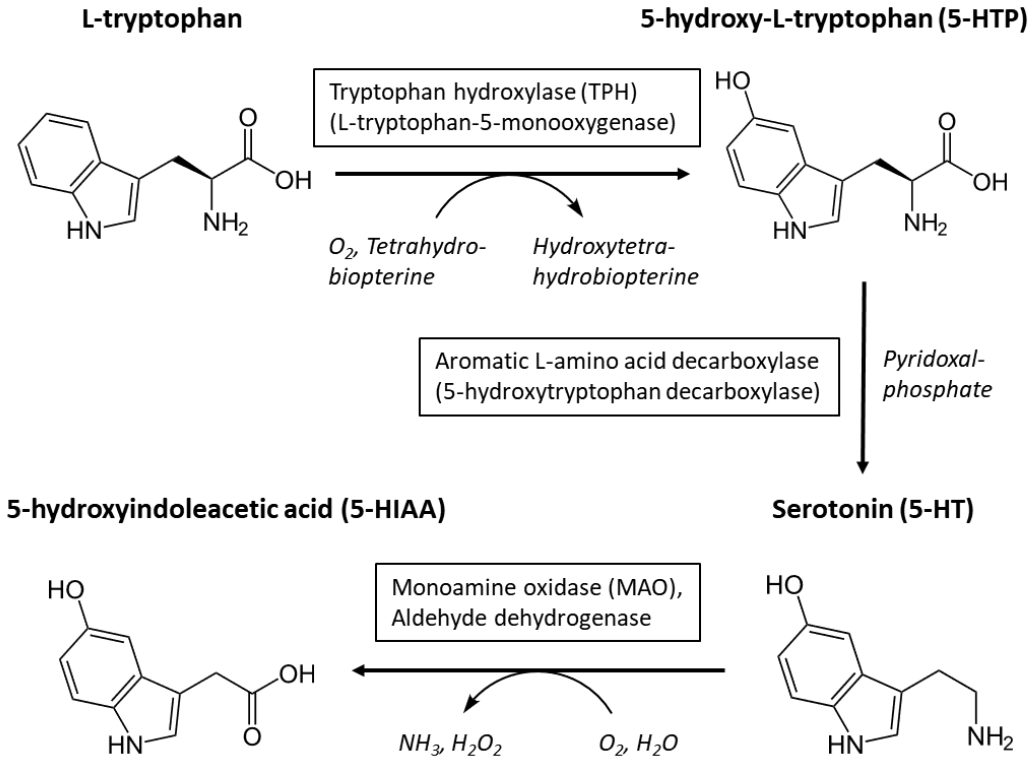

Fig. 1.1. Biosynthesis of serotonin (5-HT). The essential amino acid L-tryptophan obtained from the diet is converted into 5-hydroxy-L-tryptophan (5-HTP) by the rate limiting enzyme tryptophan hydroxylase (TPH; also known as L-tryptophan-5-monooxygenase). TPH requires tetrahydrobiopterin as a cofactor. Produced 5-HTP is then converted to 5-HT by aromatic L-amino acid decarboxylase (also known as 5-hydroxytryptophan decarboxylase). 5-HT is metabolized to 5-hydroxyindoleacetic acid (5-HIAA) by monoamine oxidase (MAO) and aldehyde dehydrogenase. Figure adapted from Araragi and Lesch, 2013 with permission.

1.2.4. Distribution and projections of brain serotonergic neurons

Although there are only about 300,000 serotonergic neurons in the human brain (Cao et al., 2017), they possess highly arborized and elongated axons which form synapses on a large number of non-serotonergic neurons. This rich connectivity of serotonergic axons with almost all other brain regions indicates broad modulatory effects of serotonergic neurons on numerous brain functions (Carey and Müller, 2013). Most of the serotonergic neurons reside in relatively small clusters in the brainstem, forming the raphe nuclei localized in the basal plate of the pons and medulla (Valiulahi et al., 2021). Serotonergic neurons in the raphe nuclei are then grouped into nine nuclei (B1, raphe pallidus; B2, raphe obscurus; B3, raphe magnus; B4, dorsal to prepositus hypoglossi; B5, raphe pontis; B6, caudal part of raphe dorsalis; B7, raphe dorsalis; B8, centralis; B9, the supralemniscal nucleus; **Fig. 1.2**). They are grouped into the caudal group (B1–4) and the rostral group (B5–9). These cell groups possess distinctive and largely non-overlapping projections areas.

The caudal group (B1–4) sends descending projections to the medulla, cerebellum, and spinal cord to control motor activity, pain perception, involuntary movement, homeostasis, and the autonomic nervous system.

The rostral group (B5–9) of serotonergic neurons sends ascending projections to the forebrain, including the cortex, amygdala, striatum, basal ganglia, hippocampus, thalamus, and hypothalamus to control cognition, mood, perception, circadian rhythms, appetite, and reproduction. The highest density of serotonergic neurons can be found in B7. It is continuous with B6, which is more caudally located, and they together form the dorsal raphe nucleus (DRN). Based on anatomical projections, B7 can further be divided into the dorsal (B7d), ventral (B7v), and lateral (B7l) subcomponents. DRN sends projections to basal parts of the forebrain, such as the amygdala. Distinct subsets of B7 also have preferential target regions: B7v innervates the cortex and amygdala, while B7d innervates the hypothalamus.

B8 also contains a high density of serotonergic neurons and forms together with its caudal counterpart, B5, the median raphe nucleus (MRN). MRN is the main 5-HT source to the hippocampus, mesopontine tegmental nuclei, and septum. Finally, the B9 cell group projects to the prefrontal cortex, caudate, substantia nigra, locus coeruleus and to the other raphe nuclei (Muzerelle et al., 2016).

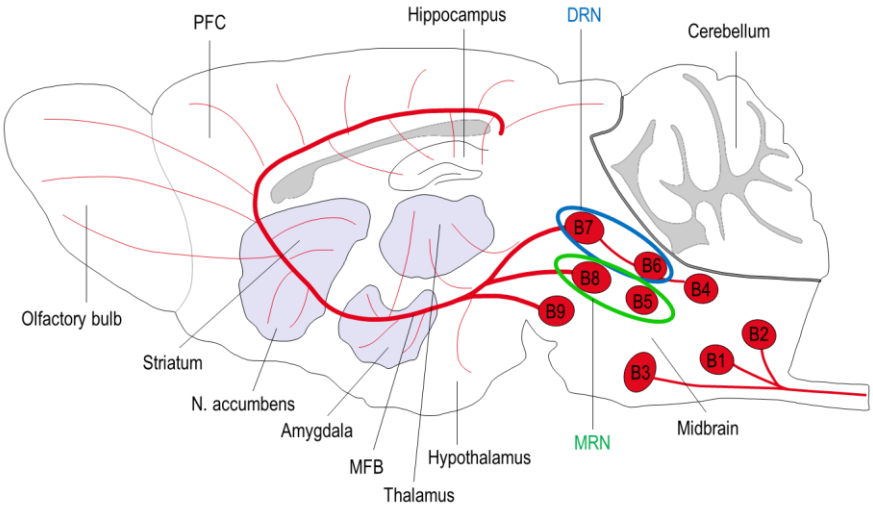

Fig. 1.2. Sources and projections of serotonergic neurons in the rodent brain. Red lines depict neuroanatomical projections. B1–B4: the caudal group of neurons in the lower brainstem which send descending projections into the medulla and spinal cord. B5–B9: the rostral group of neurons in the upper midbrain which send ascending projections into the forebrain. B6, B7: the dorsal raphe nucleus (DRN). B5, B8: the median raphe nucleus (MRN). MFB: medial frontal bundle. Figure adapted from Araragi and Lesch, 2013 with permission.

The DRN, on the other hand, receives afferent inputs from extra-raphe areas as well as within the local circuit. Neurotransmitters released from those afferents are diverse, including glutamate (cerebral cortex), dopamine (substantia nigra, ventral tegmental area), noradrenaline (locus coeruleus), acetylcholine (pedunculopontine and laterodorsal tegmental nuclei), GABA (substantia nigra pars reticulata, local interneurons), and 5-HT from other raphe nuclei (Hernandez-Lopez et al., 2013; Soiza-Reilly and Commons, 2014). In addition, anatomical and functional interconnectivity between DRN and MRN has been reported (Tischler and Morin, 2003; Beliveau et al., 2015).

It should also be noted that not all cells in the DRN are serotonergic. Indeed only 30–50% of the neurons in the DRN were shown to be serotonergic and many neurons release other neurotransmitters, such as GABA, glutamate, dopamine, nitric oxide, and various neuropeptides (e.g., neuropeptide Y, galanin, somatostatin, thyrotropin-releasing hormone; Lesch and Waider, 2012; Huang et al., 2019). Moreover, recent genetic and cell fate analyses revealed that serotonergic neurons in the DRN are heterogeneous, comprising several different subtypes with distinct molecular and anatomical characteristics (Andrade and Haj-Dahmane, 2013; Huang et al., 2019). Importantly, serotonergic neurons in the DRN and MRN

were also shown to be different in terms of their electrophysiological properties including responsiveness to 5-HT_{1A} receptor-mediated autoinhibition (Beck et al., 2004).

1.3. Adult neurogenesis

1.3.1. Location of adult neurogenesis

Adult neurogenesis is a biological phenomenon in which functional, mature neurons generated throughout life integrate into existing neuronal circuits after fetal and early postnatal development has completed. Adult neurogenesis takes place in restricted brain areas and has been reported in various species such as birds, fish, reptiles, and mammals. In rodents, the major areas of adult neurogenesis are the subgranular zone (SGZ) of the hippocampal dentate gyrus (DG) and the subventricular zone (SVZ) of the lateral ventricles. Adult neurogenesis in the DG generates only one type of neuron, namely, glutamatergic granule cells (Kempermann et al., 2015). Newborn neurons in the SVZ migrate toward the olfactory bulb (OB) and differentiate into local GABAergic/dopaminergic olfactory neurons (Jessberger and Gage, 2014; Song et al., 2017). On the other hand, adult neurogenesis in humans is present in the DG and the SVZ, with no detectable OB neurogenesis. New neurons born in the SVZ integrate into the adjacent striatum, which plays an important role in movement coordination, procedural learning, and memory, as well as in emotional and motivational control. One major difference between rodent and human adult neurogenesis is thus the migration destination of neuroblasts generated in the SVZ, with the OB being the major destination in most mammals including rodents (Ernst and Frisén, 2015). Striatal neuronal dysfunctions have been implicated in neurodegenerative diseases such as Huntington’s disease and Parkinson’s disease as well as in neuropsychiatric disorders such as schizophrenia and addiction. Interestingly, increased cell proliferation and neuroblast production have been observed in the SVZ of patients with Huntington’s disease, probably as a compensatory mechanism. In advanced stages of the disease, however, the neuronal loss cannot be compensated for anymore. Similarly, increased adult neurogenesis in the SVZ has been reported after striatal stroke in humans but also in rodents and non-human primates (Ernst and Frisén, 2015).

1.3.2. Neurobiological mechanisms

I) Phases of adult neurogenesis

Adult neurogenesis undergoes four different phases: a precursor cell phase, an early survival phase (fate specification), a postmitotic maturation phase, and a late survival phase (integration). The precursor cell phase is characterized by an expansion of the cell population that might differentiate into neurons. At the early survival phase, cells exit from their miotic cell cycle. Most of the newborn cells die within days after they are generated. The postmitotic maturation phase is linked to the establishment of functional neuronal connections, axonal and dendritic growth, and synaptogenesis. The late survival phase marks a period of fine-tuning. The total duration of adult neurogenesis takes approximately seven weeks (**Fig. 1.3**; Hsieh, 2012; Kempermann et al., 2015).

Of particular interest is that stimuli that control precursor cell proliferation tend to be nonspecific (e.g., seizures, physical exercise), whereas stimuli which represent hippocampus-dependent function influence survival of newborn cells. Past studies have demonstrated that exposure to an enriched environment or to learning stimuli for hippocampus-dependent learning increased cell survival (Kempermann et al., 2015). Quantitative regulation of neurogenesis, for the most part, stems from the regulation of cell survival. Using different mouse strains, it was shown that the genetically determined level of cell survival accounted for 85% of the variance in net neurogenesis, whereas the contribution of cell proliferation was only 19% (Kempermann et al., 2006).

II) Types of newborn neurons

New neurons are produced from a group of dividing cells called neural stem cells (NSCs). NSCs are characterized by their potential of self-renewal and multipotency, meaning that they can divide and differentiate into all the three main cell classes of the nervous system, namely, neurons, astrocytes, and oligodendrocytes (Aimone et al., 2007).

The process of adult neurogenesis can be divided into six stages based on cell morphology and marker proteins: a radial glia-like precursor stage (1^{st}), the highly proliferative progenitor stages (2^{nd}–4^{th}), a postmitotic maturation stage (5^{th}), and a new mature granule cell stage (6^{th}; Kempermann et al., 2015).

In the SGZ and SVZ, proliferating cells comprise four different cell types, which correspond to the first four stages of adult neurogenesis mentioned above, namely, type 1 (1st stage), type 2a/b (2nd and 3rd), and type 3 (4th) cells (Alenina and Klempin, 2015).

Type 1 (or type B in the SVZ) radial glia-like cells (RGLs) resemble the radial glial cells observed during development and have a morphology and physiology similar to mature astrocytes. Type 1 cells (= B cells) are relatively quiescent or slowly dividing and thought to represent the NSC population. They possess a single radial process protruding from the GCL and express such markers as glial fibrillary acidic protein (GFAP) and nestin. Recently, another class of type 1 cells has been identified, characterized by short horizontal processes. These horizontal type 1 cells appear to divide more quickly than radial type 1 cells. The lineage relationship between the radial and horizontal type 1 cells, however, is still unknown. Once quiescent NSCs proliferate, they give rise to type 2 cells, also known as intermediate progenitor cells (IPCs) or transit-amplifying progenitors (TAPs), which possess high proliferative activity with a small round morphology and short tangential processes (Hsieh, 2012).

Type 2 (or type C in the SVZ) cells are further categorized into a more glial-like (type 2a) and a neuronally determined (type 2b) cell. To be precise, type 2a cells are those cells that still express glial markers (the SRY-box transcription factor 2; Sox2) like type 1 cells but lack the typical morphology of RGLs. On the other hand, type 2b cells are defined as cells that, together with type 1 cells, express intermediate filament nestin, which shows first indications of neuronal cell fate determination. They start to express other neuronal markers such as the transcription factors NeuroD1 and Prox1. Prox1, in particular, is unique to granule cell development, and manipulation of this transcription factor terminates adult neurogenesis at this phase. Another transcription factor characteristic for type 2 cells is Eomes (Tbr2), which identifies the basal progenitor cells with self-renewing properties during embryonic cortical development and can differentiate into neurons. Tbr2 seems to suppress Sox2 expression and thus plays an important role for the transition from stem sells to IPCs (Kempermann et al., 2015).

Type 3 (or type A in the SVZ) cells are derived from type 2 cells (= C cells) and represent the population of neuroblasts that eventually mature into dentate granule cells (DGCs; Aimone et al., 2007; Kempermann et al., 2015; Gonçalves et al., 2016). They are characterized by the expression of the immature neuronal marker doublecortin (DCX). Although type 3 cells normally show only little proliferative activity, they can disproportionally proliferate under

certain pathological conditions such as experimentally induced seizures (Kempermann et al., 2015). As a final step, there is down-regulation of DCX and up-regulation of calretinin and NeuN as immature neurons mature to glutamatergic granule neurons. It takes ~6–8 weeks until new-born neurons in the SGZ structurally and functionally mature (**Fig. 1.3**; Hsieh, 2012 and references therein).

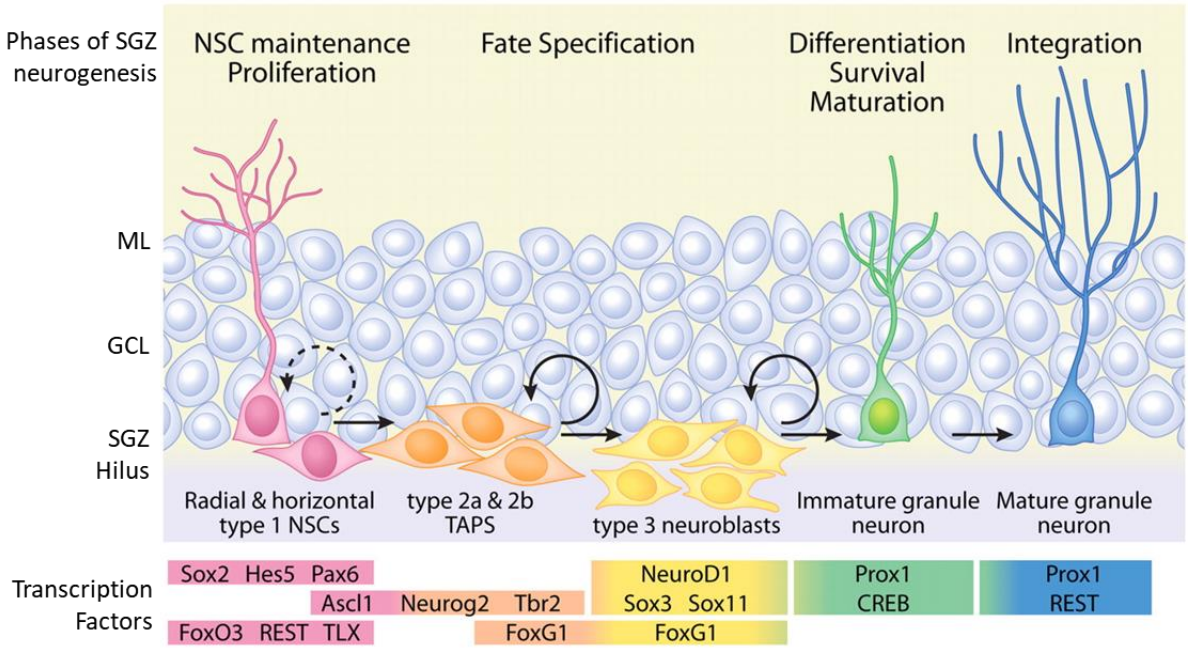

Fig. 1.3. Hippocampal adult neurogenesis in the subgranular zone (SGZ) of the dentate gyrus. Adult neurogenesis progresses in multiple steps, represented by different cell types, whose occurrence is controlled by the sequential expression of various transcription factors. NSC: neural stem cell. ML: molecular layer. GCL: granule cell layer. TAP: transit-amplifying progenitor. Figure modified from Hsieh, 2012 under a Creative Commons License (CC BY-NC 4.0).

1.4. Serotonin and adult neurogenesis

1.4.1. Serotonin receptors and neurogenesis

The idea that 5-HT could promote neurogenesis comes from the evidence that selective serotonin reuptake inhibitor (SSRI) antidepressants, which enhance 5-HT communication by blocking 5-HT reuptake, positively influence adult neurogenesis (Mahar et al., 2014; Segi-Nishida, 2017). Accumulating evidence suggests that 5-HT_{1A} receptors, which are Gi/o-coupled receptors, play an important role in SSRI-mediated neurogenesis. Santarelli and colleagues demonstrated that SSRI-mediated enhancement of cell proliferation in the DG was absent in 5-HT_{1A} receptor knockout (KO) mice, although baseline neurogenesis was not altered by this gene KO (Santarelli et al., 2003).

Antidepressants are known to have several weeks of latency until they unfold therapeutic effects. In accordance with this, Klempin and colleagues demonstrated that chronic but not acute administration of an SSRI fluoxetine promoted neurogenesis. Using specific agonists and antagonists, they proposed that the positive effect of 5-HT_{1A} receptors on neurogenesis is antagonized by 5-HT_2 receptors under acute condition (Klempin et al., 2010). Chronic administration, however, is shown to promote neurogenesis through 5-HT_{2C} receptor activation (Soumier et al., 2010; Klempin et al., 2010).

Growth factors such as BDNF and VEGF play an essential role in the regulation of adult hippocampal neurogenesis. Samuels and colleagues demonstrated that a fluoxetine-induced increase in BDNF and VEGF expression levels observed in control animals was abolished in 5-HT_{1A} receptor KO mice (Samuels et al., 2015). Evidence suggests that the increase of such growth factors are necessary for fluoxetine to unfold therapeutic effects in behavior and adult hippocampal neurogenesis (Samuels et al., 2015 and references therein). Furthermore, direct activation and inactivation of 5-HT_{1A} receptors through agonists and antagonists were shown to increase and decrease VEGF levels in the hippocampus, respectively (Greene et al., 2009).

5-HT_{2B} receptors are in general coupled to Gq/11 proteins and are expressed in both the raphe nucleus and the DG. SSRI-induced long-term behavioral and neurogenic effects as well as an increase in hippocampal extracellular 5-HT concentration were abolished in mice with genetically or pharmacologically inactivated 5-HT_{2B} receptors. In contrast, a selective 5-HT_{2B} agonist was shown to mimic behavioral and neurogenic effects of SSRI. Compared to wild type (WT) mice, baseline cell proliferation and survival were not altered in 5-HT_{2B} KO mice, which shows similarity to 5-HT_{1A} KO mice (Diaz et al., 2012).

Two recent reviews featured 5-HT_4 receptors, in addition to 5-HT_{1A} receptors, in the regulation of antidepressant action and neurogenesis (Samuels et al., 2016; Segi-Nishida, 2017). 5-HT_4 receptors are coupled to Gs proteins and expressed abundantly in the mouse or rat DG (Segi-Nishida, 2017 and references therein). Pharmacologically, direct application of 5-HT_4 receptor agonists such as RS67333 was reported to show antidepressant-like behavioral effects and to facilitate neuronal proliferation in the DG (Lucas et al., 2007; Pascual-Brazo et al., 2012). Unlike fluoxetine, however, anxiolytic effects of 5-HT_4 receptor agonists did not require hippocampal neurogenesis (Mendez-David et al., 2014). Blocking 5-HT_4 receptors by an antagonist GR125487, on the other hand, prevented neurogenic and anxiolytic/antidepressant-like effects of chronic fluoxetine administration, suggesting that 5-HT_4 receptor activation is necessary for SSRI to unfold its effects. Similarly, constitutive

$5HT_4$ receptor KO mice failed to demonstrate a fluoxetine-induced increase in the number of progenitors and immature (= DCX-positive) neurons, although the expression of these neurons at baseline was not affected (Imoto et al., 2015). Since 5-HT_4 receptors were found in mature granule cells rather than immature neurons in the DG, the authors of this study suggested that 5-HT_4 receptor mediates neurogenesis indirectly by inducing dematuration of granule cells. Importantly, such a dematuration process is accompanied by enhanced 5-HT- and dopamine-induced synaptic potentiation at the dentate-to-CA3 synapses (the mossy fiber synapses) via 5-HT_4 and D1-like receptors (Kobayashi et al., 2010; 2012). Evidence suggests that such neurogenic effects are modulated by intracellular signaling and neurotrophic factors such as CREB, BDNF (Lucas et al., 2007; Pascual-Brazo et al., 2012; Imoto et al., 2015). Moreover, it has been demonstrated that 5-HT_4 receptors in the prefrontal cortex increase the activity of DRN, suggesting that 5-HT_4 receptors outside of the DG or raphe nuclei could affect neurogenesis (Segi-Nishida, 2017 and references therein).

1.4.2. Pharmacological serotonin depletion

Pharmacologically, serotonergic depletion can be achieved either by 5,7-dihydroxytryptamine (5,7-DHT), which destroys serotonergic fibers and probably cells, or *para*-chlorophenylalanine (PCPA), which inhibits the serotonin-synthesizing enzyme TPH. Both methods have been shown to decrease 5-HT and decrease the number of newly generated cells in the hippocampus as well as in the SVZ (Brezun and Daszuta, 1999; 2000). At the molecular level, serotonergic denervation led to reduced expression of PSA-NCAM, a cell adhesion molecule transiently expressed by newly generated granule cells, thus facilitating neuronal plasticity. Importantly, this effect was reversed when the hippocampus was reinnervated by 5-HT fibers with time (Brezun and Daszuta, 2000). Ueda and colleagues demonstrated that 5,7-DHT reduced the number of BrdU-positive cells in the DG of rats housed in an enriched environment, which otherwise enhances cell proliferation (Ueda et al., 2005). Morphologically, 5-HT depletion in neonatal rats was shown to induce atrophy of dendritic spines in granule cells and its effects were counteracted by applying 5-HT_{1A} receptor agonist buspirone. Similarly, dendritic atrophy induced by 5-HT depletion in the early postnatal period was mimicked by applying the 5-HT_{1A} receptor antagonist NAN-190 (Yan et al., 1997).

Contradicting results, however, have been reported. It has been shown that only PCPA, but not 5,7-DHT, treatment decreases the number of precursor cells (Huang and Herbert, 2005; Jha et al., 2006). Since PCPA treatment led to a reduction of not only 5-HT but also

norepinephrine, the combined reduction of both monoamines could have played a role in suppression of precursor cell proliferation (Jha et al., 2006). In another study, chronic PCPA treatment was shown to increase survival of precursor cells in the DG, an effect which was normalized by 5-HT_{1A} receptor agonist 8-OH-DPAT. Of note is that such a pro-survival trait was observed also in transgenic mouse models of constitutive 5-HT deficiency such as $Pet1^{-/-}$ and $VMAT2^{f/f}$; $SERT^{cre/+}$ mice (Diaz et al., 2013).

1.4.3. Pharmacological serotonin increase

To investigate effects of acute serotonin increase on the proliferation of adult hippocampal progenitors in the DG, Jha and colleagues administered in rats either a combination of the monoamine oxidase inhibitor tranylcypromine (TCP) and the serotonin precursor L-tryptophan (L-Trp) or *para*-chloroamphetamine (PCA). The number of proliferating cells was quantified as BrdU-positive cells two hours after the single injection of BrdU. It was shown that neither TCP/L-Trp nor PCA treatment changed the proliferation of adult hippocampal progenitors in the SGZ or GCL of the DG (Jha et al., 2006).

1.4.4. Transgenic animal models with altered serotonergic neurotransmission

I) Tph2 KO mice

5-HT deficiency could result from various mutations in genes involved in the serotonergic system. Tph2 KO mice shows >90% reduction in most brain regions (Gutknecht et al., 2012). Baseline proliferation of hippocampal neuronal precursors was unaltered (Klempin et al., 2013). On the other hand, exercise-induced proliferation of precursor cells in the DG was absent in Tph2 KO mice. Lack of proliferation after exercise was especially evident with type 2a, Sox2+/GFAP− cells, which represent precursor cells. Alterations of cell proliferation at the stage of Sox2 expression indicates that physiological adaptation mechanisms took place in order to maintain homeostasis in the neurogenic niche under life-long depletion of brain serotonin (Klempin et al., 2013).

II) Tph2 KI mice

The Tph2 (R439H) knock-in (Tph2 KI) mouse shows ~60–80% reductions in brain 5-HT (Jacobsen et al., 2012). Baseline proliferation of hippocampal neuronal precursors was shown to be unaltered in these mice. Tph2 KI mice, however, showed increased survival of newborn neurons, a phenomenon known in other genetic models of brain serotonin reduction (Sachs et al., 2013; Pratelli and Pasqualetti, 2019 and references therein). Moreover, the SSRI

antidepressant fluoxetine failed to promote neurogenesis in these mice and did not increase BDNF mRNA, which was already increased even without fluoxetine, compared with WT mice (Sachs et al., 2013).

III) Conditional KO mice

The previous two studies mentioned above utilized constitutive knockout or knockin mice, meaning that the genetic modification was present from the beginning of life. The limitation of such animal models is that a compensation mechanism counteracting genetic modification takes place and confounds contribution of genetic products which are knocked out or knocked in. To overcome such limitations, Song and colleagues made use of tamoxifen (TM)-induced Cre in *Pet1*-CreER^{T2} mice to either deplete serotonergic neurons in the CNS or inactivate 5-HT synthesis only in adulthood. In both models of central 5-HT deficiency, a dramatic increase in hippocampal neurogenesis and the enhanced survival of new-born neurons was observed. Moreover, chronic treatment with a 5-HT$_{2C}$ receptor agonist prevented increased neurogenesis in these model mice (Song et al., 2016). In a subsequent study, Song and colleagues revealed that the dendritic length of hippocampal newborn neurons was dramatically increased in two other central 5-HT-deficient mouse models: Tph2 conditional knockout mice with deficient 5-HT from embryonic stage, and Pet1-Cre;Rosa26-DTR mice lacking serotonergic neurons exclusively in adulthood (Song et al., 2017). These findings suggest that reduced central 5-HT in adulthood can enhance adult hippocampal neurogenesis by increasing proliferation, survival, and dendritic growth of new neurons.

IV) 5-Htt KO mice

5-Htt KO mice have elevated extracellular 5-HT and reduced net 5-HT contents in the brain. In these mice, proliferation of hippocampal adult neural stem cells measured by BrdU staining was increased in aged mice (~14.5 months) but not in younger mice (up to ~3.0 months; Schmitt et al., 2007). Moreover, both the proliferation marker Ki67 and immature neuron marker NeuroD were increased in 5-Htt KO mice compared to WT mice (~6 months; Karabeg et al., 2013.)

1.4.5. Manipulation on other enzymes or genes

Enzymes which are primarily involved in physiological systems not directly related to neuronal development could influence neurogenesis. ACE2 is an enzyme which plays an important role in the regulation of blood pressure. It is mainly expressed in the lung and

converts AngII into Ang-(1–7). AngII binds to AT1 receptors, which work pro vasoconstrictive and pro-inflammatory, whereas another receptor for AngII, AT2 receptors, and receptors for Ang-(1–7), Mas receptors, work pro vasodilatory and anti-inflammatory. Apart from its role in the cardiovascular system, ACE2 is involved in resorption of Trp, the serotonin precursor, in the intestine. Genetic manipulation of ACE2 gene is therefore expected to trigger changes in serotonin homeostasis, which then could influence hippocampal neurogenesis. Klempin and colleagues showed that knockout of ACE2 gene in mice, as expected, resulted in decreased Trp and 5-HT levels in the brain. On the other hand, the number of BrdU-positive cells in the DG was not different from that of WT controls. The running-induced enhancement of cell proliferation, however, was absent in ACE2 KO mice, resembling the result obtained for Tph2 KO mice (Klempin et al., 2018).

1.5. Dentate gyrus

1.5.1. Anatomy

The mammalian hippocampus is in the temporal lobe and, based on cytoarchitectural criteria, divided into CA1, CA2 (area between CA1 and CA3), CA3, and the dentate gyrus (DG). The DG is, like other areas in the hippocampus, a highly layered structure and, starting from the fissure which forms a border to the neighboring CA1, is divided into the molecular layer (ML), granule cell layer (GCL), and the polymorphic layer. The ML is further divided into the outer ML (OML), the middle ML (MML), and the inner ML (IML). The polymorphic layer, commonly known as the hilus, contains numerous cell types and axons from granule cells called mossy fibers (**Fig. 1.4**).

Mossy fibers are the outputs of the DG and project to the CA3. Part of the CA3 pyramidal neurons in turn send glutamatergic projections back to the DG. For example, the hilus receives inputs from CA3, and the axons from ventral CA3 (vCA3) pyramidal cells innervate the IML (reviewed in Scharfman, 2016).

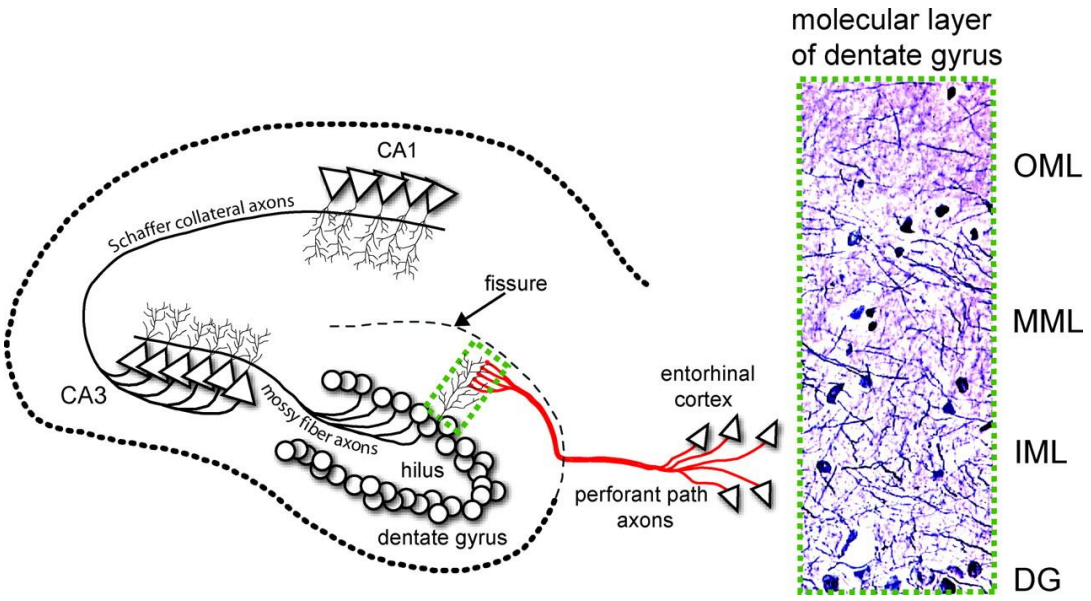

Fig. 1.4. Hippocampal structure. The hippocampus can be divided into CA1, CA2 (area between CA1 and CA3), CA3, and the dentate gyrus (DG). The hippocampal fissure is an embryonic remnant and physically separates the DG from the dendritic field of CA1 neurons. Perforant path axons come from large neurons in the layer II of the entorhinal cortex and project to dendrites of granule cell neurons in the molecular layer. The axons from the granule cells are called mossy fibers and project to CA3 pyramidal neurons, which in turn send Schaffer collateral axons to CA1 pyramidal neurons. These three axonal projections comprise the trisynaptic circuit of the hippocampus, serving functionally as a memory module. OML: outer molecular layer. MML: middle molecular layer. IML: inner molecular layer. Figure from Wong et al., 2009 with permission.

1.5.2. Cell types

Neurons in the DG are largely categorized into two groups: I) glutamatergic principal cells and II) GABAergic interneurons.

I) Principal cells

There are only two types of principal cells in the DG: A) the granule cells in the GCL and B) the mossy cells in the hilus (**Fig. 1.5**, **Fig. 1.6**).

A) Granule cells

Granule cells (GCs) have relatively low resting membrane potential compared to that of CA1 or CA3 pyramidal neurons, although the action potential threshold is similar to that of CA1 or CA3 pyramidal neurons. Consequently, relatively high depolarization is required to induce action potentials in GCs compared to the other two cell types. This results in sparse spontaneous firing of GCs *in vivo*. GCs become active only in certain behavioral tasks, such

as odor-guided tasks or when the animal is in a place field (Andersen, 2007 and references therein). Although most GCs are in the GCL, there is a small population of GCs in the IML and hilus. Stem cells reside in the SGZ and proliferate throughout life, a phenomenon known as adult hippocampal neurogenesis. The proliferated progenitor cells migrate mainly into the GCL, where they become mature GCs and integrate into the preexisting DG circuitry, just like other GCs which already exist from early life. GCs in the GCL differ depending on their position in the GCL. GCs in the suprapyramidal blade (closest to CA1) are generally larger and have more spines than those in the infrapyramidal blade (Andersen, 2007).

The dendrites of GCs are spread out in the molecular layer and receive afferent inputs from various sources. The OML and MML receive glutamatergic projections from layer II of the entorhinal cortex (EC), a pathway known as the performant path (PP). To be precise, inputs from the lateral part of EC (lateral entorhinal cortex; LEC) into the OML are called the lateral performant path (LPP) and projections from the medial part of EC (medial entorhinal cortex; MEC) into the MML are called the medial performant path (MMP). Functionally, the LPP carries contextual information and the MPP provides spatial information; in concert, they mediate context distinction according to environmental cues (Umschweif et al., 2019 and references therein).

In contrast, the IML receives inputs from the associational/commissural pathways, which consist mainly of axon fibers from the mossy cells (mossy cell fibers, MCF; Andersen, 2007; **Fig. 1.5**). The associational pathway is the input from the ipsilateral DG and the commissural pathway is the input from the contralateral DG (Yeh et al., 2018 and references therein).

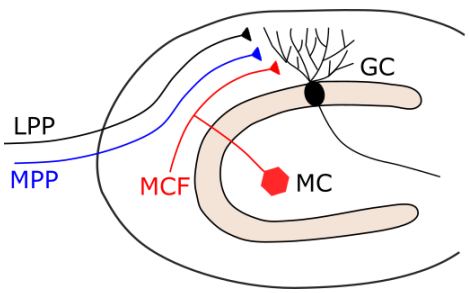

Fig. 1.5. Excitatory synapses from layer II of the entorhinal cortex and the mossy cell onto the granule cell. There are three types of excitatory synaptic inputs: LPP, lateral perforant path; MPP, medial perforant path; MCF, mossy cell fiber. GC: granule cell. MC: mossy cell. Figure adapted from Nozaki et al., 2016 with permission.

B) Mossy cells

As opposed to granule cells, mossy cells (MCs) are more spontaneously active, mainly due to the spontaneous, frequent, often large excitatory postsynaptic potential (EPSP) inputs they receive. Such EPSPs can trigger bursts of action potentials. MCs, however, receive also substantial inhibitory inputs, which become evident when the glutamatergic receptors on MCs

are blocked. Such inhibitory inputs may come from a variety of sources including GABAergic inputs from the medial septum, dentate basket cells, and aspiny hilar interneurons (both ipsilaterally and contralaterally; Andersen, 2007 and references therein.)

Of interest is that MCs are rapidly sensitive to behavioral stress. Moretto and colleagues showed that c-Fos expression in MCs was decreased rapidly after the animal underwent restraint stress. The reduction, however, recovered at a later time, suggesting that MCs could act as novelty detectors to sense environmental changes (reviewed in Scharfman, 2018).

Recently, MCs have attracted attention in the neurogenesis community because it was found that MCs provide the very first glutamatergic input onto adult-born GCs (Chancey et al., 2014). Using optogenetic stimulation, Kumamoto and colleagues showed that GCs receive glutamatergic inputs from MEC and LEC as well as from contralateral MCs at least 14 days after retroviral labeling of newborn GCs (Kumamoto et al., 2012). Similarly, by combining retroviral labeling of newborn GCs with retrograde tracing, Vivar and colleagues showed that newborn GCs receive intra-hippocampus inputs from MCs, interneurons, the CA3 area, and transiently from mature GCs as well as septal cholinergic inputs. Accompanying patch-clamp recordings supported innervation from the LEC rather than from the MEC (Vivar et al., 2012). Functionally, selective lesion of the perirhinal cortex (PRH), LEC, or selective loss of MCs was shown to impair pattern separation, a behavioral task that has been associated with adult-born neurons (Jinde et al., 2012; Vivar et al., 2012).

In contrast, the selective deletion of MCs in calcitonin receptor-like receptor (*Crlr*)-Cre mice treated with the diphtheria toxin did not seem to have any detectable influence on adult neurogenesis as assessed by the number of doublecortin-positive cells and proliferating cell-nuclear antigen (PCNA)-positive cells in the subgranular layer (Jinde et al., 2012).

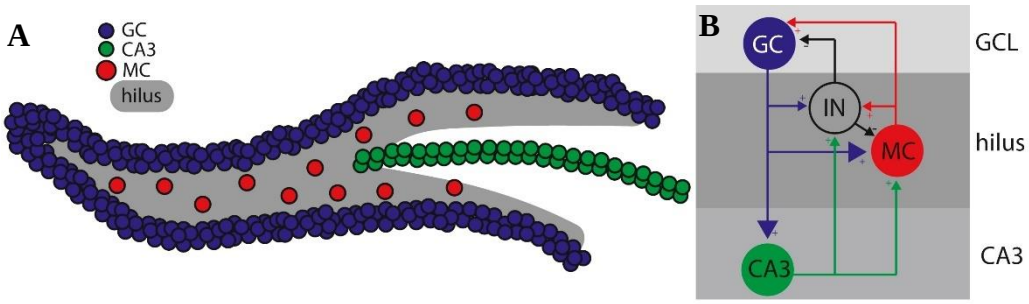

Fig. 1.6. Structure and circuit of the dentate gyrus (DG). (**A**) Schematic of the DG structure, which contains granule cell (GC; blue), mossy cell (MC; red) in the hilus (gray), and the CA3 cells (green). (**B**) Simplified circuit diagram of neurons in the DG. In addition to the cells listed in **A**, an interneuron is involved in this circuitry. Figure from GoodSmith et al., 2017 with permission.

II) Interneurons

In contrast to principal cells, interneurons present a wide diversity and are classified based on the expression of neuropeptides (such as somatostatin, neuropeptide Y, and cholecystokinin [CCK]) or calcium-binding proteins (for example, parvalbumin [PV] or calbindin). Alternatively, interneurons are categorized according to the location of cell bodies and the projection target of axons (**Fig. 1.7**). For example, the cell bodies of HIPP interneurons are in the hilus (HI) and send axons to the perforant path (PP) terminals, HICAP interneurons are associated with the hilar commissural associational path (CAP), and MOPP interneurons possess their cell bodies in the molecular layer (MO) and axons in the PP terminals (Ramaswamy, 2015). For controlling the activity of GCs, two classes of perisomatic GABAergic interneurons play a major role: PV-expressing and CCK-expressing basket cells (BCs). They both exert perisomatic GABAergic inhibition on the activity of GCs. PV neurons are fast-spiking interneurons with high glutamatergic input mediating feedforward inhibition of GCs and regulating theta-gamma oscillations, which are essential mechanisms for the processing functions of the DG (Hu et al., 2014). On the other hand, CCK neurons are regular-spiking interneurons mainly involved in feedback inhibition of GCs. In contrast to PV neurons, CCK neurons are highly modulated by neurotransmitter systems involved in mood disorders, such as the serotonergic and the cholinergic systems. This may indicate that 5-HT and 5-HT-based antidepressants, such as SSRIs, can modulate the function of CCK neurons, although its precise mechanism is still unknown (Medrihan et al., 2017 and references therein).

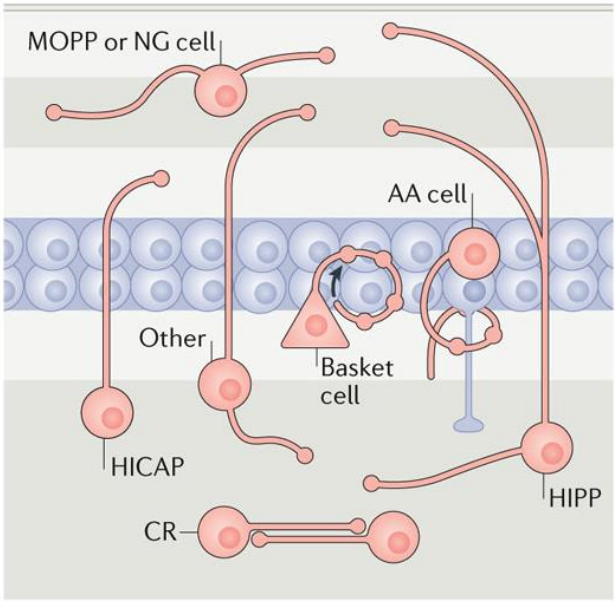

Fig. 1.7. GABAergic interneurons in the dentate gyrus. Their nomenclature is based on the location of the cell body and the axon terminal field. MOPP: interneurons with a cell body in the molecular layer and the projection area in the terminal zone of the perforant path. NG: neurogliaform cell. AA: axo-axonic cell. HICAP: interneurons with a cell body in the hilus and the axon terminal area targeting the commissural/associational pathway. HICAP cells innervate the inner molecular layer, where the commissural/associational projection from mossy cells is located. HIPP: hilar cells that project to the terminal zone of the perforant path. CR: calretinin-expression hilar cells, which innervate each other. Figure from Scharfman, 2016 with permission.

1.5.3. Serotonergic innervation

There are serotonergic (raphe nuclei), noradrenergic (locus coeruleus), dopaminergic (ventral tegmental area), and cholinergic (septal nuclei) inputs into various layers of the DG. In terms of serotonergic inputs, the MRN sends dense plexus of serotonergic fibers and terminates preferentially on GABAergic interneurons which primarily project to the distal dendrites of the GCs, i.e., the serotonergic fibers terminate on fusiform interneurons in the hilus just below the GCL and different types of BCs within the GCL (reviewed in Amaral et al., 2007; Scharfman and Myers, 2012). The suprapyramidal blade was found to be more heavily innervated. A proportion of those interneurons in the hilar region below the GCL was positive for calbindin (particularly fusiform interneurons), but the serotonergic fibers never made contact with interneurons positive for another calcium-binding protein, PV (Halasy et al., 1992). On the other hand, CCK-positive BCs are innervated by serotonergic fibers originating from the MRN. Indeed CCK-positive BCs are found to be enriched with serotonergic receptors. 5-HT_{2A} and 5-HT_{1B} receptors thereby synergistically inhibit CCK cells by inhibiting the excitability and neurotransmitter release, respectively (Leranth and Hajszan, 2007; Umschweif et al., 2019).

On the other hand, a less dense bundle of axons originating from the DRN enters the DG through the EC and projects mainly to the ML. As opposed to MRN axons, which form synapses on the target neurons, DRN afferents rarely form synapses, indicating that its transmission is primarily of the VT type (see 1.2.2. Serotonin release), exerting serotonergic influence in extended, extrasynaptic spaces. The DRN projection site overlaps with that of the LPP, which provides glutamatergic projections to the distal dendrites of the GCs in the OML. This anatomical projection suggests that serotonergic inputs from DRN are more likely to innervate GCs (Umschweif et al., 2019 and references therein). In brain slice recording, it was shown that 5-HT hyperpolarizes GCs via postsynaptic 5-HT_{1A} receptors. On the other hand, glutamatergic transmission onto GCs can be inhibited through presynaptic 5-HT_4 receptors (Kulla and Manahan-Vaughan, 2002; Ciranna, 2006). See also **Fig. 4.1** for schematic explanations.

1.6. Aims of the study

The main aim of the present study was to investigate how brain 5-HT influences proliferation of newborn cells in the DG. To this end, optogenetics and transgenic mice expressing ChR2 in serotonergic neurons were employed in order to specifically activate serotonergic neurons. In addition, electrophysiological experiments were conducted, first to validate the experimental method, and second to investigate neurophysiological actions in the DG in repose to serotonergic activation. Further, since physical activities influence proliferation of cells in the DG, animal behavior was observed during optogenetic stimulation. Thus, the present study's aim can be summarized as follows:

- Validate serotonergic-specific activation in Tph2-ChR2 mice.

For this, both *ex vivo* (= patch-clamp) and *in vivo* electrophysiological recordings were conducted. Patch-clamp recordings have an advantage in that putative serotonergic neurons can be visually identified based on morphological criteria and the anatomical location within the raphe nucleus. Moreover, since the animals used in this study had Tph2-mhChR2-EYFP genes (see Materials and Methods), serotonergic neurons with ChR2 gene expression could be identified based on the presence of fluorescent protein EYFP.

In vivo electrophysiological recordings were conducted under anesthesia to monitor firing activities of putative serotonergic neurons in response to optogenetic stimulation. A special construct called "optetrode" was used to enable simultaneous optogenetic stimulation and electrophysiological recording. For comparison, firings of putative non-serotonergic neurons as well as neuronal activities in ChR2-negative mice were also measured. Compared to *ex vivo* recordings, the *in vivo* recordings were seen here to have more relevance as they are more physiological, for example the behavioral studies conducted *in vivo*.

- Monitor neurophysiological changes in the DG in response to optogenetic stimulation of raphe nuclei.

Here, neuronal activities in the DG of anesthetized mice were measured in response to optogenetic stimulation of serotonergic neurons in the DRN and MRN. To be precise, spontaneously firing neurons in the DG were targeted and the change in their firing rates was assessed. Neurophysiological responses measured here may serve as an explanation for potential changes in cell proliferation in the DG, which will be addressed in the next section.

- **Assess influence of 5-HT on cell proliferation in the DG after overnight and one-week optogenetic stimulation in the raphe nuclei.**

  For this purpose, serotonergic neurons in the raphe nuclei (DRN and MRN) were optogenetically stimulated and cell proliferation in the DG was quantified as the number of BrdU-positive cells. To differentiate acute and long-term effects of serotonergic stimulation, two different stimulation durations, namely overnight and one-week, were chosen. Additionally, with the overnight stimulation, release and metabolism of 5-HT were examined through high-performance liquid chromatography (HPLC). This may allow inferral of a direct correlation between the amount of 5-HT and cell proliferation.

- **Investigate behavioral changes caused by optogenetic stimulation of serotonergic neurons in the raphe nuclei.**

  It has been shown in previous studies by others that physical activities influence cell proliferation in the DG. Especially, the total distances traveled have been shown to serve as an important indicator for cell proliferation. For this reason, behaviors of optogenetically stimulated mice were video recorded overnight, and for 6 nights, to quantify the total running distances in the present study. In addition, peri-stimulus effects of optogenetic stimulation were investigated during the overnight stimulation by analyzing animal behaviors immediately before, during, and immediately after the light stimulation.

2. Materials and Methods

2.1. Animal handling and strains

Animal handling and experiments followed national and institutional guidelines and were approved by the appropriate authorities (Landesamt für Gesundheit und Soziales; LAGeSo) in accordance with the European Communities Council Directive (2010/63/UE). Tph2-mhChR2-EYFP transgenic mice (also referred to as Tph2-ChR2 mice in this thesis) were obtained from The Jackson Laboratory (stock #014555; https://www.jax.org/strain/014555). This BAC transgenic mouse line expresses channelrhodopsin 2/enhanced yellow fluorescent protein – fusion protein (mhChR2::EYFP) under the control of Tph2-promotor (Zhao et al., 2011). The mhChR2 (also called hChR2-H134R) is a mammalian codon-optimized ChR2, which was modified to harbor a gain-of-function H134R substitution and thus designed to cause larger stationary photocurrents compared to ChR2. Animals were housed under a 12 hour-light/dark cycle (lights on: 06:30–18:30) at an ambient temperature of 22 ± 1 ˚C and a relative humidity of 40–50% with *ad libitum* access to food and water.

2.2. Genotyping of mice

Since the mouse strain was maintained by crossing hemizygous mice for the *ChR2* gene with wildtype (noncarrier) mice from the colony (or with C57BL/6J inbred mice), it was necessary to genotype the offspring through the polymerase chain reaction (PCR) to know whether they express the *ChR2* gene.

2.2.1. Tissue digestion and DNA isolation

For mouse genotyping, biopsies of toenail (until postnatal day 7), tail, or ear were collected and put into an autoclaved microcentrifuge tube. Tubes were stored at −20 °C until further use. To isolate genomic DNA, mixture of Ear buffer (**Table 2.1**; 50–100 µl per sample) and proteinase K (1 mg/ml; Invitrogen, Darmstadt, Germany) were dispensed into microcentrifuge tubes. Tubes were then placed in a hot water bath (55 °C) for overnight (c.a. 16–17 hours). Ideally, tubes should be under constant shaking (at 150 rpm) during this procedure to facilitate tissue digestion. On the second day, proteinase K was inactivated by incubating samples at 95 °C for 10 min, while shaking at 150 rpm. Then, 350–750 µl of 1× TE buffer (**Table 2.1**) containing RNase A (20 µg/ml; Promega, Madison, WI, USA) was added to each sample for

RNA digestion. After incubation for 15 min at room temperature, 1 µl of genomic DNA was used as a PCR template. Butter volumes were adjusted to the size of samples.

2.2.2. PCR

Primer sequences for the *ChR2* gene are as follows:

Forward primer:	5'-GCT GAG AAA GAA AAT TAC ATC G-3'
Reverse primer:	5'-GCA AGG TAG AGC ATA GAG GG-3'

Composition of the PCR mixture (for 1 sample) for the *ChR2* gene is as follows:

0.5 µl	Forward primer (10 µM stock)
0.5 µl	Reverse primer (10 µM stock)
1 µl	dNTP mix (10 mM stock; Bioline, Luckenwalde, Germany)
2.5 µl	10× PCR buffer (**Table 2.1**)
1 µl	$MgCl_2$ (50 mM stock)
0.2 µl	*Taq* DNA polymerase (5u/µl; Invitrogen)
18.3 µl	ddH_2O
1 µl	genomic DNA

Samples were kept on ice until transferred to preheated PCR machines. To ensure that the PCR occurred properly, and that samples were not contaminated, genomic DNA of a known genotype (e.g., a ChR2-positive sample from a previous successful PCR) and water (ddH_2O) was taken instead of sample genomic DNA as a positive and negative control, respectively.

The PCR program for *ChR2* gene amplification is shown below:

Cycle 1: (×1)	step 1 (Initial denaturation):	92 °C for 5 min
Cycle 2: (×34)	step 1 (Denaturation):	92 °C for 30 s
	step 2 (Annealing):	55 °C for 30 s
	step 3 (Elongation):	72 °C for 30 s
Cycle 3: (×1)	step 1 (Final elongation):	72 °C for 10 min
	end:	10 °C ∞

To prevent unspecific amplification of DNA fragments, PCR cycles were commenced as soon as possible after adding DNA to PCR mixtures and PCR probes were set into a PCR cycler (PTC-200; Bio-Rad Laboratories, Munich, Germany) only after the cycler was heated up above ~70 °C.

2.2.3. Electrophoresis

5 µl of 10× DNA loading buffer (**Table 2.1**) was mixed with each PCR product and loaded into a well on 2% (w/v) agarose (Biozym, San Diego, CA, USA) gel prepared with 1× TAE buffer (**Table 2.1**) which contains 0.5 µg/ml ethidium bromide (Invitrogen). As a reference, a

base pair (bp) size marker (100 bp ladder; New England Biolabs, Ipswich, MA, USA) was also loaded into a well. Electrophoresis was conducted at 1–8 V/cm in 1× TAE buffer and visualised under a UV transilluminator (300 nm; Alpha Innotech, Santa Clara, CA, USA). Expected bp size for the ChR2-positive genotype is 400 bp, whereas the ChR2-negative genotype has no band in electrophoresis.

Buffer/Solution	Substances	
0.1 M borate buffer	3.08 g	Boric acid
	to pH 8.5	5N NaOH
		Measure up to 500 ml with dd H_2O after adjusting pH
Cryoprotection solution	250 ml	Ethylene glycol
	250 ml	Glycerol
	500 ml	0.1 M PO_4
10× DNA loading buffer	40%	Sucrose
	0.02%	Bromophenol blue (Sigma-Aldrich, Steinheim, Germany)
		Made in 1× TE buffer
Ear buffer	100 mM	Tris (pH 8.5)
	5 mM	EDTA (Sigma-Aldrich)
	0.2 %	SDS (Serva, Heidelberg, Germany)
	200 mM	NaCl
10× PBS	80 g	NaCl
	2 g	KCl
	14.2 g	Na_2HPO_4
	2.4 g	KH_2PO_4
		Measure up to 1 L with ddH_2O (pH 7.4)
1× PBS	dilute 10× PBS ten times with ddH_2O	
10× PCR buffer	500 mM	KCl
	200 mM	Tris-HCl (pH 8.4)
1× TAE buffer	40 mM	Tris-acetate (pH 7.4)
	1 mM	EDTA
10× TBS	88 g	NaCl
	24 g	Tris-HCl
	5.6 g	Tris base
		Measure up to 1 L with ddH_2O (pH 7.6)
1× TBS	dilute 10× TBS ten times with ddH_2O	
1× TE buffer	10 mM	Tris-HCl (pH 8.0)
	1 mM	EDTA

Table 2.1. Buffers and solutions. Self-made buffers and solutions for genotyping and histological studies are listed here. ddH_2O: double-distilled water. EDTA: ethylenediaminetetraacetic acid. PBS: phosphate-buffered saline. TBS: Tris-buffered saline.

2.3. Patch-clamp recordings from brain slices

2.3.1. Preparation of brain slices

Mice (4–6 weeks old; male and female) of the Tph2-mhChR2-EYFP strain (n = 3) were anesthetized with isoflurane and decapitated. The whole head was immediately immersed in modified sucrose-based ice-cold artificial cerebrospinal fluid (sucrose-ACSF) comprising the following (mM): 230 Sucrose; 2.5 KCl; 1.25 NaH_2PO_4; 26 $NaHCO_3$; 10 $MgSO_4$; 0.5 $CaCl_2$; 11 D-Glucose. This solution replaces NaCl in normal ACSF with an equimolar sucrose and increases the ratio of Mg^{2+} to Ca^{2+} in order to improve neuronal viability. The composition minimizes Na^+ and Ca^{2+} ion-associated overexcitability and neurotoxicity during slice preparation and Cl^- ion-associated water influx and subsequent cell swelling (Aghajanian and Rasmussen, 1989; Moyer and Brown, 1998). The sucrose-ACSF was continuously bubbled with a gas composed of 95% O_2 and 5% CO_2 (pH 7.4). Then the brain was rapidly isolated and placed in a Petri dish for dissection, completely submerged by oxygenated, ice-cold, sucrose-ACSF. About one third of the rostral brain and the cerebellum were cut off to leave the block of brain containing the raphe nucleus. The rostral end of this brain block was glued onto the plunger of a specimen tube and installed in a vibratome (Model: VF-310-0Z, Precisionary Instruments, Greenville, NC, USA), whose chamber was filled with ice-cold sucrose-ACSF, bubbled with a gas mixture. Brainstem slices of 200 µm thickness (typically F66–72, corresponding to −4.24 – −4.96 mm from the Bregma, in Mouse Brain Atlas by Paxinos and Franklin, 2001) were made with the vibratome and transferred to a multi-well incubation chamber filled with bubbled ACSF, comprising the following (mM): 124 NaCl; 2.75 KCl; 1.25 NaH_2PO_4; 26 $NaHCO_3$; 1.3 $MgSO_4$; 2 $CaCl_2$; 11 D-Glucose. The ACSF was preheated at 33 ℃ and left at room temperature after slice transfer.

2.3.2. Patch-clamp setup and visualization of neurons

After 30–60 min of recovery time, a single slice was transferred to the recording chamber and perfused with ACSF, which was bubbled and warmed up (29–30 ℃), at the rate of 1.5–2 ml/min. The slice in the recording chamber was secured with a slice grid (commonly called “Harp”; Model: HSG-5F, ALA Scientific Instruments, Farmingdale, NY, USA). Neurons were visualized by a Dodt Gradient Contrast (DGC) tube (Scientifica, Uckfield, UK) and a halogen lamp (Model: TH4-200, Olympus, Tokyo, Japan). For identifying serotonergic neurons indicated by the presence of EYFP fluorescence, green-yellow-red LED light (peak spectrum ca. 570 nm wavelength) was delivered from a pE-300^{ultra} illumination system (CoolLED, Andover, UK) and transmitted through a YFP filter set (Scientifica) to excite

EYFP in brain slices and detect EYFP emission. Visualized images were captured with a SciCam Pro camera (Scientifica) mounted on a SliceScope Pro 6000 upright fixed microscope (Scientifica). Image capture was controlled by Ocular software version 2.0 (Teledyne Photometrics, Birmingham, UK). Patch pipettes were pulled from borosilicate glass capillaries with filament (Model: GC150TF-10; 1.5 mm OD, 1.17 mm ID; Harvard Apparatus, Holliston, MA, USA) using a Smart Pull microelectrode puller (UniPix, Préverenges, Switzerland). Both edges of the glass capillaries were fire-polished in advance, in order to prevent scratching of a Cl-coated silver wire used for electrophysiological recording. The pulled pipettes had a resistance of 3–5 MΩ when filled with the following intracellular (IC) solution (mM): 125 K-gluconate, 5 NaCl, 2 $MgCl_2$, 10 EGTA, 10 HEPES, 2 Na_2ATP (pH 7.2 with KOH, ~280 mmol/kg, filtered by 0.2 µm pore filter; Stuart, 2001). Filling of the glass pipettes was conducted with non-metallic needles (MicroFil™, World Precision Instruments, Sarasota, FL, USA) to prevent contamination of IC solution with ions from metallic surfaces. The pipette was placed in an electrode holder containing the Cl-coated silver wire mounted on the headstage of the amplifier. Slight positive pressure was given to the recoding pipette and lowered into the perfused recording chamber using a PatchStar motorized micromanipulator (Scientifica). Liquid junction potential (any voltage caused by the concentration difference between the bath and the IC solution) was compensated for using "pipette offset" function of the amplifier. Putative serotonergic neurons were first morphologically identified by their large cell bodies (~15–35 µm), whereas non-serotonergic neurons have relatively small cell bodies (~10 µm; Li et al., 2001; Liu et al., 2002). Moreover, serotonergic neurons are most likely to be located along the midline of the raphe nucleus, whereas non-serotonergic neurons are off the midline and rather scattered (Day et al., 2004; Brown et al., 2008). Finally, the serotonergic identity of a neuron was confirmed by the presence of EYFP, although its absence does not necessarily mean a neuron is non-serotonergic since it is known that not all serotonergic neurons express ChR2 in this transgenic mouse line (80–90% expression rate; Zhao et al., 2011).

2.3.3. Electrophysiological recording

The recording patch pipette was lowered under visual guidance onto the surface of the targeted neuron using a fine movement wheel of the micromanipulator. Gigaseal (>1 GΩ resistance) between the pipette and the cell surface was formed when the positive pressure was released, and gentle negative pressure was applied to the pipette. After the Gigaseal was formed, fast and slow capacitance of the patch pipette ("C_p Fast" and "C_p Slow", respectively) were compensated by the auto-compensatory function of the amplifier. The cell membrane

was then ruptured by applying negative suction to establish the whole-cell recoding mode. During the formation of Gigaseal, the holding command potential was gradually reduced and once the whole-cell mode was established, the holding potential was set to −65 mV. After entering the whole-cell configuration, the capacitance of the cell (C_m) was compensated by the auto-compensatory function of the amplifier. Series resistance (R_s) was compensated for when it exceeded around 20 MΩ by adjusting the bandwidth and correction/prediction % on the amplifier. Electrophysiological signals were amplified by a MuliClamp 700B microelectrode amplifier (Molecular Devices, San Jose, CA, USA) and digitized at 10 kHz and low-pass filtered at 4 kHz (Bessel filter) using a Digidata 1550B digitizer (Molecular Devices). Acquired data were analyzed using Clampfit 11.2 (Molecular Devices), NeuroExplorer v5 (Nex Technologies, Colorado Springs, CO, USA), and GraphPad Prism (GraphPad Software, San Diego, CA, USA).

2.3.4. Optogenetic light stimulation

Blue LED light was delivered from a 470 nm LED light source (BLS-FCS-0470-200; Mightex, Toronto, Ontario, Canada) and a BioLED Light Source Control Module (BLS-13000-1E, Mightex). Light was passed through an optic fiber (400 µm core diameter, 0.39 NA, N118L03; Thorlabs GmbH, Bergkirchen, Germany), which was positioned using a micromanipulator above the brain slice (~1 mm away) in the recording chamber. Optogenetic stimulation was triggered by 5 V voltage signals sent from a digital output of the Digidata 1550B digitizer (Molecular Devices) to the analog input of the BioLED Light Source Control Module (Mightex), whose stimulation pattern was controlled by custom-made protocols in the pClamp 11.2 software (Molecular Devices). Pulsed (1–20 Hz, 1–15 ms) or continuous (1 second) light (40 mW [irradiance: 322 mW/mm^2] at the optic fiber tip) was applied to induce inward currents in the voltage-clamp mode from the holding potential set at the resting membrane potential (−65 mV), or action potential firing in the current-clamp mode. In case the patched neurons were tonically active, light-induced action potential firing was monitored either on top of basal firing or after silencing basal firing with the minimal necessary hyperpolarizing current injection (Zhao et al., 2011).

2.4. *In vivo* electrophysiology in anesthetized animals

2.4.1. Optogenetic stimulation and recording in raphe nuclei

I) Construction of optrodes

For optogenetic stimulation and simultaneous electrophysiological recordings of raphe nuclei, electrodes combined with an optic fiber, a construct called “optrode”, was used. Especially when the electrodes were made by bundling four micro wires together, so called “tetrode”, the optrode can alternatively be termed as “optetrode” (Anikeeva et al., 2011). Using optrodes or optetrodes facilitates a precise positioning of electrode/optic fiber in comparison to positioning them separately when electrodes and an optic fiber need to be placed in close vicinity as in the case of raphe recording/stimulation.

First, an optic fiber (200 µm core diameter, 0.66 numerical aperture [NA]; Prizmatix, Holon, Israel) was cut to the appropriate length and fastened with epoxy resin in a 1.25 mm stainless steel fiber optic ferrule (SFLC230-10; Thorlabs GmbH, Bergkirchen, Germany). This was then inserted into one of the 1.25 mm holes on the electronic interface board (EIB; LabMaker GmbH, Berlin, Germany) supplied with the Omnetics connectors (Model A79014-001; Omnetics Connector Corporation, Minneapolis, MN, USA).

Four tungsten microwires insulated with polyimide (12.7 µm diameter; California Fine Wire, Grover Beach, CA, USA) were bundled with a bulldog clip and twisted into a tetrode using a tetrode spinner 2.0 (Neuralynx, Bozeman, MT, USA). Using a heat gun, insulation was melted to keep the wires twisted after the heat was removed. To improve the fixation, twisted tetrodes were further coated with Loctite glue (406/770 Polyolefin glue). The twisted tetrode was cut just above the bulldog clip. Two tetrodes were then directly fixed onto the optical fiber using cyanoacrylate glue. The tips of the glued tetrodes were cut with tungsten-carbide scissors (Cat. No. 14558-09; Fine Science Tools, Heidelberg, Germany) so that the tetrode tips extended ~0.5 mm below the optical fiber. Looped ends of the tetrodes were cut with scissors and threaded into pin holes of the EIB and fixed with gold pins (LabMaker), together with a stainless-steel ground wire (SS-3T/HH; Science Products GmbH, Hofheim, Germany). Fixing gold pins ensured that polyimide insulation on the surface of microwires was removed through friction. The free end of the stainless-steel ground wire was soldered to a small screw (self-tapping bone screw 4 mm; Fine Science Tools), which was to be screwed in the skull of the animal during recording to serve as an electrical ground.

Tetrodes together with an optic fiber were then immersed into colloidal gold solution (Neuralynx) and a driving current of ~50 mA was applied through an impedance meter to electrochemically deposit gold on the tip of tetrodes to lower the impedance of the microwires to ~200–250 kΩ.

II) Electrophysiological recording and optogenetic stimulation

Adult mice (n = 2) were deeply anesthetized with an intraperitoneal (i.p.) injection of urethane (1.5 g/kg body weight; Sigma-Aldrich, Germany) and placed in a stereotaxic apparatus with a warm water circulation platform set at 37 °C (RWD, Shenzhen, China). Craniotomy was conducted either above the DRN or MRN. The optetrode was connected to an optic fiber patch cable (200 µm core diameter, 0.66 NA; Plexon, Dallas, TX, USA) and inserted into either the DRN (AP: −4.60 mm, ML: +1.2 mm at an angle of 23°, DV: −2.88; in mm from the bregma) or MRN (AP: −4.60, ML: +2.0 at an angle of 25°, DV: −4.45; in mm from the bregma). Stereotaxic coordinates are based on Paxinos and Franklin, 2001. Optogenetic stimulation (10–12 mW [318–382 mW/mm^2] at the optic fiber tip) was delivered from a 465 nm PlexBright Table-Top LED Module controlled by a PlexBright 4 channel optogenetic controller (Plexon). For simultaneous electrophysiological recordings, neuronal activity was measured using a OmniPlex D Neural Data Acquisition System with HST/16D Gen2 digital head stages (Plexon). Broadband signals, filtered between 0.10 and 7500 Hz, were continuously acquired at 40 kHz. To extract neuronal spikes, signals were then band-pass filtered at 300–6000 Hz.

III) Electrophysiological data analysis

Spikes were detected using Offline Sorter v4.5.0 (Plexon, Dallas, TX, USA) by placing a negative threshold at 4 standard deviation (SD) from the mean of the peak heights' histogram. Neurons were sorted in the Offline Sorter v4.5.0 (Plexon) by manual clustering using the waveform crossing method. Waveforms and unit clusters in the 3D PCA (principal component analysis) space were visually inspected and spikes which could have derived from noise or artifacts were manually invalidated. All the channels with SNR (Signal-to-Noise Ratio) less than 4 were excluded from further analysis. Furthermore, it was ensured that none of the analyzed units contained >0.5% of events with interspike intervals below the refractory period of 1.2 ms (Hill et al., 2011; Zhang et al., 2018). Extracellularly recorded spike waveforms were inverted using the Offline Sorter in order to reflect the actual changes in the membrane potential of neurons. Putative serotonergic neurons and non-serotonergic neurons

were differentiated according to their electrophysiological characteristics (Araragi et al., 2013 and references therein). Serotonergic neurons typically have a wider action potential width, an asymmetric action potential up-to-down stroke ratio, and a lower and steady firing rate (typically <5 Hz). Non-serotonergic neurons, on the other hand, have a narrower action potential width, a symmetric action potential up-to-down stroke ratio, and a higher and somewhat varying firing rate. All the sorted spike data were analyzed and visualized using NeuroExplorer v5 (Nex Technologies, Colorado Springs, CO, USA) and GraphPad Prism (GraphPad Software, San Diego, CA, USA).

2.4.2. Optogenetic stimulation in raphe nuclei and recording in the DG

I) Electrophysiological recording and optogenetic stimulation

Adult mice (n = 13) were deeply anesthetized with an intraperitoneal (i.p.) injection of urethane (1.5 g/kg body weight; Sigma-Aldrich, Germany) and placed in a stereotaxic apparatus with a warm water circulation platform set at 37 °C (RWD, Shenzhen, China). Craniotomy was conducted either above the DRN or MRN. An optic fiber (400 µm core diameter, 0.39 NA, N118L03; Thorlabs GmbH, Bergkirchen, Germany) was inserted into the DRN (AP: −4.60, ML: +1.2 at an angle of 23°, DV: −2.88; in mm from the bregma) or MRN (AP: −4.60, ML: +2.0 at an angle of 25°, DV: −4.45; in mm from the bregma). Stereotaxic coordinates were based on Paxinos and Franklin, 2001. Optogenetic stimulation (15–20 mW [119–159 mW/mm^2] at the optic fiber tip) was delivered from a 465 nm PlexBright Table-Top LED Module (Plexon, Dallas, TX, USA) controlled by a PlexBright 4 channel optogenetic controller (Plexon) or from a 470 nm LED light source (BLS-FCS-0470-200; Mightex, Toronto, Ontario, Canada), which was controlled by a BioLED Light Source Control Module (BLS-13000-1E, Mightex) and a BioLED Analog/Digital Input and Output Control Module (BLS-IO04-US, Mightex). For simultaneous electrophysiological recordings, a multi-electrode array (4 × 4 fixed arrays, 35 µm diameter tungsten electrodes, 150 × 150 µm spacing, 4 mm or 6 mm length; Innovative Neurophysiology, Durham, NC, USA) or a silicon probe (16-channel E-2 probe; Cambridge NeuroTech, Cambridge, UK) was inserted into the DG (AP: −2.06, ML: −1.5, DV: −2.0; in mm from the bregma). Neuronal activity was measured using OmniPlex D Neural Data Acquisition System with HST/16D Gen2 digital head stages (Plexon). Broadband signals, filtered between 0.1 and 7500 Hz, were continuously acquired at 40 kHz. To extract neuronal spikes, signals were then band-pass filtered at 300–6000 Hz. Spikes were detected using the Offline Sorter v4.5.0 (Plexon) by placing a negative threshold at 4 SD from the mean of the peak heights' histogram.

For post-mortem histological verification of recording sites in the hippocampus (**Fig. 3.9A**), multi-channel electrodes were coated with a red fluorescent dye, 1,1-dioctadecyl-3,3,3,3-tetramethylindocarbocyanine perchlorate (ABD-22102, DiI perchlorate; Biomol GmbH, Hamburg, Germany; 80 mg/ml in isopropyl alcohol) and air dried for 30 minutes before insertion. After recording, the mouse brain was removed and fixed in 4% paraformaldehyde (PFA; Otto Fischar GmbH & Co. KG, Saarbrücken, Germany) at least overnight. The fixed brain was then cut with a vibratome (Model: VF-310-0Z, Precisionary Instruments, Greenville, NC, USA), whose chamber was filled with 1× phosphate-buffered saline (PBS; **Table 2.1**). Brain slices of 40–50 µm thickness were made with the vibratome and mounted on glass slides using VECTASHIELD® HardSet™ Antifade Mounting Medium with the 4', 6-diamidino-2-phenylindole (DAPI) nuclear counterstain (blue fluorescence; Cat. No. H-1500; Vector Laboratories, Newark, CA, USA). Images were taken on a fluorescent microscope (BZ-9000; Keyence, Osaka, Japan).

II) Spike sorting

Spike sorting was conducted using Offline Sorter v4.5.0 (Plexon, Dallas, TX, USA). Spikes were first sorted using the valley seeking scan method by varying a Parzen multiplier from 0.5 to 1.5 at increments of 0.2. Waveforms and unit clusters in the 3D PCA (principal component analysis) space were visually inspected and spikes which could have derived from noise or artifacts were manually invalidated. All the channels with SNR less than 3 were excluded from further analysis. To ensure clear separation of a unit from all the other noise clusters, units with an isolation distance greater than 15 and L-ratio less than 0.35 were accepted (Schmitzer-Torbert et al., 2005; Watson et al., 2014). Furthermore, it was ensured that the percentage of spikes with interspike intervals below the refractory period (1.2 ms) should not exceed 0.5% within a unit (Hill et al., 2011). All the sorted spike data were analyzed and visualized using NeuroExplorer v5 (Nex Technologies, Colorado, USA) and GraphPad Prism (GraphPad Software, San Diego, CA, USA).

III) Action potential shape analysis and burst analysis

Half-peak and trough-to-peak widths of action potentials were measured using Clampfit 11.2 software (Molecular Devices, San Jose, CA, USA). First, action potential traces were displayed in Clampfit, and the baseline potential was defined as a steady potential before the action potential threshold. Then, the polarity of peak action potential was set as positive going. With this setting, the half-peak width was measured as a half-height width (HHW) of the positive-going peak. Trough-to-peak width was measured as a distance between peak and anti-peak of an action potential (Medrihan et al., 2017; **Fig. 2.1**).

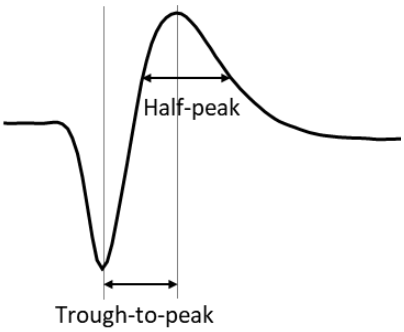

Fig. 2.1. Half-peak and trough-to-peak widths of an action potential.

To visualize the tendency of a neuron for discharging action potentials, an auto-correlogram (ACG) of a neuron was first created with 1 ms bins, using NeuroExplorer v5 (Nex Technologies, Colorado, USA). Then a burst index (BI) was calculated based on the following formula,

$$BI = \frac{Peak - Baseline}{Peak} \qquad if \quad Peak > Baseline$$

$$BI = \frac{Peak - Baseline}{Baseline} \qquad if \quad Baseline > Peak$$

where Baseline = the mean firing rate between 40–50 ms in ACG and Peak = the peak firing rate between 0–10 ms in ACG. The BI therefore ranges from −1 (tonically firing) to 1 (bursting; Fujita et al., 2014).

2.5. Optogenetic stimulation in freely behaving mice

2.5.1. Optic fiber implantation

Young adult female mice (age: 6–8 weeks) were anesthetized with an intraperitoneal (i.p.) injection of ketamine (100 mg/kg body weight; Ketavet®, Pfizer Deutschland GmbH, Berlin, Germany) and xylazine (10 mg/kg body weight; Rompun®, Bayer, Leverkusen, Germany). The deepness of anesthesia was controlled by tail-pinch. The scalp was shaved and disinfected with 70% isopropyl alcohol and 4% chlorhexidine digluconate (diluted from 20% solution; Caesar & Loretz GmbH, Hilden, Germany). The mouse was placed on an electric or warm water heating plate (37 °C) in a stereotaxic frame and its head was fixed. Eyes were covered with Bepanthen (Bayer) or Visc-Ophtal (Dr. Robert Winzer Pharma GmbH, Berlin, Germany) to protect them from dryness. The scalp was incised along the midline and kept open with a retractor. The skull was then wiped with 3–6% H_2O_2 to form micropores (Ung and Arenkiel, 2012). The skull was drilled at three positions and small screws (self-tapping bone screws 4 mm; Fine Science Tools, Heidelberg, Germany), which serve as anchors for dental cement, were screwed in. Then craniotomy was conducted either above the DRN or MRN. An optic fiber ferrule (self-made from a high NA optic fiber for DIY optogenetic implants, 200 µm core diameter, 0.66 NA, Prizmatix, Holon, Israel and a stainless steel fiber optic ferrule, SFLC230-10, Thorlabs GmbH, Bergkirchen, Germany) was inserted into the DRN (AP: −4.60, ML: +1.2 at an angle of 23°, DV: −2.88; in mm from the bregma) or the MRN (AP: −4.60, ML: +2.0 at an angle of 25°, DV: −4.45; in mm from the bregma). All the stereotaxic coordinates are based on Paxinos and Franklin, 2001. The optic fiber ferrule was then fixed with dental cement (Vertex Self-Curing Acrylic Powder, Shade: 8 [blue-pink] and Vertex Self-Curing Acrylic Liquid; Vertex Dental, Soesterberg, the Netherlands) on the skull. In order to prevent visually triggered locomotive enhancement caused by light emittance from the dental cement, the self-curing acrylic power was mixed with carbon powder (20% w/w in powder mix, end weight after hardening ca. 0.5 g; Sigma-Aldrich, Munich, Germany; Araragi et al., 2022), which made the dental cement black and thus impenetrable to light leakage. Intraoperatively and on the first postoperative day, mice were subcutaneously injected with carprofen (5 mg/kg body weight; Rimadyl®, Pfizer Deutschland) to minimize pain. In addition, bupivacain 0.25% (diluted from 0.5% solution; Jenapharm, Jena, Germany) was applied on the wound as a local analgesic. The animals recovered from an operation on a warmed plate until the effect of anesthesia had disappeared. All the animals were single caged after the operation to prevent manipulation and damage to the implanted optic fiber ferrules

by inmates. Control animals (Ctrl; ChR2-positive mice without light stimulation) underwent the same operation as the stimulated group.

2.5.2. Optogenetic light stimulation

One week after the surgery, mice were placed separately in Plexiglas cages (37.5 × 21.5 cm). Implanted optical fiber ferrules were connected to optical patch cables, which were in turn connected to PlexBright Compact LED Modules (Plexon, Dallas, TX, USA) attached on PlexBright motorized carousels (Plexon). Optical patch cables for DRN stimulation and control experiments were self-made using bare optical fibers (200 µm core diameter, 0.66 NA; Prizmatix, Holon, Israel) and heat-shrinkable rubber tubes. Optical patch cables for MRN stimulation and control experiments were purchased (200 µm core diameter, 0.66 NA, stainless steel mono-coil wrap reinforcement; Plexon). To minimize light emission in the free space, connections between ferrules and patch cables were achieved using metal sleeves (Prizmatix). Light stimulation (465 nm) was driven by a PlexBright 4 channel Optogenetic controller (Plexon). Overnight stimulations (10 mW [318 mW/mm^2] at the optic fiber tip, 20 Hz, 15 ms pulse) were applied every 5 min for the duration of 30 s starting at 0:00 over 8 hours. As an age-matched control group, the same mouse line without light stimulation was used. To analyze cell proliferation in the hippocampus, the animals received an i.p. injection of bromodeoxyuridine (BrdU; 50 mg/kg body weight dissolved in 0.9% NaCl; Sigma-Aldrich, Germany) immediately after optogenetic light stimulation and were killed 2 hours later.

For one-week stimulations of DRN, two different stimulation patterns were used: 1) 5 mW, 8 Hz, 5 ms pulse or 2) 10 mW, 20 Hz, 15 ms pulse. Stimulations were applied every 5 min for the duration of 30 s starting at 20:00 over 8 hours until 4:00 of the following day. This was repeated for 6 nights. As an age-matched control group, the same mouse line without light stimulation was used. On the last day of stimulation, animals received an i.p. injection of BrdU (the same dose as by overnight stimulation) 3 times, 6 hours apart (8:00, 14:00, 20:00) and were sacrificed 12 hours after the last injection.

The above-mentioned experimental schemes are summarized in **Fig. 2.2**.

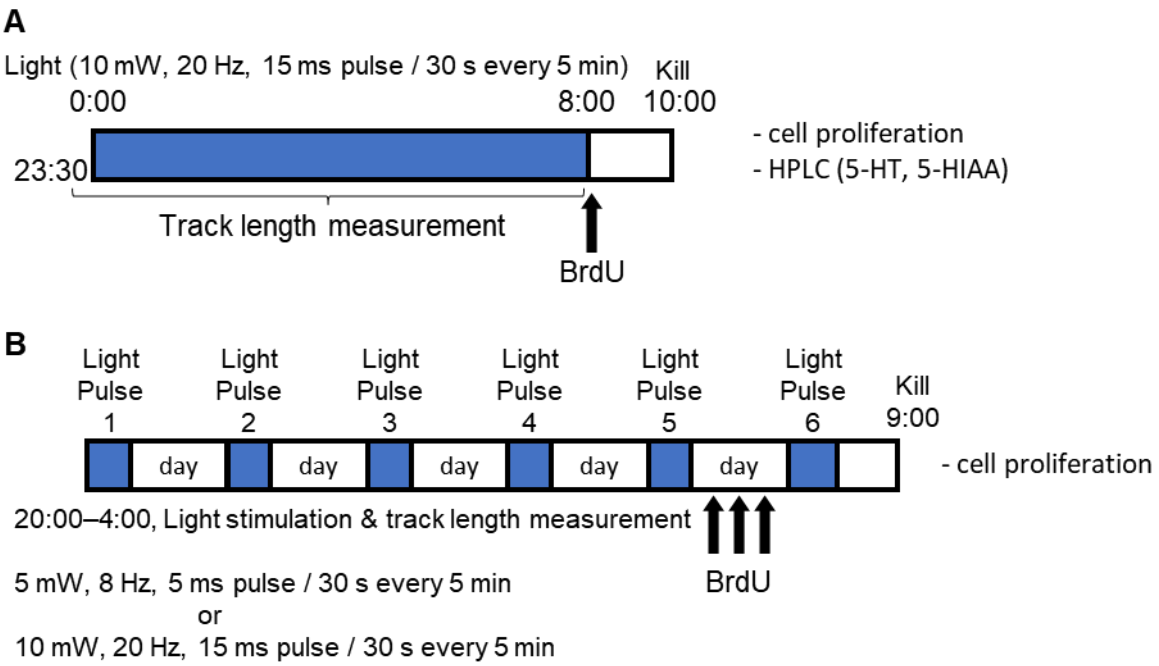

Fig. 2.2. Experimental schemes. (**A**) Experimental scheme of overnight stimulation of raphe nuclei. Light pulses were given every 5 min for the duration of 30 s starting at 0:00 over 8 hours. Mice received one BrdU injection when light activation was stopped and were perfused 2 hours later. (**B**) Experimental scheme of daily light stimulation of DRN for 6 nights. Light pulses were given every 5 min for the duration of 30 s starting at 20:00 over 8 hours until 4:00 of the following day. Mice received 3 injections of BrdU, 6 hours apart on day 5.

2.6. Behavioral analysis

2.6.1. Experimental setup and general conditions

Animal behaviors were recorded using CinePlex Behavioral Research System (Plexon, Dallas, TX, USA) under IR light (Model: MIRA II, Franz Video-Equipment, Winterhausen, Germany). Images were captured in 640 × 480 format in 30 fps. For the overnight stimulation groups, video recording was conducted from 23:30 until 8:00 on the following day. For the one-week stimulation groups, video recording was conducted from 20:00 until 4:00 on the following day and this was repeated for 6 nights. Mouse movements in pre-recorded videos were tracked and analyzed with ViewerII software (Biobserve GmbH, Bonn, Germany) at every third frame.

2.6.2. Cumulative track length

I) Overnight stimulation

Traveled track lengths were measured from the whole session (23:30–8:00) and averaged values at every 30s were obtained. Obtained track lengths were then converted into cumulative values in GraphPad Prism (GraphPad Software, San Diego, CA, USA). Data from the Ctrl group were analyzed in the same way. Data from the stimulated (Stim) groups were normalized to the respective Ctrl group within DRN and MRN experimental groups.

II) One-week stimulation

Traveled track lengths were measured from the whole session (20:00–4:00) and the total distances traveled were measured per night. Cumulative track length curves for 6 nights were generated by adding up the average total distances traveled per night and per experimental group, i.e., Ctrl vs. Stim. To statistically compare the total distances traveled between the Ctrl and Stim groups, the area under the curve was calculated using GraphPad Prism (GraphPad Software). Data from the Ctrl group were analyzed in the same way.

2.6.3. Peri-stimulus behavioral changes

Peri-stimulus behavioral changes were analyzed only for the overnight stimulation group. Peri-stimulus changes in velocity, activity, ambulation, zone crossing (ZC), rated zone crossing (RZC), and wall distance were calculated during 30 s blocks of pre-stimulation, stimulation, and post-stimulation at every 5-minute interval (Araragi et al., 2022). The values were normalized by subtracting pre-stimulation values at each stimulation within the same animal. Only peri-stimulus behavioral data obtained from after optogenetic light stimulation started until the room light was turned on (0:00–6:30) were analyzed. Data from the Ctrl group were analyzed in the same way. Activity was scored when the animal moved at least 1.00 cm per second. Ambulation is defined as a spontaneous short-term acceleration, recognized when the animal's velocity changes suddenly from inactivity to beyond 1.5 cm/s within three successive video frames. ZC was calculated by dividing an animal cage into virtual 3 × 3 cm grids and the number of line crossing events was scored. In contrast to ZC, RZC implements a rating that emphasizes linear movement and dismisses small-scale locomotion. To calculate RZC, each line crossing is weighted by a discrete factor between zero and four (see the formula below). The factor is calculated by looking at the last three line-crossings, of which the distances from the first two to the last are summed up. Distances

are expressed as the number of line crossings necessary to get from the starting zone to the final zone. Finally, one count is subtracted. Track oscillations at only one zone's margin are thus leveled to zero. Wall distance measures the positions of the animal body to the nearest wall at any time of the experiment (for all the details of behavioral parameters, see Viewer manual).

RZC weight factor: $\sum_{n=1}^{n} \overline{(N_{(n+1)},\ N_{(n+3)})} + \overline{(N_{(n+1)},\ N_{(n+4)})} - 1$

2.7. Immunohistochemistry and quantification

The mice were deeply anesthetized and transcardially perfused with 0.9% NaCl followed by 4% PFA (Otto Fischar GmbH & Co. KG, Saarbrücken, Germany). Brains were removed from the skulls, postfixed in 4% PFA at 4 °C overnight, and transferred to 30% sucrose. Sequential 40 µm coronal sections were cut on a microtome and kept in cryoprotection solution (**Table 2.1**) for long-term storage. For BrdU staining, DNA was denatured in 2N HCl for 20 min at 37 °C. Sections were rinsed in 0.1 M borate buffer (**Table 2.1**) and washed in 1× Tris-buffered saline (TBS; **Table 2.1**). Sections were stained free-floating with antibodies diluted in 1× TBS containing 3% donkey serum and 0.1% Triton X-100. Immunohistochemistry for BrdU followed the peroxidase method with biotinylated secondary antibody (Donkey Anti-Rat Biotin, 1:500; Jackson ImmunoResearch Laboratories, West Grove, PA, USA), ABC Elite reagent (Vector Laboratories, Newark, CA, USA), and di-aminobenzidine (DAB; Vector Laboratories) as chromogen. For quantification, one-in-six series of sections of each brain were BrdU stained for light microscopy, and immunoreactive cells were counted throughout the rostro-caudal extent of the DG. Results were multiplied by six to obtain the total number of BrdU-positive cells per DG.

The laterality index of the number of BrdU-positive cells in brain slices obtained after one week of DRN stimulation was calculated as follows: Since the ipsilateral and contralateral hemispheres in relation to the implanted optic fiber ferrules were not marked on the brain slices obtained from mice after 8 Hz stimulation, the lower number of BrdU-positive cells in one hemisphere was divided by the higher number in the other hemisphere. For the 20 Hz stimulation, the number of BrdU-positive cells in the ipsilateral side was divided by the number in the contralateral side.

2.8. HPLC

Another set of animals (n = 5 each for the control and light-stimulated group) was used for HPLC analysis after overnight optogenetic light stimulation. Animals were deeply anesthetized with an i.p. injection of ketamine/xylazine (100/10 mg/kg body weight) and subsequently perfused transcardially with 0.9% NaCl. Brains were removed, weighed, and snap-frozen on dry ice. Frozen brain tissue was homogenized in lysis buffer containing 10 µM ascorbic acid and 1.8% perchloric acid, and deproteinized by centrifugation for 30 min at 20,000 × g and 4 °C (Klempin et al., 2018). Tissue levels of Trp, 5-HT, and 5-HIAA were analyzed using high-sensitive HPLC with fluorometric detection (Shimadzu, Tokyo, Japan) and normalized to wet tissue weight for statistical analysis.

2.9. Experimental design and statistical analysis

Data are expressed as the mean ± SEM unless otherwise stated. Group differences were tested by unpaired *t* test unless otherwise stated. Data from DRN and MRN groups (controls and stimulated) were treated separately and not compared with each other. All the statistical tests were performed by GraphPad Prism (GraphPad Software, San Diego, CA, USA). In all cases, $p \leq 0.05$ was considered statistically significant and indicated by stars as follows: *$p \leq 0.05$; **$p \leq 0.01$; ***$p \leq 0.001$; ****$p \leq 0.0001$. P value of $0.05 < p \leq 0.10$ was considered a trend of significance.

3. Results

3.1. Patch-clamp recordings from raphe brain slices

3.1.1. Putative serotonergic neurons can be identified by their cell size and the presence of EYFP

To confirm the validity of the experimental animal model (Tph2-mhChR2-EYFP mice) used in this study, the slices obtained for patch-clamp recordings were first checked for their EYFP expression under the microscope. As shown in **Fig. 3.1D**, clear EYFP expression was observed in a group of neurons in the DRN and MRN. Under high magnification (**Fig. 3.1E**–**F**), neurons which do not express EYFP corresponded to the morphology of non-serotonergic neurons, characterized by their small cell bodies (~10 µm in **Fig. 3.1E, E'**). Although there were variations in the level of EYFP (i.e., ChR2) expression, the neurons expressing EYFP are tendentially bigger (~20 µm in **Fig. 3.1F**) than those without EYFP expression, indicating that EYFP is selectively expressed in serotonergic neurons. Some of the recorded serotonergic neurons identified by their EYFP expression also showed the clock-like slow and regular spontaneous firings typical of serotonergic neurons. The presence of spontaneous firings seems to depend on the availability of noradrenergic inputs in brain slices, which drive spontaneous firings *in vivo* (Levine and Jacobs, 1992).

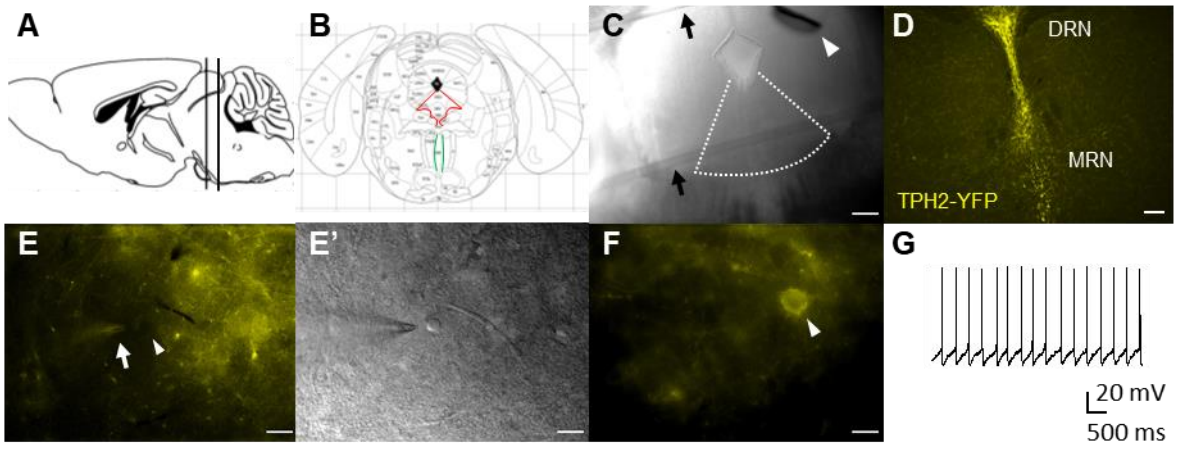

Fig. 3.1. Patch-clamp recordings obtained from dorsal raphe brain slices. (**A**) Slices were typically obtained from the region located at −4.24 – −4.96 mm from the bregma in the mouse brain atlas (Paxinos and Franklin, 2001), which is demarcated by two vertical lines. (**B**) Illustration of the brain slice containing raphe nuclei. The dorsal raphe nucleus (DRN) and the median raphe nucleus (MRN) are demarcated by the red and green lines, respectively. Shown here is the slice obtained at −4.60 mm from the bregma. Grid lines are spaced at 1 mm distance. (**C**) Brain slice containing the DRN (its approximate position is demarcated by dotted lines). The slice is placed in a perfused recording chamber and secured by a slice anchor of which the wires can be seen in the image (arrows). An optic fiber (arrowhead) is placed in the vicinity of the slice. Scale bar: 200 µm. (**D**) Fluorescent image of a slice containing the DRN and the MRN. Serotonergic neurons which express channelrhodopsin 2 (ChR2) are marked by enhanced yellow fluorescent protein (EYFP). Scale bar: 100 µm. (**E**) Putative non-serotonergic neuron (arrowhead) expressing no ChR2 (and thus no EYFP). Patch pipette (arrow) with positive pressure is positioned near the cell to clear away the surrounding materials. (**E'**) The same image as in **E**, obtained by the Dodt contrast method. (**F**) Putative serotonergic neuron (arrowhead) expressing a high level of ChR2, which can be identified by strong EYFP expression. (**E–F**) Scale bar: 20 µm. (**G**) Spontaneous firing of a serotonergic neuron recorded in the current clamp mode. Its firing is characterized by slow and regular firing patterns.

3.1.2. Optogenetic stimulation specifically activated serotonergic neurons

Subsequently, *ex vivo* electrophysiological recordings in the DRN were conducted to see whether optogenetic stimulation specifically activates serotonergic neurons. A putative serotonergic neuron identified morphologically and by the presence of EYFP protein showed prompt and reliable one-to-one responses to optogenetic stimulation with increasing frequencies both in the current clamp mode (**Fig. 3.2A**, left) and in the voltage clamp mode (**Fig. 3.2B**, left). In response to 1 s continuous light stimulation, the neuron showed sustained inward current (photocurrent) in the voltage clamp mode (**Fig. 3.2C**, top) or sustained action potential firings in the current clamp mode (**Fig. 3.3A**, left). Interestingly, the serotonergic neuron in response to 1 s continuous light stimulation in the current clamp mode displayed an

almost identical response to 20 Hz pulsed light stimulation (**Fig. 3.2A**, left panel, bottom), indicating that serotonergic neurons can fire up to this frequency. A putative non-serotonergic neuron identified morphologically and by the absence of EYFP fluorescence showed no detectable responses to pulsed or continuous light stimulation in both the current clamp mode (**Fig. 3.2A**, right; **Fig. 3.3A**, right). and the voltage clamp mode (**Fig. 3.2B**, right; **Fig. 3.2C**, middle). The same neuron, however, responded to 1 s continuous 100 pA current injection with repeated action potential firings (**Fig. 3.3B**, right***)***, confirming that the lack of responses to light stimulation was not due to some artifact, e.g., death of the recorded neuron. The amount of photocurrent in response to 1 s continuous light stimulation was significantly different between putative serotonergic neurons and non-serotonergic neurons (**Fig. 3.2C** bottom; non-serotonergic vs. serotonergic, −0.23 ± 3.50 vs. −124.1 ± 33.46, $t_{(10.22)} = 3.682$, $p = 0.0041$, unpaired *t* test with Welch-correction for unequal variances; n = 8 and 11, respectively).

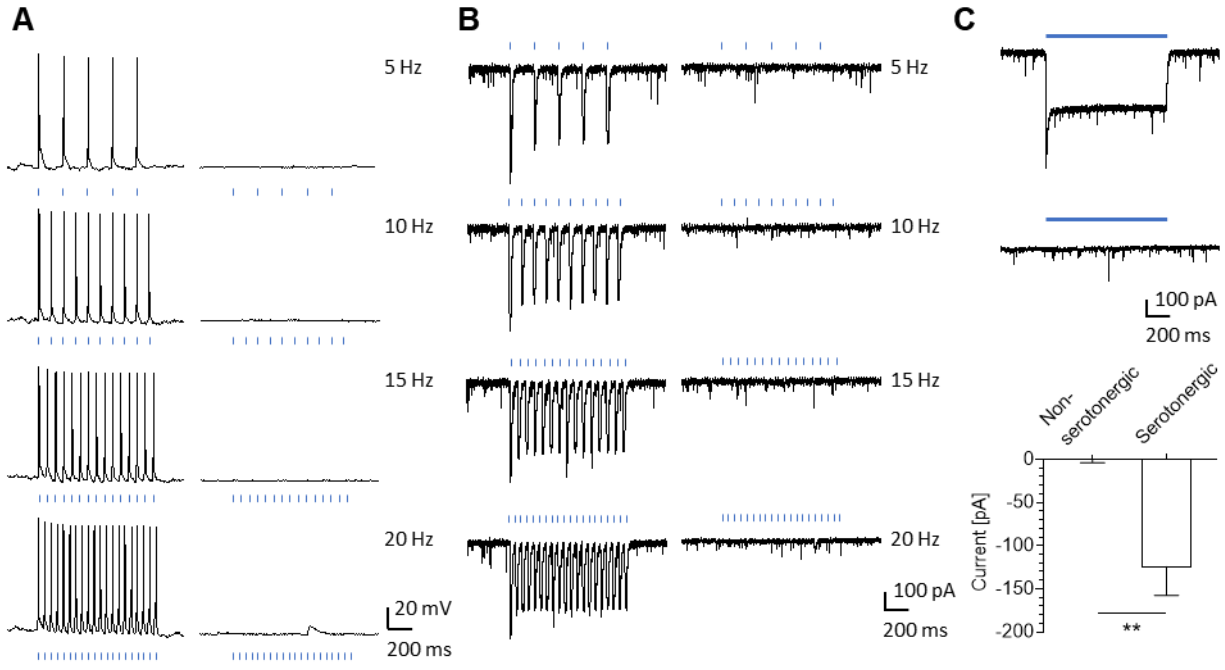

Fig. 3.2. Patch-clamp recordings obtained from dorsal raphe brain slices in response to optogenetic stimulation. (**A**–**B**) Optogenetically induced action potentials recorded in the current clamp mode (**A**) or inward current (photocurrent) recorded in the voltage clamp mode (**B**). Putative serotonergic (left panel) and non-serotonergic (right panel) neuron. (**C**) Photocurrent in response to 1 s continuous blue light stimulation recorded in the voltage clamp mode. Response of a putative serotonergic neuron (top) and non-serotonergic neuron (middle). The amount of photocurrent between serotonergic (n = 11) and non-serotonergic (n = 8) neurons was significantly different (bottom). $^{**}p \leq 0.01$, unpaired *t* test. Data are presented as mean + SEM.

Action potentials collected in response to current injection showed recognizable shape differences between the recorded serotonergic (**Fig. 3.3C**, up) and non-serotonergic (**Fig. 3.3C**, down) neurons, which correspond to previous reports (Vandermaelen and Aghajanian, 1983; Asaoka et al., 2017; Hernández-Vázquez et al., 2019). Namely, that serotonergic neurons have a wide action potential (typically ~2–4 ms) with a slight inflexion or 'shoulder' in the repolarizing phase due to a Ca^{2+} entry, a prominent asymmetric upstroke-to-downstroke ratio, and a long-lasting afterhyperpolarization. Non-serotonergic neurons, e.g., GABAergic interneurons, have narrower action potential widths (~1.5 ms) without a shoulder in the repolarizing phase. Specific activation of serotonergic neurons by blue light was observed in recordings in the MRN as well (data not shown). In sum, the data demonstrated that serotonergic neurons in the raphe nuclei of the model organism can be specifically activated by blue light stimulation, while non-serotonergic neuron activities were unaffected.

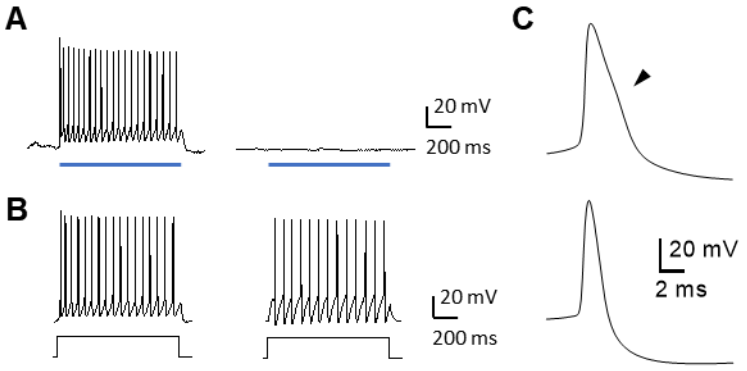

Fig. 3.3. Patch-clamp recordings obtained from dorsal raphe brain slices in response to optogenetic stimulation and current injection. (**A**–**B**) Current clamp recordings in response to 1 s continuous light stimulation (**A**) and 1 s 100 pA current injection (**B**). Putative serotonergic (left) and non-serotonergic (right) neuron. (**C**) Averaged action potential shapes (excluding first few spikes), obtained from responses in **B**. Putative serotonergic neuron (up, corresponding to **B** left; HHW = 2.7 ms) and non-serotonergic neuron (down, corresponding to **B** right; HHW = 1.5 ms). Arrowhead: a shoulder in the repolarizing phase. HHW: Half-Height-Width of the action potential.

3.1.3. Wider light pulses increase the chance of eliciting action potentials

The pulsed light stimulation presented above used a pulse width of 15 ms. To show that this width was appropriate, patched serotonergic neuron was illuminated with blue light at increasing pulse widths both in the current clamp (**Fig. 3.4A**) and in the voltage clamp (**Fig. 3.4B**) mode. As shown here, pulsed light partially failed to elicit action potentials in the current clamp mode when the pulse width was below 15 ms. Only when the pulse width was as long as 15 ms, reliable one-to-one responses to pulsed light stimulation were observed. In

the voltage clamp mode, temporally reliable one-to-one responses were observed regardless of the pulse width, although inward current in response to 1 ms pulse stimulation was noticeably smaller than other pulse widths. By other pulse widths, the amplitudes of inward currents were more or less similar, but the width of inward currents increased as the pulse width increased. This indicates that in response to wider light pulse widths, the amplitude and/or the width of inward currents also increases, enhancing the chance that light pulses can successfully trigger action potentials by driving membrane potential to the action potential threshold.

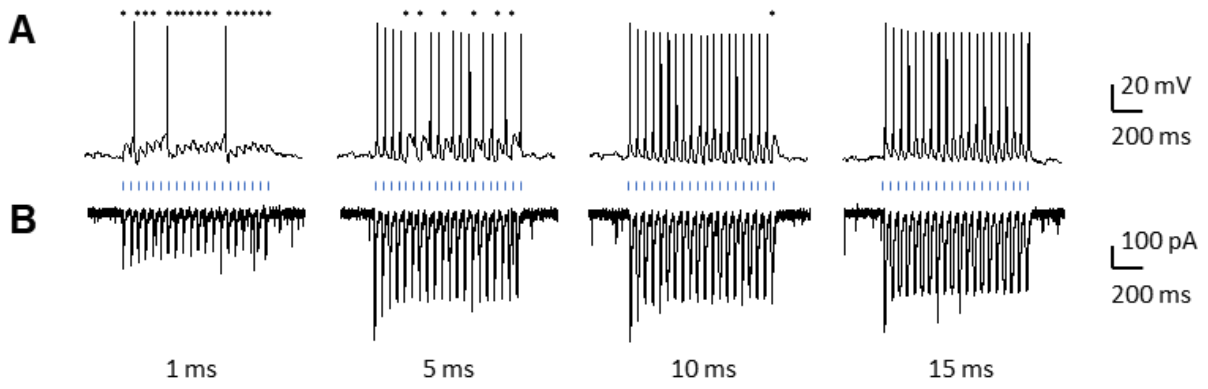

Fig. 3.4. Patch-clamp recordings in response to pulsed optogenetic stimulation with increasing pulse widths. (**A**) Current clamp recordings. Blue ticks indicate light pulses. Note that they are depicted at the same widths in the figure. The actual pulse widths are shown at the bottom. Shorter pulse widths are more likely to fail in eliciting action potentials. Asterisks (*) indicate missed action potentials. (**B**) Same recordings in the voltage clamp mode.

3.2. *In vivo* recordings from anesthetized animals

3.2.1. Optogenetic stimulation specifically activates serotonergic neurons

To confirm the validity of the experimental model (Tph2-mhChR2-EYFP mice), *in vivo* extracellular electrophysiological recordings were first conducted in the DRN to see whether optogenetic stimulation specifically activates serotonergic neurons. A spontaneously active putative serotonergic neuron (**Fig. 3.5**) promptly responded to optogenetic stimulation with increasing frequencies (**Fig. 3.6A**). At higher stimulus frequencies (>15 Hz), the neuron started to fail in following individual light stimuli, which resulted in single drops in frequency as shown in the instantaneous firing frequency plots. It should be noted that the shape of action potentials detected during the light stimulation (**Fig. 3.6A**) was identical to that detected at baseline (**Fig. 3.5**), confirming that the observed reactions to light stimuli were not

caused by optically induced electrical artifacts (Cardin et al., 2010). To note is also that the brief negative deflection at the start of the action potential waveforms (**Fig. 3.5**, **Fig. 3.6A**) is attributed to the capacitive current of the cell membrane and its occurrence in recordings depends on the position of the recording electrodes (Gold et al., 2006). Contrarily, a putative non-serotonergic neuron did not respond to light stimulation (**Fig. 3.6B**). Similar results were obtained from recordings in the MRN (data not shown). In sum, serotonergic neurons in the raphe nuclei of the model organism were specifically activated by blue light stimulation, while non-serotonergic neuron activities were unaffected. Together with the results derived in the previous section, serotonergic specific activation by blue light could be confirmed both under *ex vivo* and *in vivo* conditions (see 3.1. Patch-clamp recordings from raphe brain slices).

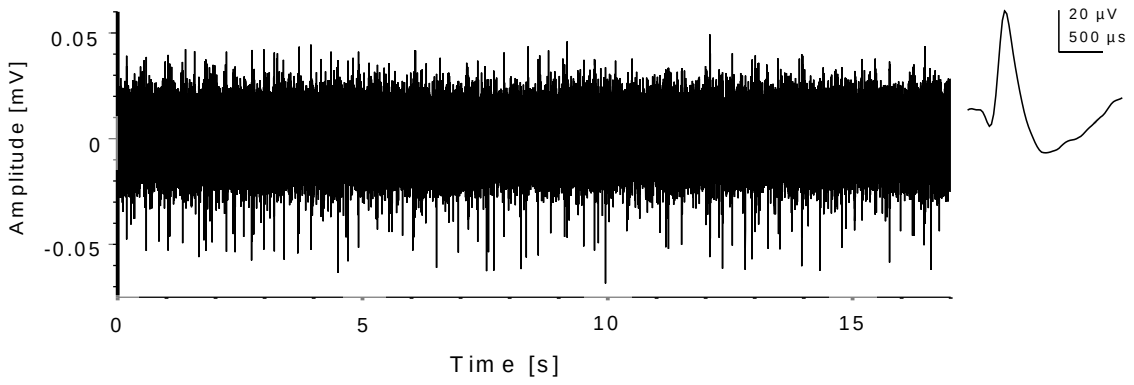

Fig. 3.5. Continuous trace of baseline firings recorded from a putative serotonergic neuron in an anesthetized mouse. The recorded neuron displays spontaneous action potential firings. Inverted action potential shape is shown in the inlet.

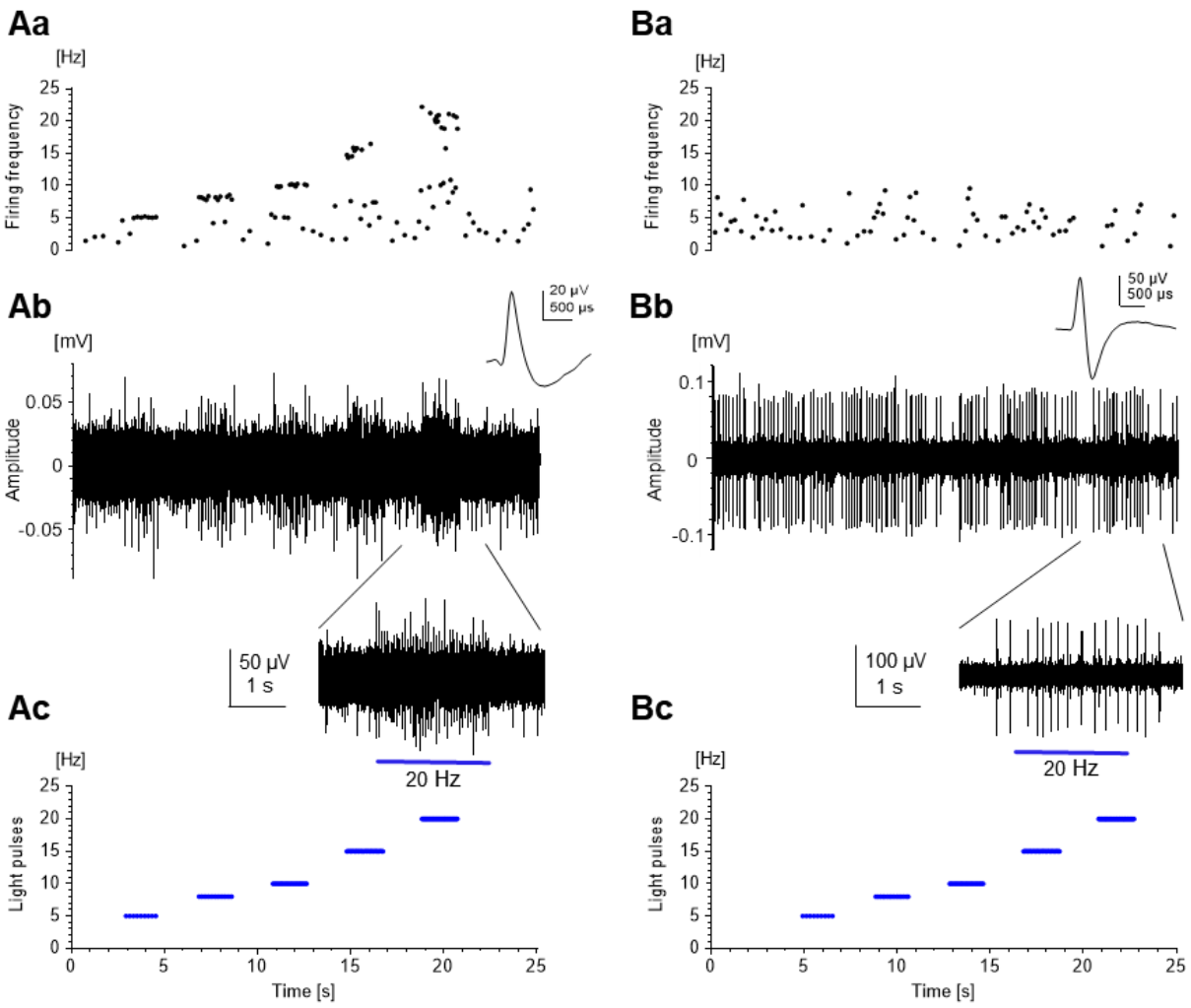

Fig. 3.6. Continuous traces of action potential trains recorded from a putative serotonergic neuron and non-serotonergic neuron. Pulsed light stimuli (465 nm, 10 mW, 15 ms pulse) in increasing frequency steps (5–20 Hz; **Ac, Bc**) produced temporally precise activation in a serotonergic neuron (**A**), but not in a non-serotonergic neuron (**B**). At higher stimulus frequencies, the serotonergic neuron failed to follow each individual stimulus, resulting in single drops in frequency as seen in the instantaneous firing frequency plots (**Aa**). Non-serotonergic neuron did not show any response to light stimuli (**Ba, Bb**). Inverted action potential shapes are shown in inlets (**Ab, Bb**). To note are the unchanged action potential shapes between baseline (**Fig. 3.5**) and response to the light stimuli (**Ab**).

To show that serotonergic neuron activation is due to activation of ChR2, recordings were conducted in the raphe nuclei of ChR2-negative mice. As shown in **Fig. 3.7Aa**, optogenetic stimulation did not induce any firing activity responses of serotonergic neurons. This was also seen with non-serotonergic neurons (**Fig. 3.7Ba**), which lack ChR2 in any case. Action potential shapes of serotonergic (**Fig. 3.7Ab**) and non-serotonergic (**Fig. 3.7Bb**) neurons were similar to those of their counterparts observed in ChR2-positive mice (serotonergic: **Fig. 3.5, Fig. 3.6A**; non-serotonergic: **Fig. 3.6B**). This may indicate that the presence of ChR2 does not

change the basic electrophysiological properties of serotonergic and non-serotonergic neurons in the raphe nuclei.

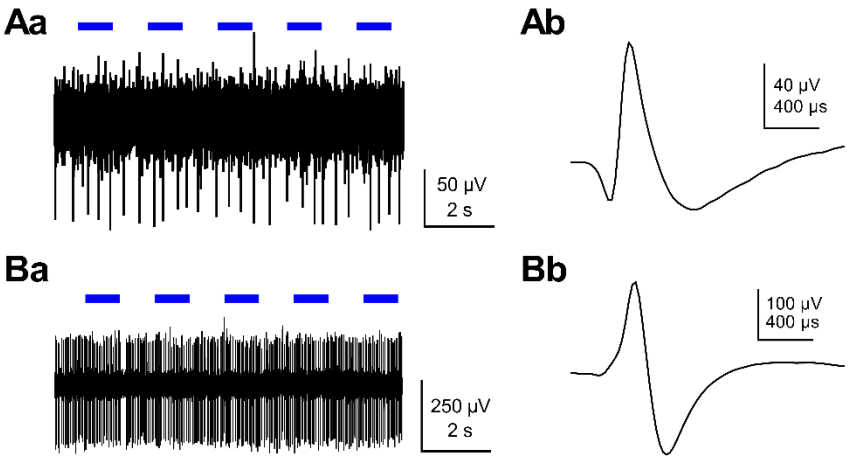

Fig. 3.7. Continuous traces and action potential waveforms recorded in a ChR2-negative mouse. Continuous trace (**Aa**) and action potential waveform (**Ab**) obtained from a putative serotonergic neuron. Continuous trace (**Ba**) and action potential waveform (**Bb**) obtained from a putative non-serotonergic neuron. Blue bars = light stimulation (465 nm, 12 mW).

Fig. 3.8, on the other hand, shows time courses of instantaneous frequencies in response to light stimuli in a ChR2-negative mouse. As shown here, instantaneous frequencies did not change in response to light both in a putative serotonergic neuron (**Fig. 3.8A**) and in a putative non-serotonergic neuron (**Fig. 3.8B**). Statistical analyses confirmed the absence of statistically significant differences in the instantaneous frequency between the light stimulation period and non-stimulated period both in a putative serotonergic neuron (**Fig. 3.8Ab**; Stim vs. Non-Stim, 2.796 ± 0.137 vs. 2.704 ± 0.131, unpaired *t* test, $t_{(48)} = 0.483$, $p = 0.632$; n = 24, n = 26, respectively; 95% confidence interval (CI) of the difference, Stim − Non-Stim, −0.2901 to 0.4731) and in a putative non-serotonergic neuron (**Fig. 3.8Bb**; Stim vs. Non-Stim, 23.44 ± 0.52 vs. 24.49 ± 0.60, unpaired *t* test, $t_{(413)} = 1.319$, $p = 0.188$; n = 205, n = 210, respectively; 95% CI of the difference, Stim − Non-Stim, −0.5134 to 2.61).

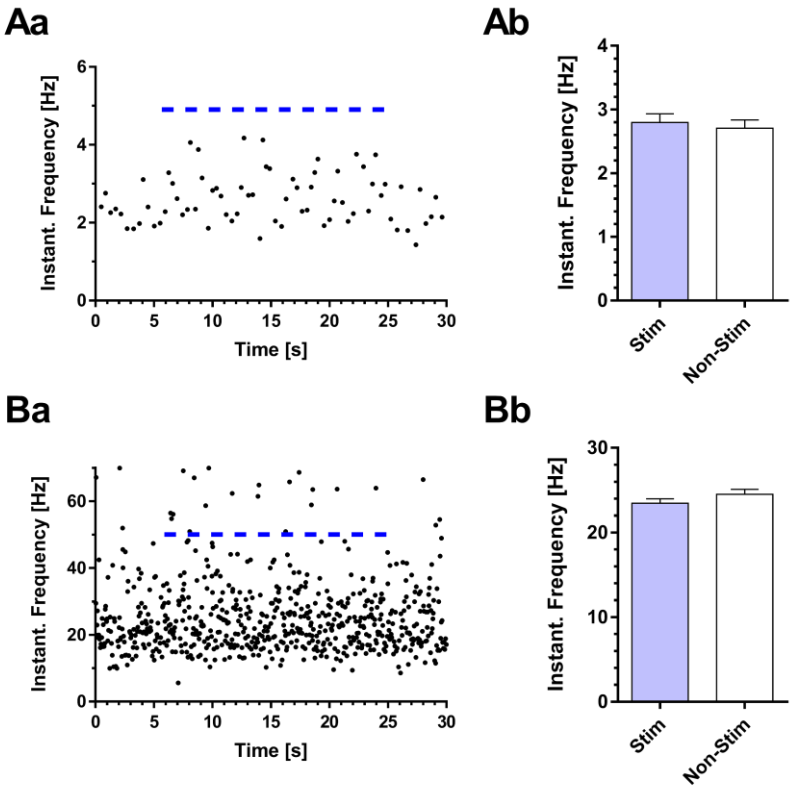

Fig. 3.8. Instantaneous firing frequency in response to light stimulation in a ChR2-negative mouse. Time course of instantaneous frequency (**Aa**) and averaged instantaneous frequency during (Stim) and between (Non-Stim) light stimulation (**Ab**) obtained from a putative serotonergic neuron. Time course of instantaneous frequency (**Ba**) and averaged instantaneous frequency during (Stim) and between (Non-Stim) light stimulation (**Bb**) obtained from a putative non-serotonergic neuron. Blue bars = light stimulation (465 nm, 12 mW). There were no statistically significant differences in instantaneous frequency during and between light stimulation (unpaired *t* test). Data are presented as mean + SEM.

3.2.2. Optogenetic stimulation in the raphe nuclei led to suppression of neuronal activities in the DG

Next, *in vivo* electrophysiological recordings were conducted in the DG on responses to optogenetic light stimulation of raphe nuclei. **Fig. 3.9A** shows the position of the recording electrode, which spans over the hilus, the granule cell layer, and the molecular layer of the DG. **Fig. 3.9B** shows an exemplary continuous trace from one of the neurons recorded. As shown here, neuronal firings were promptly suppressed, gradually reversing with time after cessation of light stimulation. **Fig. 3.9C** demonstrates multiple unit activities measured from a 16-channel multi-electrode array (4 × 4, 150 µm separation). In this example, a total of 11 units (= cells) were identified, which passed the sorting criteria (see Materials and Methods). Although there were differences in the degree of inhibition among the units, the net influence

of raphe stimulation was inhibition. Reduction in the firing rate during stimulation was statistically significant, as indicated in the SD plot (SD <−2; **Fig. 3.9D**)

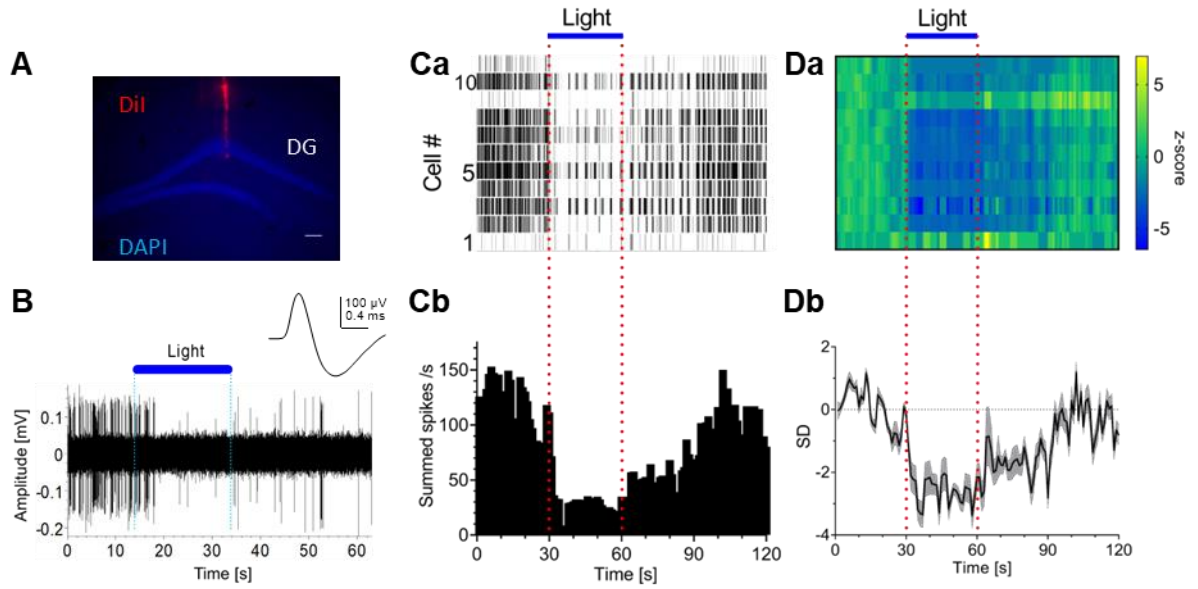

Fig. 3.9. Neuronal responses in the dentate gyrus (DG) after optogenetic stimulation of the dorsal raphe nucleus. (**A**) Image showing the position of the recording electrode (DiI staining, red). Slice was counterstained with DAPI (blue). Scale bar = 100 µm. (**B**) Exemplary trace and action potential shape (inset). Blue light stimulation (20 mW) suppressed firings. (**C**) Single-unit activities measured by a 16-channel multi-electrode array inserted into the DG. Activities of identified 11 units presented as raster plots (**Ca**) and a summed rate histogram (**Cb**). Light stimulation caused net suppression of firing activities in the DG. (**D**) Heat map (**Da**) and standard deviation (SD) plot (**Db**) corresponding to **C**. Z = 0 or SD = 0 was set based on the baseline firing rate at 0–30 s. Firing was significantly suppressed (SD <−2) during light stimulation and recovered gradually after the light stimulation ceased. Data are presented as mean ± SEM.

On a single neuron level, recorded neurons can be classified based on their action potential shapes (wide or narrow) and firing patterns (bursting or non-bursting). To be precise, wide waveform cells can be further distinguished based on whether they are bursting or non-bursting. Narrow waveform cells are in principle all non-bursting (**Fig. 3.10**). Exemplary firing rate changes at a single neuron level are shown in **Fig. 3.11**. For both DRN and MRN stimulation, suppression of action potential firings was observed.

In sum, optogenetic light stimulation of raphe nuclei of Tph2-mhChR2-EYFP mice, regardless of whether it is in the DRN or MRN, caused prompt and robust inhibition of neuronal firings in the DG, either on a single neuron level or as a population in the DG.

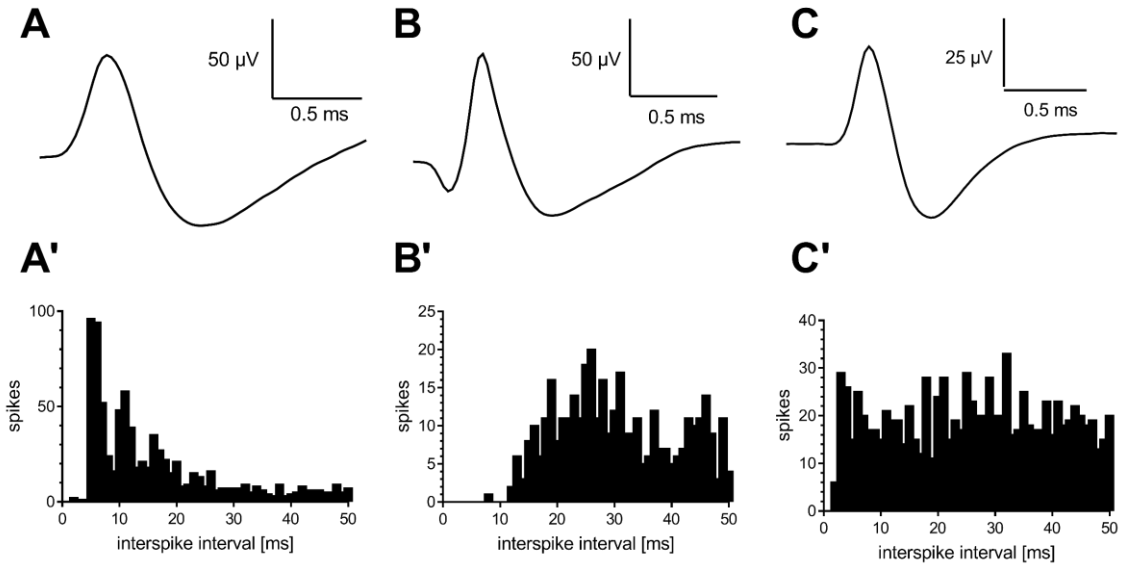

Fig. 3.10. Autocorrelograms (ACGs) of spontaneously firing cells in the dentate gyrus (DG). ACGs were created by counting spikes in 1-ms time bins up to 50 ms. Wide waveform cells (**A**, **B**) exhibit either bursting (**A'**; BI = 0.94) or non-bursting (**B'**; BI = −0.88) firing patterns. Narrow wave form cells (**C**) exhibit in principle non-bursting firing patterns (**C'**; BI = 0.36). Burst firing is characterized by a sharp peak between the 0–10 ms interspike interval, which gradually decays with increasing interspike interval. BI: burst index (see Materials and Methods).

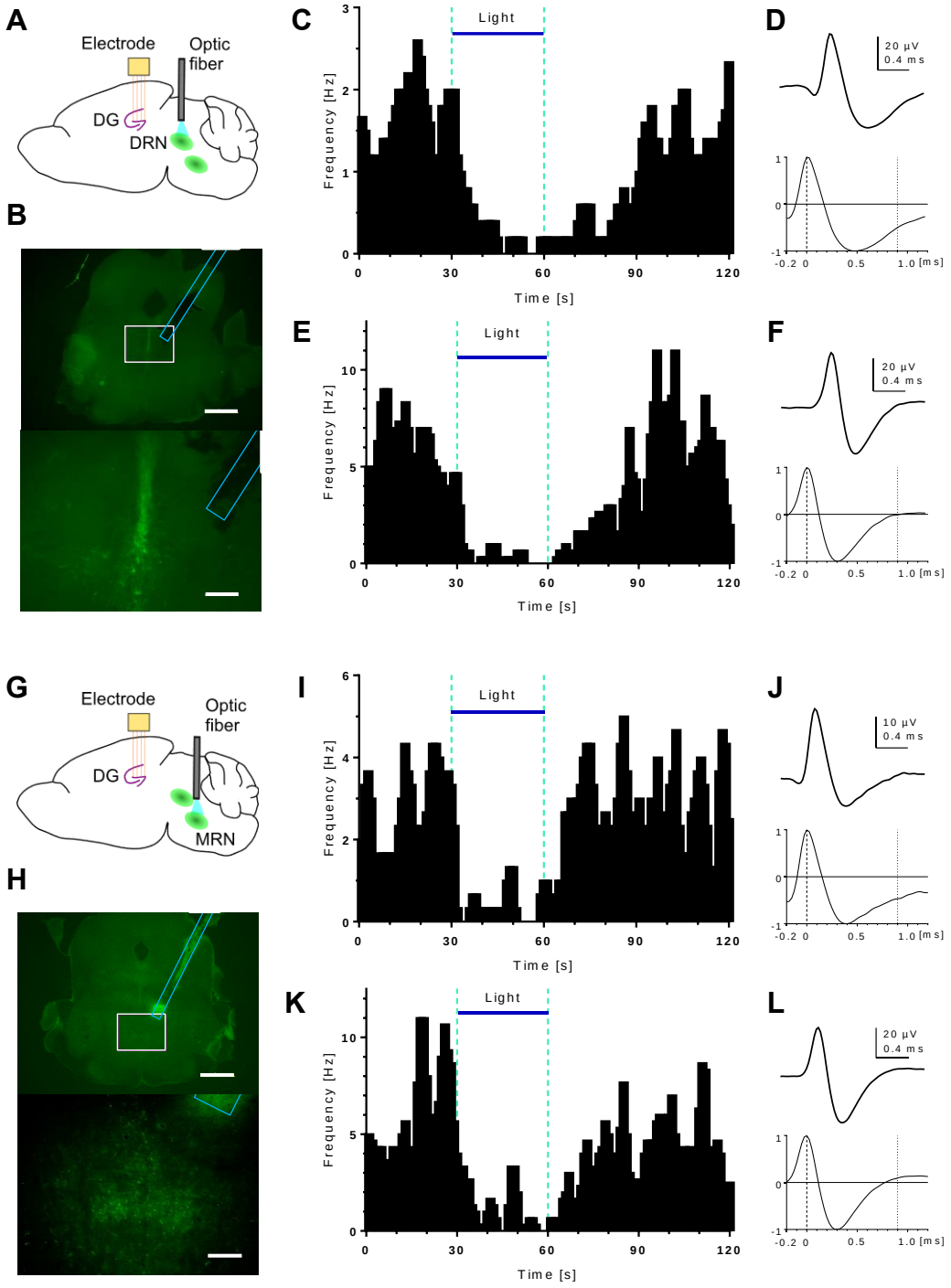

Fig. 3.11. Neuronal firings in the dentate gyrus (DG) in response to optogenetic stimulation of the dorsal raphe nucleus (DRN; **A**–**F**) or the median raphe nucleus (MRN; **G**–**L**). Schematics illustrating the designs of the experiments (**A, G**). Brain slices showing the lesions made by an optic fiber (outlined by blue lines) in the DRN (**B**) or MRN (**H**). Squares in the top images are magnified in the bottom images. Scale bars = 1 mm (top) or 200 µm (bottom). Firing rate histogram of a wide action potential cell (**C, I**) and its corresponding action potential shape (**D, J**; bottom: normalized action potential). Firing rate histogram of a narrow action potential cell (**E, K**) and its corresponding action potential shape (**F, L**; bottom: normalized action potential). Blue light stimulation (18 mW) suppressed action potential generation in the DG. After the stimulation ceased, firing rates recovered gradually to baseline level.

To differentiate between these three types of neurons, trough-to-peak and half-peak widths of action potentials of recorded neurons are plotted on the x-, y-axis, respectively (**Fig. 3.12**).

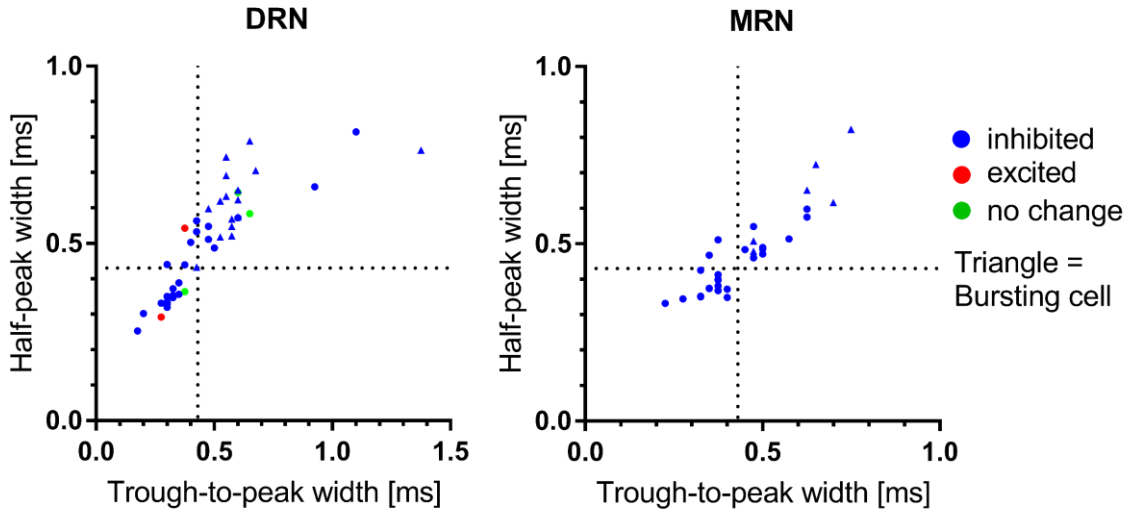

Fig. 3.12. Plots of trough-to-peak and half-peak widths of action potentials. Recorded neurons in the dorsal raphe nucleus (**DRN**) and median raphe nucleus (**MRN**) are characterized based on their action potential trough-to-peak and half-peak widths. Here neurons with trough-to-peak and half-peak widths of less than ca. 0.43 ms (dotted lines) are considered as narrow waveform neurons, and those above these thresholds are considered as wide waveform neurons. Wide waveform neurons which displayed bursting firing patterns are designated with triangle signs. Inhibited: firing rate decrease of 20% or more from the baseline. Excited: firing rate increase of 20% or more from the baseline. No change: less than 20% firing rate change from the baseline.

Based on this cell classification, the firing rate changes were summarized of recorded neurons in the DG in response to optogenetic stimulation in the dorsal or median raphe nucleus (**Fig. 3.13**, **Table 3.1**). As shown here, optogenetic stimulation of either dorsal or median raphe nucleus suppressed all these three cell types in the DG. Suppressed firings recovered gradually (**Fig. 3.9**, **Fig. 3.11**) and one minute after stimulation, there were no statistically significant changes in firing rates compared to respective baselines (**Fig. 3.13**, **Table 3.1**).

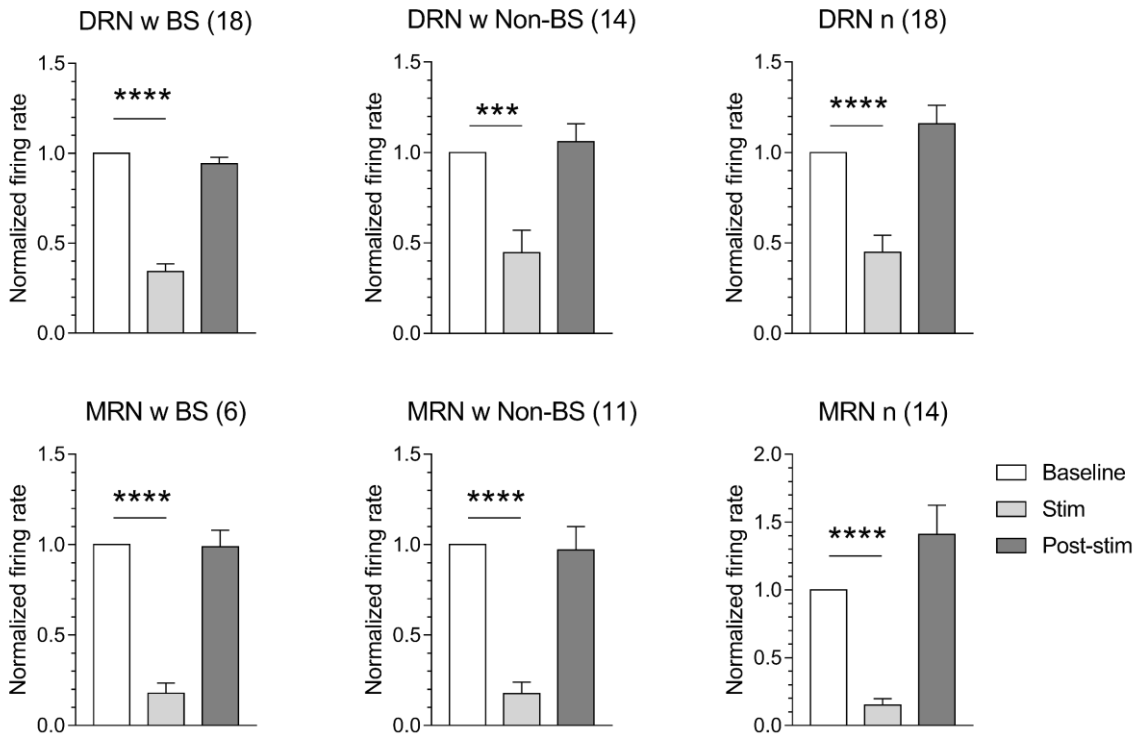

Fig. 3.13. Normalized firing rates recorded in the dentate gyrus. Changes in action potential firing rates in response to optogenetic stimulation in the dorsal raphe nucleus (DRN) or median raphe nucleus (MRN) are shown based on cell types. Firing rates are normalized by taking the firing rates before optogenetic stimulation as baselines. Mean ± SEM. ***$p \leq 0.001$, ****$p \leq 0.0001$; one-sample *t* test compared to respective baselines (= 1). Baseline: averaged firing rates before optogenetic stimulation. Stim: averaged firing rates during 30 s optogenetic stimulation. Post-stim: averaged firing rates 30–60 s after optogenetic stimulation. w BS: wide action potential with bursting. w Non-BS: wide action potential without bursting. n: narrow action potential. Number of recorded cells are shown in parentheses.

	DRN			MRN		
	w BS (18)	w Non-BS (14)	n (18)	w BS (6)	w Non-BS (11)	n (14)
Stim	0.343 ± 0.043 ****$p <$ 0.0001	0.447 ± 0.124 ***$p =$ 0.0006	0.448 ± 0.095 ****$p <$ 0.0001	0.178 ± 0.057 ****$p <$ 0.0001	0.176 ± 0.063 ****$p <$ 0.0001	0.151 ± 0.045 ****$p <$ 0.0001
Post-stim	0.942 ± 0.035 $p = 0.1227$	1.06 ± 0.099 $p = 0.5551$	1.159 ± 0.103 $p = 0.1399$	0.987 ± 0.092 $p = 0.8946$	0.972 ± 0.128 $p = 0.8294$	1.41 ± 0.21 $p = 0.0783$

Table 3.1. Numerical results corresponding to **Fig. 3.13**. Values are shown as means ± SEM. ***$p \leq 0.001$, ****$p \leq 0.0001$; one-sample *t* test compared to respective baselines (= 1). Number of recorded cells are shown in parentheses. See **Fig. 3.13** legend for abbreviations.

3.3. Optogenetic stimulation in freely behaving mice and cell proliferation in the DG

3.3.1. Optogenetic stimulation of raphe neurons reduces cell proliferation in the DG

To evaluate the effect of overnight stimulation of serotonergic neurons on cell proliferation in the hippocampus, the number of BrdU-positive cells in the DG was quantified after 8 hours of optogenetic stimulation. **Fig. 3.14A** shows representative images of brain slices with BrdU-positive cells (black dots) in the DG. A lower number of BrdU-positive cells in the SGZ can be recognized in the stimulated animal compared with control. Mice with optogenetic stimulation (Stim) had lower numbers of BrdU-positive cells compared to control groups (Ctrl) both in the DRN (Ctrl vs. Stim, 799.5 ± 61.8 vs. 557.3 ± 46.3, unpaired *t* test, $t_{(15)}$ = 3.181, p = 0.0062; n = 8, n = 9, respectively) and the MRN (Ctrl vs. Stim, 945 ± 130.3 vs. 514.3 ± 51.13, unpaired *t* test, $t_{(7)}$ = 2.79, p = 0.0269; n = 5, n = 4, respectively) experimental groups (**Fig. 3.14B**).

3.3.2. Optogenetic stimulation did not significantly change total distances traveled

Since previous studies had shown that running exerts a positive influence on hippocampal cell proliferation (Klempin et al., 2013), the cumulative traveled distances from the 30-minute baseline prior to optogenetic stimulation until completion of optogenetic stimulation were compared among the experimental groups (**Fig. 3.14C**–**E**). **Fig. 3.14C, D** displays the time course of cumulative distances, whereas **Fig. 3.14E** shows a comparison of total traveled track lengths at the end of experiments. The traveled distances of optogenetically stimulated animals (normalized to respective control groups) were not significantly different from those of control animals in either the DRN (Ctrl vs. Stim, 100 ± 20.0 vs. 133 ± 21.5, value in % control, unpaired *t* test, $t_{(15)}$ = 1.114, p = 0.2828; n = 8, n = 9, respectively) and MRN (Ctrl vs. Stim, 100 ± 22.5 vs. 68.0 ± 16.9, value in % control, unpaired *t* test, $t_{(7)}$ = 1.085, p = 0.3140; n = 5, n = 4, respectively) groups. These data indicate that a decrease in cell proliferation in the DG is not due to reduced physical activities but is rather directly mediated by serotonin signaling in the DG.

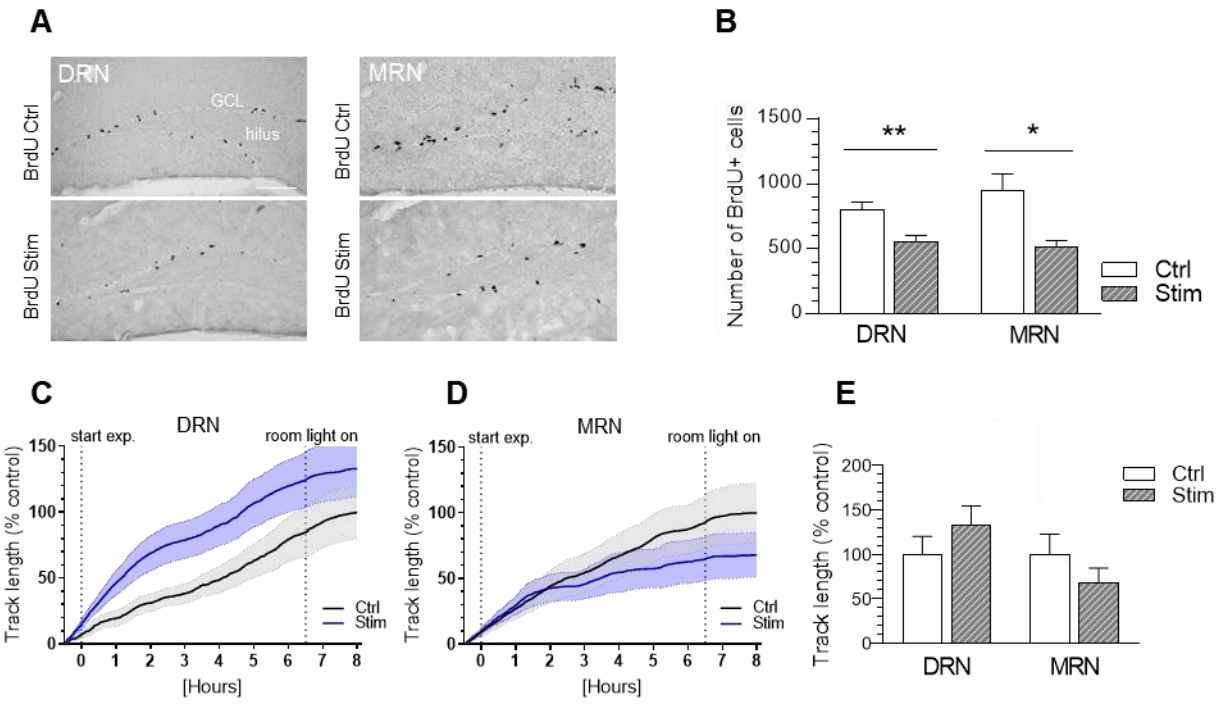

Fig. 3.14. Cell proliferation and behavior of mice after overnight stimulation. (**A**) Representative images of peroxidase-stained BrdU cells in the granular cell layer (GLC) following dorsal or median raphe nuclei (DRN, MRN) light stimulation (Stim) vs. control (Ctrl); Scale bar 100 µm. (**B**) The number of BrdU-positive cells in the DG is significantly decreased following overnight stimulation of either DRN (Ctrl vs. Stim; n = 8 vs. n = 9) or MRN (Ctrl vs. Stim; n = 5 vs. n = 4); unpaired *t* test, *$p \leq 0.05$, **$p \leq 0.01$. Data are presented as mean + SEM. (**C, D**) Cumulative curves of track lengths obtained from overnight-stimulated mice (DRN, **C**; MRN, **D**) revealed no statistically significant differences in distances traveled compared to control mice. Data are normalized to Ctrl and presented as mean ± SEM. (**E**) Comparison of total distances traveled. There were no statistically significant differences between the Ctrl and Stim in the DRN and MRN stimulation groups (unpaired *t* test). Data are presented as mean + SEM.

3.3.3. Optogenetic stimulation of serotonergic neurons transiently facilitates animal locomotion.

Behavioral changes from the prestimulus status during and immediately after optogenetic light stimulation are averaged for the dark phase of the experiment (0:00–6:30) and summarized in **Fig. 3.15, Table 3.2** (for DRN stimulation), and **Fig. 3.16**, **Table 3.3** (for MRN stimulation). As evident here, all the parameters measured, except wall distance, increased during the stimulation, which lasted at least for the next 30 seconds after stimulation. Some parameters in DRN stimulated animals showed delayed increase, i.e., increase was first observed in the poststimulus period rather than during stimulation. It could be that the mouse behavior was under the mixed influence of behavioral facilitation and inhibition during the stimulation phase. In MRN stimulated group, on the other hand,

behavioral facilitation was evident during stimulation and lasted or further increased in the poststimulation period. This difference in the pattern of behavioral changes between DRN and MRN stimulation implies involvement of different behavioral circuitry mediating locomotion.

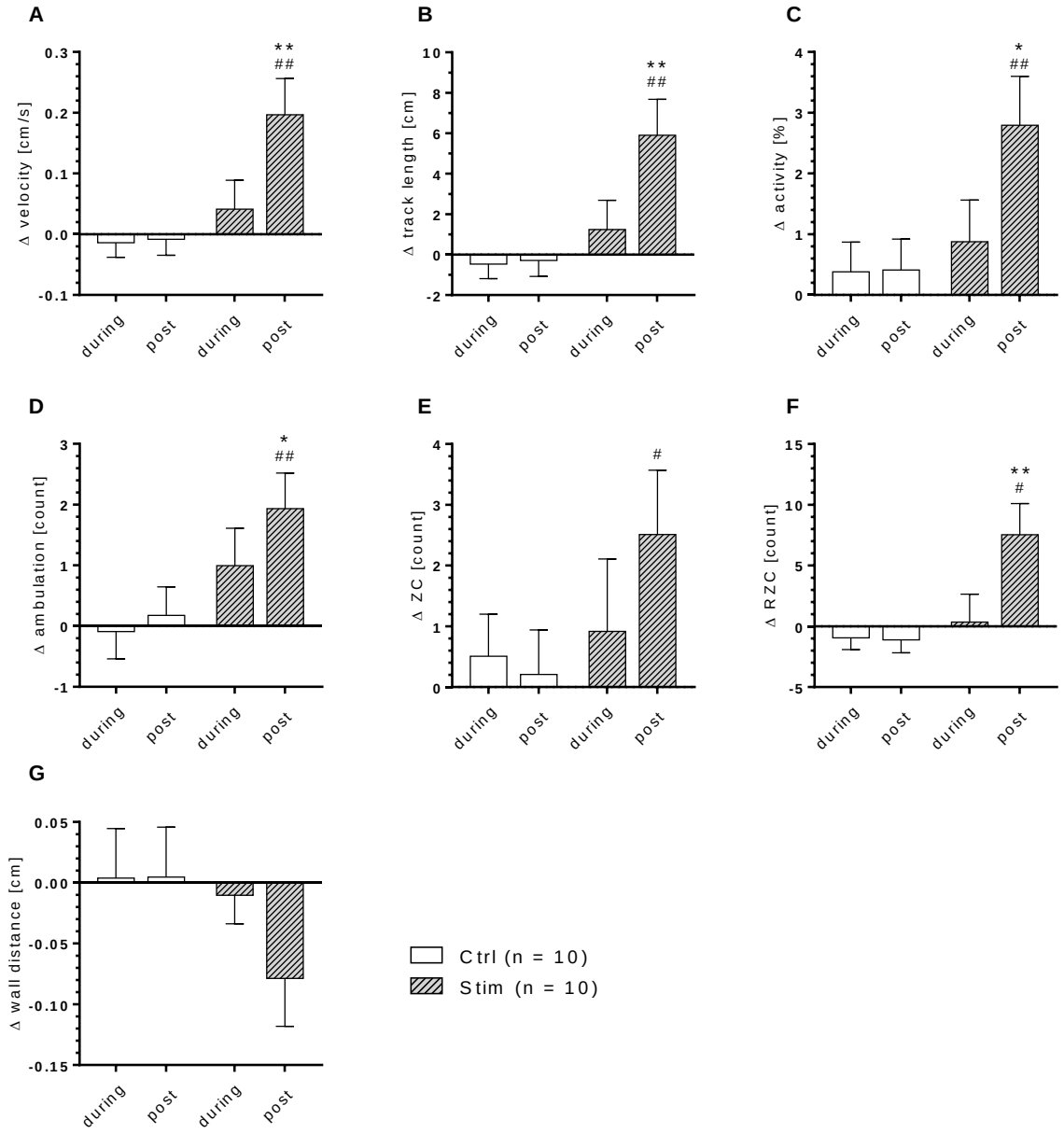

Fig. 3.15. Optogenetic stimulation of the dorsal raphe nucleus transiently facilitates locomotion. Averaged changes of velocity (**A**), track length (**B**), activity (**C**), ambulation (**D**), zone crossing (ZC; **E**), rated zone crossing (RZC; **F**), and wall distance (**G**) at night (0:00–6:30 hour). Data were collected during the 30-second stimulation period (during) and preceding (pre) and succeeding (post) 30-second periods. Data were normalized by subtracting pre values of each animal, at each light stimulation. Data are presented as mean + SEM. n = number of animals. $*p \leq 0.05$, $**p \leq 0.01$; unpaired *t* test, compared to the control group (Ctrl) within the same experimental period, i.e., (during/post-)stimulation. $^{\#}p \leq 0.05$, $^{\#\#}p \leq 0.01$; one-sample *t* test, compared to the pre-stimulation value (= 0) in the same group. Ctrl: mice without optogenetic stimulation. Stim: mice with optogenetic stimulation. Numerical results are presented in **Table 3.2**.

Variable	Ctrl (n = 10)		Stim (n = 10)	
	During	Post	During	Post
ΔVelocity [cm/s] vs. Ctrl vs. pre-stim.	−0.01 ± 0.02 $p = 0.58$	−0.01 ± 0.03 $p = 0.75$	0.04 ± 0.05 $p = 0.32$ $p = 0.41$	0.20 ± 0.06 $^{**}p = 0.008$ $^{\#\#}p = 0.009$
ΔTrack length [cm] vs. Ctrl vs. pre-stim.	−0.47 ± 0.72 $p = 0.53$	−0.29 ± 0.79 $p = 0.72$	1.24 ± 1.44 $p = 0.30$ $p = 0.41$	5.90 ± 1.78 $^{**}p = 0.007$ $^{\#\#}p = 0.009$
ΔActivity [%] vs. Ctrl vs. pre-stim.	0.38 ± 0.49 $p = 0.45$	0.41 ± 0.51 $p = 0.44$	0.88 ± 0.69 $p = 0.56$ $p = 0.23$	2.79 ± 0.80 $^{*}p = 0.02$ $^{\#\#}p = 0.007$
ΔAmbulation [count] vs. Ctrl vs. pre-stim.	−0.09 ± 0.45 $p = 0.84$	0.18 ± 0.47 $p = 0.71$	1.00 ±0.62 $p = 0.17$ $p = 0.14$	1.94 ± 0.59 $^{*}p = 0.03$ $^{\#\#}p = 0.009$
ΔZC [count] vs. Ctrl vs. pre-stim.	0.51 ± 0.69 $p = 0.48$	0.21 ± 0.73 $p = 0.78$	0.92 ± 1.19 $p = 0.76$ $p = 0.46$	2.51 ± 1.06 $p = 0.09$ $^{\#}p = 0.04$
ΔRZC [count] vs. Ctrl vs. pre-stim.	−0.95 ± 0.96 $p = 0.35$	−1.11 ± 1.06 $p = 0.33$	0.35 ± 2.30 $p = 0.60$ $p = 0.88$	7.54 ± 2.56 $^{**}p = 0.008$ $^{\#}p = 0.02$
ΔWall distance [cm] vs. Ctrl vs. pre-stim.	0.004 ± 0.041 $p = 0.92$	0.005 ± 0.041 $p = 0.91$	−0.010 ± 0.023 $p = 0.76$ $p = 0.67$	−0.079 ± 0.039 $p = 0.15$ $p = 0.07$

Table 3.2. Numerical results corresponding to **Fig. 3.15**. Values are means ± SEM. n = number of animals. $^{*}p \leq 0.05$, $^{**}p \leq 0.01$; unpaired *t* test, compared to the control group (Ctrl) within the same experimental period, i.e., (during/post-)stimulation. $^{\#}p \leq 0.05$, $^{\#\#}p \leq 0.01$; one-sample *t* test, compared to the pre-stimulation (pre-stim.) value (= 0) in the same group. See **Fig. 3.15** legend for abbreviations.

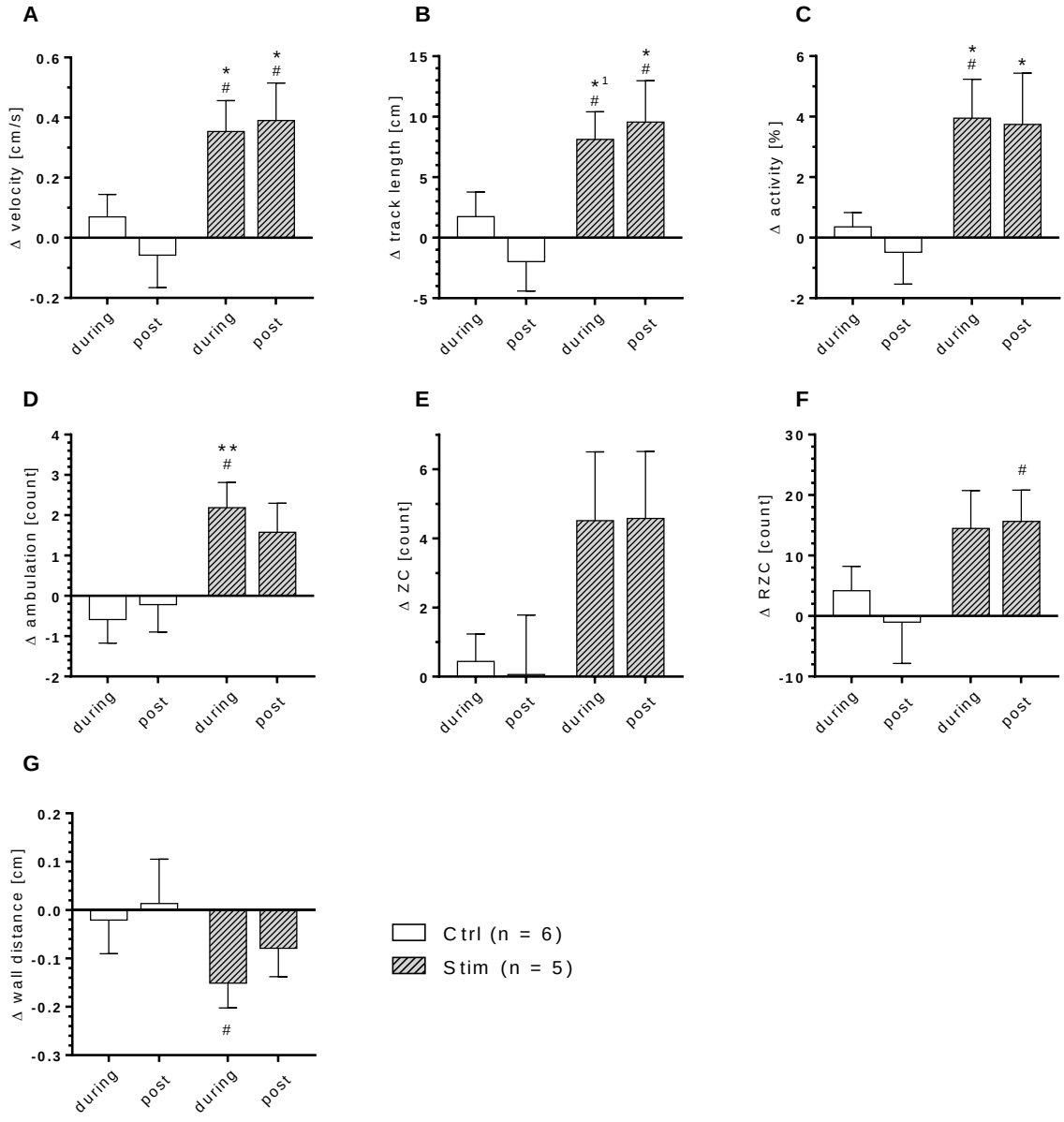

Fig. 3.16. Optogenetic stimulation of the median raphe nucleus transiently facilitates locomotion. Averaged changes of velocity (**A**), track length (**B**), activity (**C**), ambulation (**D**), zone crossing (ZC; **E**), rated zone crossing (RZC; **F**), and wall distance (**G**) at night (0:00–6:30 hour). Data were collected during the 30-second stimulation period (during) and preceding (pre) and succeeding (post) 30-second periods. Data were normalized by subtracting pre values of each animal, at each light stimulation. Data are presented as mean + SEM. n = number of animals. $*p \leq 0.05$, $**p \leq 0.01$, $*^{1}p = 0.06$; unpaired *t* test, compared to the control group (Ctrl) within the same experimental period, i.e., (during/post-)stimulation. $^{\#}p \leq 0.05$; one-sample *t* test, compared to the pre-stimulation value (= 0) in the same group. Ctrl: mice without optogenetic stimulation. Stim: mice with optogenetic stimulation. Numerical results are presented in **Table 3.3**.

Variable	Ctrl (n = 6)		Stim (n = 5)	
	During	Post	During	Post
ΔVelocity [cm/s] vs. Ctrl vs. pre-stim.	0.07 ± 0.07 $p = 0.39$	−0.06 ± 0.11 $p = 0.61$	0.35 ± 0.10 $*p = 0.04$ $^{\#}p = 0.02$	0.39 ± 0.12 $*p = 0.02$ $^{\#}p = 0.03$
ΔTrack length [cm] vs. Ctrl vs. pre-stim.	1.75 ± 2.03 $p = 0.42$	−1.97 ± 2.43 $p = 0.45$	8.13 ± 2.28 $*^{1}p = 0.06$ $^{\#}p = 0.02$	9.56 ± 3.42 $*p = 0.02$ $^{\#}p = 0.04$
ΔActivity [%] vs. Ctrl vs. pre-stim.	0.36 ± 0.47 $p = 0.48$	−0.48 ± 1.06 $p = 0.66$	3.95 ± 1.29 $*p = 0.02$ $^{\#}p = 0.03$	3.74 ± 1.70 $*p = 0.05$ $p = 0.09$
ΔAmbulation [count] vs. Ctrl vs. pre-stim.	−0.59 ± 0.59 $p = 0.36$	−0.22 ± 0.68 $p = 0.76$	2.19 ± 0.62 $**p = 0.01$ $^{\#}p = 0.02$	1.58 ± 0.72 $p = 0.10$ $p = 0.09$
ΔZC [count] vs. Ctrl vs. pre-stim.	0.44 ± 0.79 $p = 0.60$	0.06 ± 1.72 $p = 0.97$	4.51 ± 1.99 $p = 0.07$ $p = 0.08$	4.57 ± 1.94 $p = 0.11$ $p = 0.07$
ΔRZC [count] vs. Ctrl vs. pre-stim.	4.19 ± 4.02 $p = 0.34$	−1.01 ± 6.83 $p = 0.88$	14.48 ± 6.28 $p = 0.18$ $p = 0.08$	15.65 ± 5.15 $p = 0.09$ $^{\#}p = 0.03$
ΔWall distance [cm] vs. Ctrl vs. pre-stim.	−0.02 ± 0.07 $p = 0.77$	0.01 ± 0.09 $p = 0.88$	−0.15 ± 0.05 $p = 0.18$ $^{\#}p = 0.04$	−0.08 ± 0.06 $p = 0.44$ $p = 0.25$

Table 3.3. Numerical results corresponding to **Fig. 3.16**. Values are means ± SEM. n = number of animals. $*p \leq 0.05$, $**p \leq 0.01$, $*^{1}p = 0.06$; unpaired *t* test, compared to the control group (Ctrl) within the same experimental period, i.e., (during/post-)stimulation. $^{\#}p \leq 0.05$; one-sample *t* test, compared to the pre-stimulation (pre-stim.) value (= 0) in the same group. See **Fig. 3.16** legend for abbreviations.

3.3.4. Reduced cell proliferation was accompanied by reduced 5-HT contents in the hippocampus

Next was investigated whether optogenetic stimulation in the DRN led to increased or decreased tissue levels of 5-HT and its metabolite 5-HIAA in the hippocampus and in raphe nuclei using HPLC. **Fig. 3.17** shows HPLC data normalized to respective control groups without light stimulation in percentage. As shown here, 5-HT levels were decreased in the stimulated groups in both the raphe nuclei (Ctrl vs. Stim, 100 ± 17.67 vs. 38.2 ± 23.21, value in % control, unpaired *t* test, $t_{(8)} = 2.119$, $p = 0.0670$; n = 5 per group) and the hippocampus (Ctrl vs. Stim, 100 ± 23.67 vs. 35.6 ± 13.41, value in % control, unpaired *t* test, $t_{(8)} = 2.375$, $p = 0.0449$; n = 5 per group). The ratio of 5-HT to 5-HIAA (= 5-HT/5-HIAA) was reduced (i.e.,

higher turnover) in stimulated groups in both the raphe nuclei (Ctrl vs. Stim, 100 ± 9.778 vs. 33.4 ± 19.38, value in % control, unpaired *t* test, $t_{(8)} = 3.068$, $p = 0.0154$; n = 5 per group) and the hippocampus (Ctrl vs. Stim, 100 ± 19.71 vs. 39.4 ± 18.29, value in % control, unpaired *t* test, $t_{(8)} = 2.261$, $p = 0.0536$; n = 5 per group). In sum, optogenetic DRN stimulation resulted in reduced 5-HT contents both in the raphe nuclei and in the serotonergic projection target (e.g., hippocampus), which is accompanied by higher turnover rate of 5-HT into 5-HIAA, compared to the non-stimulated control group.

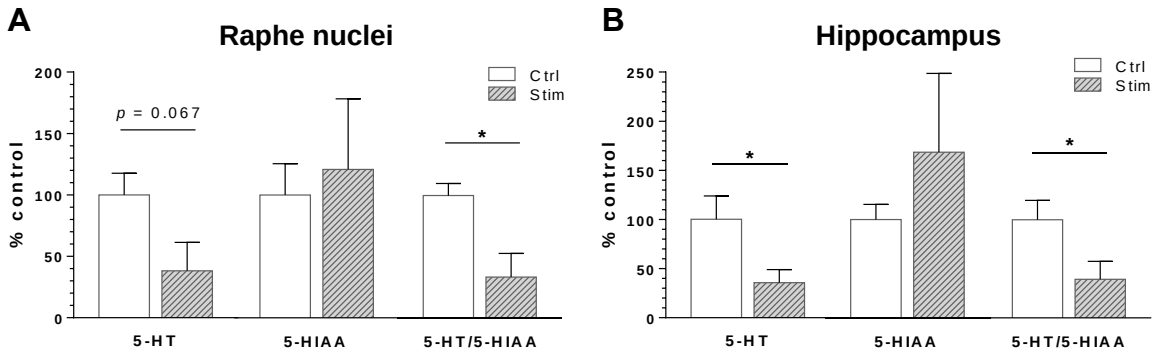

Fig. 3.17. Change in serotonin (5-HT) levels after overnight stimulation. High-performance liquid chromatography (HPLC) analysis of 5-HT and its metabolite, 5-hydroxyindoleacetic acid (5-HIAA). 5-HT and the ratio of 5-HT to 5-HIAA (= 5-HT/5-HIAA) was reduced in raphe nuclei (**A**) and hippocampus (**B**) following overnight stimulation of the dorsal raphe nucleus. Data are normalized to the control group (Ctrl; 100%); unpaired *t* test, $*p \leq 0.05$; n = 5 per group. Data are presented as mean + SEM. Ctrl: mice without optogenetic stimulation. Stim: mice with optogenetic stimulation.

3.3.5. One week of DRN optogenetic stimulation reduced BrdU-positive cells only in the ipsilateral hemisphere

So far, the results obtained from overnight optogenetic stimulation have been presented. To elucidate long-term effects of optogenetic stimulation of serotonergic neurons on cell proliferation in the DG, the DRN was stimulated for 6 nights using two different stimulation protocols (see Materials and Methods). Moreover, the total distance traveled was measured during the 6-night stimulation at 20 Hz. At the end of one-week optogenetic stimulation, no significant difference in the number of BrdU-positive cells was observed between control and stimulated animals in both the 8 Hz (Ctrl vs. Stim, 1723 ± 251.8 vs. 1695 ± 199.8, unpaired *t* test $t_{(15)} = 0.0900$, $p = 0.9295$; n = 7, n = 10, respectively) and the 20 Hz (Ctrl vs. Stim, 1786 ± 306.9 vs. 1743 ± 169.6, unpaired *t* test, $t_{(11)} = 0.1337$, $p = 0.8961$; n = 5, n = 8, respectively) stimulation protocols (**Fig. 3.18A**). Next, the number of BrdU-positive cells in two hemispheres was separately assessed and it was found that there was a significant inequality

(expressed as laterality index; see Materials and Methods) between the hemispheres in both the 8 Hz (Ctrl vs. Stim, 0.8477 ± 0.0238 vs. 0.7104 ± 0.0392, unpaired *t* test, $t_{(15)} = 2.678$, $p = 0.0172$; n = 7, n = 10, respectively) and the 20 Hz (Ctrl vs. Stim, 0.996 ± 0.1089 vs. 0.815 ± 0.0357, unpaired *t* test, $t_{(11)} = 1.896$, $p = 0.0422$; n = 5, n = 8, respectively) stimulated animals (**Fig. 3.18B**). Comparison of the number of BrdU-positive cells between ipsilateral (ipsi) and contralateral (contra) hemispheres in each animal revealed that the number of BrdU-positive cells was significantly lower in the ipsilateral side than in the contralateral side in 20 Hz stimulated animals (contra vs. ipsi, 1918 ± 218.1 vs. 1568 ± 134.4, paired *t* test, $t_{(7)} = 2.756$, $p = 0.0283$, n = 8) but not in control animals without light stimulation (contra vs. ipsi, 1762 ± 226.4 vs. 1811 ± 401.5, paired *t* test, $t_{(4)} = 0.223$, $p = 0.8345$, n = 5; **Fig. 3.18C**). The significant difference can be explained not only by the reduced number of BrdU-positive cells in the ipsilateral hemisphere but also by a slight increase of BrdU-positive cells in the contralateral side. The total daily running distances of mice stimulated at 20 Hz or their control counterparts tendentially increased with time, except the last night, probably because the mice received BrdU injections during the daytime and their sleep was disturbed, resulting in less activities during the night (**Fig. 3.19A**). There were no statistically significant differences in the total daily running distances between the Ctrl and Stim groups (unpaired *t* test). The cumulative track length curve for the 6 nights was obtained by adding up the daily average total track lengths (**Fig. 3.19B**). As shown here, the cumulative track length traveled was slightly higher in the Ctrl group than in the Stim group. Since not all the animals were successfully tracked for the whole 6 nights (success rate: Ctrl (n = 5), 93.3% (28/30 data points); Stim (n = 8), 93.8% (45/48 data points)), the total track length traveled for the 6 nights was represented as area under the curve (AUC) in **Fig. 3.19C**. Statistical analysis showed that there was no statistically significant difference in AUC between the two groups (Ctrl vs. Stim, 115028 ± 30958 vs. 86038 ± 16134, unpaired *t* test, $t_{(11)} = 0.918$, $p = 0.378$; n = 5, n = 8, respectively; **Fig. 3.19C**).

Overall, the results obtained from one-week stimulation suggest the presence of adaptive mechanisms to compensate for the suppressive effects of acute optogenetic light stimulation of serotonergic neurons as shown in the present study. As a result, the total number of BrdU-positive cells returned to the control level without light stimulation, but the significant hemispheric difference persisted.

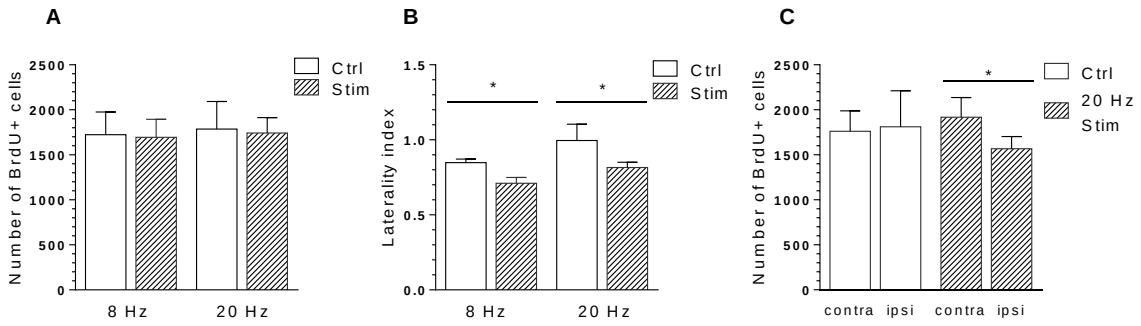

Fig. 3.18. Cell proliferation in the dentate gyrus following 6 nights of dorsal raphe nucleus (DRN) stimulation. Quantification of BrdU-positive (BrdU+) cells in mice with (Stim) and without light stimulation (Ctrl). No difference in cell proliferation in the hippocampus was observed (**A**). However, data reveal a shift in the laterality index for the Stim group (**B**), which was accompanied by decreased cell numbers in the ipsilateral hippocampus (**C**; ipsi=location of the implanted fiber optic ferrule in the DRN). *$p \leq 0.05$, unpaired *t* test (**A**, **B**), paired *t* test (**C**). 8 Hz: Ctrl vs. Stim, n = 7 vs. n = 10. 20 Hz: Ctrl vs. Stim, n = 5 vs. n = 8. Data are presented as mean + SEM.

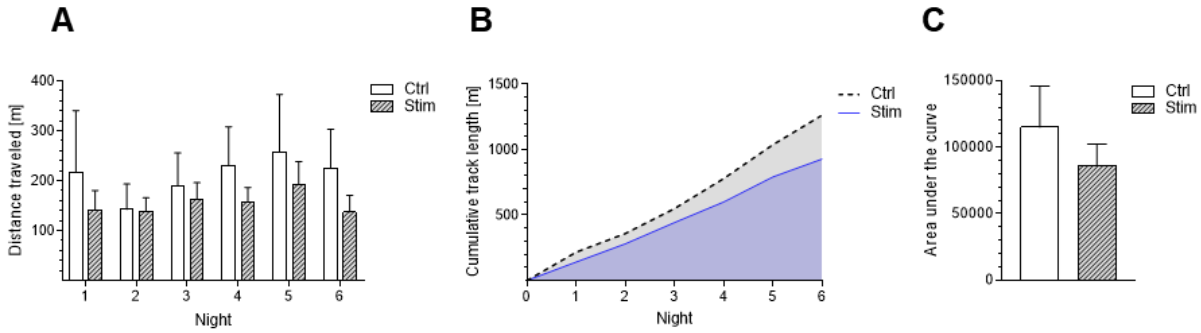

Fig. 3.19. Comparison of total distances traveled after one-week optogenetic stimulation of the dorsal raphe nucleus. (**A**) Total distances traveled for each night. Mice were either optogenetically stimulated at 20 Hz (Stim) or not stimulated (Ctrl). There were no statistically significant differences in the total daily running distances between the Ctrl and Stim groups. (**B**) Time course of the cumulative track length for 6 nights. (**C**) Statistical comparison of the cumulative track length represented as area under the curve (AUC). There was no statistically significant difference in AUC between the two groups (unpaired *t* test). Ctrl vs. Stim, n = 5 vs. n = 8. Data are presented as mean + SEM.

4. Discussion

4.1. Optogenetic stimulation specifically activates serotonergic neurons in brain slices of Tph2-mhChR2-EYFP mice

The presented data obtained on optogenetic stimulation of raphe neurons in brain slices and simultaneous patch-clamp recordings confirm the validity of the experimental animal models used in the current study. Namely, optogenetic stimulation specifically activated serotonergic neurons without affecting activities of non-serotonergic neurons in transgenic Tph2-mhChR2-EYFP mice. This is important for the investigation of the contribution of serotonergic neurons to the proliferation of new cells in the DG, as discussed below. To differentiate between serotonergic and non-serotonergic neurons, neurons were first sorted based on morphological criteria and their serotonergic identity was confirmed by the presence of EYFP (see Materials and Methods). As expected, putative serotonergic neurons were activated by blue light, whereas non-serotonergic neurons did not show any response to blue light. Importantly, action potentials observed in response to current injection had the same morphology as previously reported for each cell type, confirming that the light-reactive neuron was serotonergic. The stimulation frequency used in the presented study (20 Hz) has commonly been used in other studies employing optogenetic activation of serotonergic neurons (Warden et al., 2012; Dugué et al., 2014; Liu et al., 2014). This reflects physiological patterns of serotonergic activity, where firing rates of 2–20 Hz have been reported *in vivo* (Teixeira et al., 2018). Indeed, the data in response to 1 s continuous light stimulation indicate that serotonergic neurons can fire up to about 20 Hz. Although precise neuronal activation in brain slices at high frequencies (>15 Hz) was observed in a different study (Liu et al., 2014) as well, a partial failure to evoke action potentials at high frequencies has also been previously reported (Zhao et al., 2011). It should be noted that the efficacy of optogenetic activation also depends on the expression level of ChR2 proteins, which may vary from neuron to neuron.

The optogenetic pulse width of 15 ms used in the present study is not typical since shorter pulse widths, such as 5 ms, are more commonly used, although some authors already reported that at least a 10 ms duration was necessary to induce full response of ChR2 (Erofeev et al., 2019). The present study has demonstrated, however, that a 15 ms pulse width is more effective in triggering action potentials compared to other pulse widths that have been tested (1–10 ms). This is probably because neurons require a certain time to reach the action potential threshold after the depolarizing process starts in response to blue light illumination. When the pulse width is too short, the depolarizing process ends before the membrane

potential of the neuron reaches the action potential threshold. A longer pulse width therefore ensures that the optogenetic stimulation is given enough time to raise the membrane potential of the illuminated neuron to its action potential threshold. Since the maximum stimulation frequency used in the current study was 20 Hz, i.e., 50 ms inter-stimulus intervals, a 15 ms pulse width still leaves enough time between spikes so that the depolarized membrane potential can be repolarized to its resting membrane potential and be ready for the generation of the next action potential.

In sum, optogenetically stimulating a serotonergic neuron at 20 Hz with 15 ms pulses is most likely to activate the neuron at its maximum activity level, which is ideal for investigating the role of 5-HT in the following studies presented in this thesis.

4.2. *In vivo* optogenetic stimulation specifically activates serotonergic neurons in the raphe nuclei of Tph2-mhChR2-EYFP mice

Data on optogenetic stimulation of raphe neurons and simultaneous extracellular recordings also confirmed the *in vivo* validity of the experimental animal models used in the present study. As with the patch-clamp recordings in the previous section, optogenetic stimulation specifically activated serotonergic neurons without affecting the activities of non-serotonergic neurons in the transgenic animals used in the study. Since serotonergic contribution to the proliferation of new cells in the DG was to be investigated in living animals, the *in vivo* recording has more relevance for the present study. To confirm serotonergic specificity, spontaneously firing neurons were first differentiated between serotonergic and non-serotonergic based on electrophysiological criteria (see Materials and Methods). As expected, only a putative serotonergic neuron was activated by blue light, whereas a non-serotonergic neuron did not show any response to blue light. Importantly, action potentials observed in response to light pulses had the same morphology as those observed during spontaneous firing, confirming that the responses observed were not light-induced electrical artifacts. Indeed, it has been reported that tungsten electrodes with small exposed tip surfaces as used in the current study, i.e., tetrodes with wire diameters <20 µm, show smaller optically induced electrical artifacts than do tungsten electrodes with larger exposed metal tips (Cardin et al., 2010). As opposed to the patch-clamp recordings in the previous section, partial failure to evoke action potentials at high frequencies (>15 Hz) was observed *in vivo*. It should be noted however that under *in vivo* conditions, the positioning of a recording electrode, an optic fiber, and a target cell is not as straightforward as in patch-clamp recordings since the experimenter

cannot see them in the brain of living animals. Moreover, optogenetic light substantially attenuates in brain tissues (see Introduction). Partial failure to evoke action potentials at high frequencies could be explained by an interplay of such confounding factors *in vivo*. In addition, the efficacy of optogenetic activation depends on the varying expression level of ChR2 proteins, as mentioned in the previous section. Nonetheless, together with the results obtained from patch-clamp recordings, it appears that serotonergic neurons in raphe nuclei can be activated at up to 20 Hz, confirming the validity of the stimulation frequency used in the following studies.

4.3. Optogenetic stimulation of raphe nuclei led to reduced cell proliferation and suppression of neuronal activities in the DG, which was accompanied by reduced 5-HT content

Here it was demonstrated that overnight optogenetic stimulation of raphe nuclei led to a lower number of newly proliferated cells in the DG compared to non-stimulated control groups. Further, electrophysiological recordings showed that optogenetic stimulation of raphe nuclei and the resulting release of 5-HT inhibited neuronal activities in the DG. Intriguingly, reduced cell proliferation was accompanied by reduced 5-HT levels in both the raphe nuclei and the hippocampus, as revealed by HPLC analysis from DRN-stimulated animals. This could be attributable to the repeated optogenetic raphe stimulation, resulting in repeated 5-HT release and thus depletion of 5-HT storage. In accordance with this, stimulated mice showed a lower 5-HT/5-HIAA ratio compared to the control group, indicating that more 5-HT was released and metabolized into 5-HIAA.

One of the possible explanations for reduced cell proliferation after overnight optogenetic stimulation is that electrophysiological activities in the DG were inhibited by 5-HT. Indeed, coupling between neuronal activities and cell proliferation has been demonstrated in previous studies (Deisseroth, 2004; Paez-Gonzalez et al., 2014). It was shown thereby that excitatory stimuli act on adult hippocampal neural stem/progenitor cells (NSPC) to favor neuron production. In the present study, electrical activities were not specifically measured in new-born cells, but it is plausible that an overall inhibitory tone in the GCL/SGZ was intrinsically sensed by NSPC and disturbed excitation-neurogenesis coupling. Importantly, inhibitory effects of 5-HT on electrophysiological activities of neurons have also been reported in other areas in the hippocampus, for example, optogenetic stimulation of raphe nuclei has been

shown to suppress ripples in the CA1 (Wang et al., 2015) or spiking activities in the ventral hippocampus (Yoshida et al., 2019).

In the present study, both DRN and MRN stimulation showed inhibitory effects on neuronal activities in the DG. Based on the action potential properties observed in the current study, such an inhibitory influence seemed to work on both principal cells and interneurons. Principal cells are primarily GCs and interneurons can be, among others, GABAergic interneurons such as CCK-expressing or PV-expressing interneurons in the DG. According to a previous study by Medrihan and colleagues (Medrihan et al., 2017), GCs, CCK neurons, and PV neurons correspond to bursting cells with wide action potential (w BS), non-bursting cells with wide action potential (w non-BS), and cells with narrow action potential (n), respectively. The results obtained in the present study indicate that optogenetic stimulation of raphe nuclei suppresses activities of all these measured cell types.

Anatomically, serotonergic inputs to the DG mainly originate from the MRN and project most densely to the hilus, especially to its subgranular portion (reviewed in Scharfman and Myers, 2012). The suprapyramidal blade was found to be more heavily innervated. Especially, it was shown that the CCK neurons are highly responsive to 5-HT and are a major target of serotonergic projections from the MRN (**Fig. 4.1**; Umschweif et al., 2019). The results from the current study suggest that optogenetic stimulation of MRN induced 5-HT release in the hilus and SGZ, which directly exerted inhibitory effects on the CCK neurons via inhibitory 5-HT_{2A} and 5-HT_{1B} receptors. A previous study has shown that 5-HT_{2A} activation hyperpolarizes the membrane potential of CCK neurons, whereas activation of 5-HT_{1B} receptors, which are expressed in axon terminals, inhibits GABA release from CCK neurons. Since CCK neurons exert GABAergic inhibition on GCs, it is counterintuitive that serotonin-mediated inhibition of CCK neurons is accompanied by inhibition of GCs. This can be explained in that GCs receive GABAergic inhibition from PV neurons, which in turn are inhibited by CCK neurons. Serotonin-mediated inhibition of CCK neurons is thus supposed to lead to disinhibition of PV neurons (Umschweif et al., 2019), resulting in the suppression of GCs, although disinhibition of PV neurons was not observed in the current study (**Fig. 4.1**). This discrepancy could be partly explained by the difference in experimental conditions, i.e., *ex vivo* vs. *in vivo* recordings or whether the activities of PV neurons were measured after direct chemogenetic inhibition of CCK neurons (Medrihan et al., 2017) vs. after optogenetic activation of raphe serotonergic neurons as in the current study.

On the other hand, DRN sends a less dense bundle of axons to the OML through the entorhinal cortex and its projection site overlaps with that of the LPP (**Fig. 4.1**). DRN stimulation supposedly inhibits activities of GCs via volume transmission of 5-HT onto the molecular layer, mediated by inhibitory 5-HT_{1A} receptors. Inhibition of both principal cells and interneurons in response to DRN stimulation is probably because DRN projections do not form synaptic connections but that rather 5-HT release from their terminals is mediated by volume transmission, exerting effects of 5-HT in a wider area extrasynaptically.

As an entity already highly integrated into the hippocampal circuitry, past studies have proposed interneurons as a prime candidate to influence the proliferation, survival, and maturation of adult-generated cells in the DG (Masiulis et al., 2011; Song et al., 2013; Catavero et al., 2018; Yi et al., 2020; Groisman et al., 2020). Song and colleagues showed that optogenetic activation of PV-positive GABAergic interneurons maintain the quiescence of neural stem cells by tonic release of GABA while promoting newborn neuronal progeny survival and development (Song et al., 2013). Augmented inhibition on GCs from PV cells, which was mediated by inhibition of CCK cells via 5-HT, may have disturbed this balance of tonic inhibition and led to excessive inhibition of GCs, resulting in suppression of cell proliferation. Interestingly, a recent study has shown that after chronic administration of SSRI antidepressants, inhibitory effects from PV cells on GCs became mitigated through expression of inhibitory 5-HT_{5A} receptors on PV cells (Sagi et al., 2020). In accordance with this, it was shown that the delayed behavioral effects of chronic SSRI treatment is mediated by 5-HT_{5A} receptors on PV cells (Sagi et al., 2020), whereas the initial behavioral effects induced by SSRIs start with the inhibition of CCK cells in the DG, leading to disinhibition of PV cells and reduced excitability of GCs (Medrihan et al., 2017).

Taken together, it can be postulated that 5-HT as an inhibitory neurotransmitter inhibits neuronal activities in the DG, at least in its acute phase, which then reduces the generation of new cells. In response to altered 5-HT levels in the long term, receptor compositions may change, which may counteract the acute inhibitory effects of 5-HT.

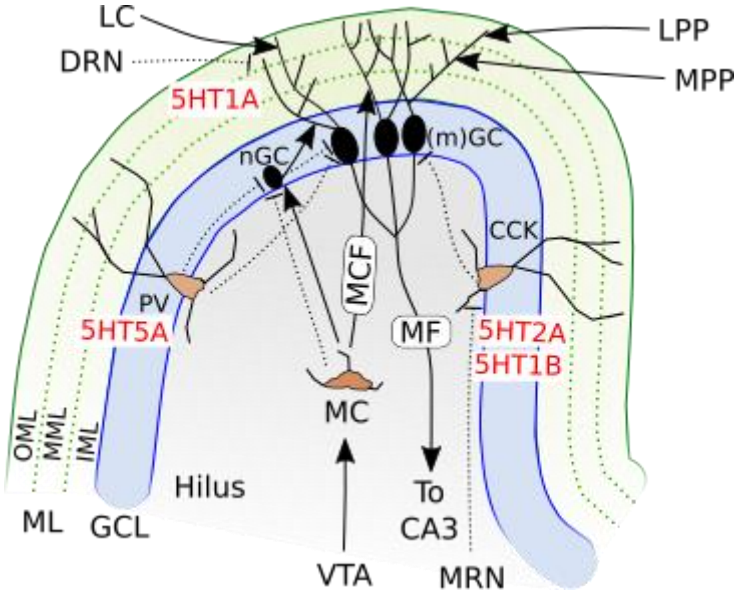

Fig. 4.1. Neuronal connection and serotonergic inputs in the rodent dentate gyrus (DG). The main excitatory input to the granule cells (GC) is the perforant path (PP). The lateral perforant path (LPP) projects to the distal dendrites of GC located in the outer molecular layer (OML). The medial perforant path (MPP), on the other hand, projects to the more proximal dendrites located in the middle molecular layer (MML). Moreover, the distal dendrites of the GC receive serotonergic inputs from the dorsal raphe nucleus (DRN). Dopaminergic neurons in the locus coeruleus (LC) project to the distal dendrites of the GC and excite GC through activation of dopaminergic receptors. Another dopaminergic projection originates from the ventral tegmental area (VTA), which sends axonal projections to the hilar mossy cells (MC) and indirectly modulates GC activity. MC activate the mature GC through glutamatergic inputs, called mossy cell fibers (MCF), onto the proximal dendrites located in the inner molecular layer (IML). Inhibition in the DG is mediated by GABAergic interneurons such as cholecystokinin (CCK) basket cells and parvalbumin (PV) basket cells. These neurons strongly inhibit the GC through perisomatic inhibition to keep them mostly silent. The inhibition via CCK cells is regulated by serotonergic inputs from the median raphe nucleus (MRN). PV cells modulate neurogenesis by keeping the newborn granule cells (nGC) quiescent. nGCs then modulate activities of mature GCs (mGCs) in response to PP synaptic inputs from the entorhinal cortex (EC). To be precise, nGCs inhibit mGCs in response to LPP inputs from the lateral EC, whereas nGCs excite mGCs in response to MPP inputs from the medial EC (Luna et al., 2019). After integrating all distal and proximal synaptic inputs, GCs transmit the information through hilar mossy fibers (MF) to CA3. Arrows indicate excitation, dashed lines inhibition. Figure modified from Umschweif et al., 2019 with permission.

An alternative explanation for reduced cell proliferation and reduced 5-HT contents is that 5-HT indeed works positively for cell proliferation and the reduced cell proliferation resulted from reduced 5-HT release. It is rather counterintuitive, however, that optogenetic stimulation of raphe nuclei led to a reduced release of 5-HT. For the understanding of this phenomenon, autoinhibitory regulation of 5-HT release plays an important role. That is, optogenetically activated serotonergic neurons released 5-HT, but the released 5-HT bound to the inhibitory 5-HT_{1A} receptors on the soma of the serotonergic neuron, hyperpolarizing the neuron and

limiting further release of 5-HT (Araragi et al., 2013; Andrade et al., 2015). Moreover, 5-HT_{1B} receptors located on the axon terminals of serotonergic neurons also worked as inhibitory autoreceptors to inhibit 5-HT release (Nautiyal et al., 2016). Due to this autoinhibition, it is plausible that 5-HT release was inhibited at intervals between optogenetic stimulation, and the net 5-HT release was reduced despite the repeated optogenetic stimulation, which took place every 5 minutes in the current study. Autoinhibition and reduced 5-HT release despite serotonergic activation has previously been reported in a study using electrical stimulation of raphe nuclei (Mokler et al., 1998). They had reported that electric stimulation of DRN and MRN led to a significant decrease of 5-HT release in the dorsal hippocampus in a frequency-dependent manner. At 20 Hz, the frequency used in the current study, electrical stimulation resulted in reduced 5-HT release while 5 or 10 Hz stimulation led to less pronounced 5-HT reduction. Contrarily, the same stimulation protocol led to a significant increase in 5-HT release in the anesthetized animals. Mokler and colleagues have postulated that such a difference may relate to the difference in the degree of autoinhibition of serotonergic neurons between anesthetized and unanesthetized animals. The observed inhibitory effect of 5-HT release on the electrical activities in the DG can be explained by less prominent autoinhibition since all the recordings were conducted in anesthetized animals in the current study. In short, although optogenetic stimulation of serotonergic neurons in raphe nuclei induced 5-HT release, released 5-HT inhibited the further release of 5-HT at intervals between optogenetic stimulation through autoinhibition *in vivo*, which may have resulted in the net decrease of 5-HT contents in both the hippocampus and raphe nuclei.

To summarize, reduced cell proliferation in the DG could be mediated by an electrophysiologically measured inhibitory influence of 5-HT on the DG. Repeated optogenetic stimulations of serotonergic neurons in raphe nuclei and subsequent 5-HT release may have resulted in depletion of 5-HT storage or significant autoinhibition of 5-HT release between stimulations. Both scenarios could explain reduced 5-HT contents in the tissues, as measure by HPLC analysis. Reduction of 5-HT as a mitogenic factor then could have further contributed to reduced cell proliferation in the hippocampus.

4.4. Potential relevance to antidepressant drugs action on the serotonergic system

Past studies have demonstrated that diverse classes of antidepressant drugs such as fluoxetine, imipramine, reboxetine, and tranylcypromine increase cell proliferation in the DG of mice and rats (Boldrini et al., 2009 and references therein). Among such antidepressants, SSRI are known to specifically block serotonin transporters, which take up released 5-HT in the synaptic cleft into presynaptic terminals. As a result, an SSRI is believed to unfold its effects by enhancing synaptic 5-HT transmission. Past studies have shown that chronic administration of SSRIs, such as fluoxetine, facilitates progenitor proliferation, survival, and the early maturation phase in the DG, which is associated with improvement of depressive symptoms (reviewed in Segi-Nishida, 2017). It has been demonstrated that chronic SSRIs can also restore stress- or corticosterone-induced reduction in neurogenesis (see Segi-Nishida, 2017). Moreover, postmortem brains of SSRI-treated patients with major depressive disorder showed a higher number of neuronal progenitors and mature granule cells in the DG than those of untreated patients (Boldrini et al., 2009; 2013 as in Segi-Nishida, 2017). Not only SSRI but other antidepressants such as tricyclic antidepressants (TCAs) which work rather unspecifically on several neurotransmitter systems have also been shown to positively influence neurogenesis. Interestingly, it was shown in a postmortem study of human brains, that the number of NPCs in the DG was not different between SSRI- and TCA-treated patients with major depressive disorder (MDD). Moreover, dividing cell numbers were greater in TCA-treated patients than in SSRI-treated patients (Boldrini et al., 2009).

Given this, the observation that direct serotonergic activation resulted in 5-HT reduction and inhibited hippocampal cell proliferation was rather unexpected. It should be noted, however, that pro-neurogenic effects of fluoxetine, such as increased cell proliferation in the hippocampus, emerge only after chronic treatment and not from an acute administration of this drug (Malberg et al., 2000; Santarelli et al., 2003; Encinas et al., 2006; Klempin et al., 2010). Moreover, the effects of therapeutic antidepressant themselves become apparent only after chronic treatment of several weeks and, by initiation of treatment, an exacerbation of anxiety is often observed (Burghardt and Bauer, 2013). Further, in healthy human subjects, acute SSRI administration has been shown to impair learning and cognitive flexibility (Skandali et al., 2018) or to affect the processing of social cues such as recognition of fearful and happy facial expressions (Harmer et al., 2003). Therefore, effects of SSRIs should be differentiated as to whether they are acute or chronic effects. The results from overnight optogenetic stimulation in the current study may mimic acute effects of SSRIs, which largely

manifest as adverse effects on neural functions. The delayed therapeutic effects of chronic SSRI are likely to be mediated by desensitization of autoinhibitory 5-HT_{1A} receptors. This in turn leads to disinhibition of serotonergic neurons from the negative feedback of 5-HT release, resulting in enhanced 5-HT neurotransmission (Turcotte-Cardin et al., 2019 and references therein). Indeed, in an pharmacokinetic study, it was demonstrated that after acute administration of increasing concentrations of an SSRI, further release of new 5-HT was blocked, indicating the presence of negative feedback mediated by inhibitory 5-HT autoreceptors (Bundgaard et al., 2006). Thus, a therapeutic benefit of combining an SSRI with a 5-HT_{1A} receptor antagonist had been discussed, at least for a short time at the initial phase of the SSRI-antidepressant treatment (Newman et al., 2004; Castro et al., 2008).

Moreover, it should be noted that the fact that antidepressant treatment is associated with increased neurogenesis does not necessarily mean that it is the mechanism of antidepressant action. Nonetheless, evidence suggests that cell proliferation in the DG is most likely required for antidepressants to unfold their therapeutic effects since inhibition of neurogenesis has been demonstrated to block some behavioral effects of antidepressants (Santarelli et al., 2003).

4.5. Cell proliferation normalized after one week of optogenetic stimulation

In the current study, raphe nuclei were optogenetically stimulated for the maximum duration of 6 nights to compare the results with those obtained from one-night stimulation experiments. Moreover, a 6-night approach was chosen to mimic results obtained earlier, to determine whether the running-induced increase in cell proliferation is due to increased 5-HT synthesis in raphe nuclei that directly affects the DG (Klempin et al 2013). After 6 nights of stimulation, however, the total number of BrdU-positive cells was not different from that of unstimulated control groups. Instead, only hemispheric differences were observed, i.e., the ipsilateral side to the optic fiber insertion had a lower number of BrdU-positive cells. Anatomically, serotonergic projections from the DRN were shown to have more laterality than those from the MRN, whereby ipsilateral projections are more predominant (Azmitia, 1981; Kanno et al., 2008). Moreover, neurons in the dorsolateral dorsal raphe nucleus (dlDR) or lateral areas have more ipsilateral projections compared to raphe neurons located along the midline of the raphe nucleus (Kanno et al., 2008; Waselus et al., 2011). In the present study, optic fiber ferrules were implanted into the right hemisphere at a specific angle. Given that

light intensity is exponentially attenuated with increasing distance in the brain (Aravanis et al., 2007; Yizhar et al., 2011; Stark et al., 2012), it is plausible that the right side of the DRN was more intensely illuminated than the left side. Although acute overnight stimulation reduced the number of BrdU-positive cells in the whole brain, it is also likely that after repeated stimulations of 6 nights, adaptive changes occurred, revealing inhibitory influence of stimulation only in the ipsilateral hippocampus, which received more intense serotonergic projections than the contralateral hippocampus. Taking the HPLC data from the acute experiments into account, 5-HT content might either have recovered, or cell proliferation increased to compensate for the earlier loss after one-week stimulation. The observed laterality in the present study could have derived from such an interplay of adaptive changes and anatomical projections. Such compensation was unlikely to be mediated by increased running activities since the cumulative track length after 6 nights was not significantly different between the Ctrl and Stim groups. One of the potential mechanisms, which may have contributed to the recovery of cell reduction is desensitization of 5-HT_{1A} autoinhibitory receptors. The receptors are known to inhibit 5-HT release, which would have worked negatively on cell proliferation. After repeated optogenetic activation of serotonergic neurons and the accompanying acute release of 5-HT for 6 nights, 5-HT_{1A} receptors could have become gradually desensitized, limiting autoinhibition-induced reduction of 5-HT at intervals between optogenetic stimulation. The proposed mechanism has a close resemblance to the mechanism of delayed therapeutic effects of chronic SSRI treatment (see the previous section).

Similarly, repeated optogenetic stimulation of serotonergic neurons for 6 nights may have caused adaptive changes in the postsynaptic sites, for example, in the hippocampus, which may explain the partial recovery from the initial reduction in cell proliferation. In particular, it is plausible that electrophysiologically observed inhibitory effects on DG neuronal activities during the optogenetic stimulation of serotonergic neurons may have become attenuated after repeated optogenetic stimulation of serotonergic neurons and subsequent 5-HT release. As an analogue to this, a past study demonstrated that chronic administration of an SSRI, fluoxetine, increased population spike amplitude and EPSP slopes in the DG of anesthetized rats compared to placebo controls (Stewart and Reid, 2000), although a more recent study conducted in freely moving rats could not demonstrate this electrophysiological alteration after chronic fluoxetine treatment (Keith et al., 2007).

It would be interesting, therefore, to see if even longer stimulation paradigms, e.g., 2–3 weeks of stimulation, as in correspondence with a typical latency until therapeutic effects of SSRI

antidepressants take place, reverse the inhibitory effects of acute optogenetic stimulation on cell proliferation and turn into pro-proliferative stimuli for adult hippocampal neurogenesis.

4.6. Optogenetic stimulation transiently enhanced locomotion without significantly changing the total distances traveled.

In this study, the total traveled distances during the overnight and one-week optogenetic stimulation were measured since a number of past studies had demonstrated positive effects of locomotion on adult neurogenesis (1999b; van Praag et al., 1999a; Kronenberg et al., 2003). The reasoning was that acute and long-term exercises may influence 5-HT release. Microdialysis studies in rats have shown that running exercises significantly increased 5-HT concentration in the hippocampus during exercise, which however returned to baseline with 1–2 hours delay (Meeusen et al., 1996; Béquet et al., 2001). The 5-HT increase was accompanied by an increase in Trp, or was augmented by supplementation of Trp, implicating involvement of 5-HT synthesis (Meeusen et al., 1996; Gomez-Merino et al., 2001).

Since the traveled distances in the present study were not significantly different between the stimulated and control groups, it can be assumed that reduced cell proliferation observed in the DG was not due to reduced locomotive activity. Instead, it can be postulated that the release of 5-HT in the DG, which resulted from the optogenetic raphe stimulation, influenced cell proliferation in the DG.

In the current study, however, optogenetic stimulation of DRN or MRN was shown to transiently facilitate locomotive behaviors. This finding corresponds with recent reports, where optogenetic approaches also had been used (Balázsfi et al., 2017; Gölöncsér et al., 2017; Teixeira et al., 2018). In classical studies, effects of 5-HT on locomotion were assessed by direct electrical stimulation of raphe nuclei. It was shown that the electrical stimulation (100 Hz, 0.1 ms pulses) of the DRN produced locomotion accompanied by hippocampal and cortical activities. The same stimulation of the MRN, on the other hand, produced behavioral freezing or an unnatural forced movement with cerebral activities (Peck and Vanderwolf, 1991). To be precise, it has been suggested that ascending serotonergic projections are involved in the so-called Type 1 behavior (walking, moving the head about, changing posture, or in general, enhanced locomotion), whereas cholinergic inputs play a role in the Type 2 behavior (waking immobility, face-washing, gnashing the teeth together, tremor; Peck and Vanderwolf, 1991; Gölöncsér et al., 2017). It should also be noted that central 5-HT can

modulate locomotor activities at the peripheral level by directly acting on the spinal cord (Bacqué-Cazenave et al., 2020 and references therein).

In the study presented here, the total distances traveled were not significantly different between the DRN-stimulated group and its control group, both after overnight and one-week stimulation. Transient behavioral changes of DRN-stimulated animals showed certain characteristics, namely, behavioral increase was first observed after the light stimulation, not during the stimulation. Interestingly, Correia and colleagues showed that optogenetic stimulation of DRN transiently and rapidly slows down the locomotion, although repeated stimulations facilitate locomotion in the long-term (Correia et al., 2017). More precisely, acute stimulation suppressed spontaneous locomotion in the open field with rapid onset (≤1 s), independent of anxiety or motor impairment. Inhibition of locomotion, however, could be overcome by strong motivational drive such as food intake. Contrarily, repeated 15 min daily stimulation over three weeks led to an increase in locomotion, indicating that DRN serotonergic stimulation has short-term and long-term effects on locomotion (Correia et al., 2017). The delayed increase in behavioral parameters observed in the current study could be due to the mixed effects of facilitation and inhibition during the light stimulation. Immediately after the light stimulation, such inhibitory effects ceased, resulting in the net increase in behavioral parameters measured.

The cumulative curve of traveled distances from MRN-stimulated animals revealed a particular characteristic; at the beginning it showed almost the same or a slightly higher slope than that of controls but was followed by a sudden decrease after a few hours of stimulation. A previous study demonstrated a similar phenomenon, i.e., optogenetic stimulation of MRN led to a sudden increase in locomotive activities, while total explorative behaviors were reduced (Gölöncsér et al., 2017; Balázsfi et al., 2017). The hypothesis states that MRN stimulation is perceived as an unpleasant aversive stimulus as with electric shocks. This may have resulted in shock-induced runs, i.e., sudden increase in locomotive activities, while reducing total explorative behaviors. In line with this, it has been shown that MRN stimulation results in the activation of neural regions involved in the processing of stress and aversive stimuli (Balázsfi et al., 2017). Similarly, it was shown in another study that long-term optogenetic stimulation of MRN led to an increased freezing 7 days after the stimulation (Gölöncsér et al., 2017).

Moreover, as shown in the present study, the absolute changes in peri-stimulus behavioral parameters were more pronounced in MRN stimulated animal groups than in the DRN

stimulated animals. This corresponds to another reported study, where the authors assumed that this could be explained as stress responses in the MRN-stimulated animals (Teixeira et al., 2018). Taken together, MRN stimulated animals may have experienced additional stressful and unpleasant effects compared to DRN-stimulated animals after repeated light stimulation, resulting in reduced total traveled distances, although not significant, compared to non-stimulated control groups.

Conclusion

First, it was shown that *ex vivo* and *in vivo* optogenetic stimulation of raphe nuclei specifically activated serotonergic neurons in Tph2-mhChR2-EYFP mice, confirming the validity of the experimental animal model used in the current study. Optogenetic stimulation of raphe led to suppression of neuronal firing activities in the DG. Stimulation overnight (8 hours) in freely behaving mice resulted in reduced cell proliferation in the DG, accompanied by a reduction of 5-HT levels in the raphe nuclei and hippocampus. Reduced cell proliferation in the DG could be mediated by an inhibitory influence of 5-HT on the DG, as measured by electrophysiological recordings. Repeated optogenetic stimulations of raphe nuclei and subsequent 5-HT release caused depletion of 5-HT storage or substantial autoinhibition of 5-HT release between stimulations, leading in either way to reduced 5-HT contents in the tissues. When taking 5-HT into account as a mitogenic factor, this reduction in the 5-HT level itself may have further contributed to reduced cell proliferation in the DG.

Continued raphe activation for one week had no effect on the total number of newly generated cells but resulted in reduced cell proliferation on the ipsilateral side of fiber optic implantation. Although optogenetic raphe stimulation transiently increased locomotive behaviors of mice, the total distances traveled overnight and after 6 nights were not significantly different between control and stimulated groups, indicating that reduced cell proliferation cannot be explained by reduced physical activities. The results may be important in the understanding of antidepressant mechanisms that include an exacerbation in depressive symptoms in patients during the acute early phase of SSRI treatment. It needs to be seen if an even longer stimulation paradigm of 2–3 weeks, which corresponds to the typical latency in the therapeutic effects of SSRIs, would reverse the inhibitory effects of acute stimulation on cell proliferation, and become a pro-proliferative stimulus for adult neurogenesis in rodents.

References

Aghajanian GK, Rasmussen K (1989) Intracellular studies in the facial nucleus illustrating a simple new method for obtaining viable motoneurons in adult rat brain slices. Synapse 3. 4:331–338.

Aimone J, Jessberger S, Gage F (2007) Adult neurogenesis. Scholarpedia 2. 2:2100.

Alenina N, Klempin F (2015) The role of serotonin in adult hippocampal neurogenesis. Behavioural Brain Research 277:49–57.

Amaral DG, Scharfman HE, Lavenex P (2007) The dentate gyrus: fundamental neuroanatomical organization (dentate gyrus for dummies). In: Progress in Brain Research : The Dentate Gyrus: A Comprehensive Guide to Structure, Function, and Clinical Implications (Scharfman HE, ed), pp 3–790. Elsevier.

Andersen P (2007) The hippocampus book. Oxford, New York: Oxford University Press.

Andrade R, Haj-Dahmane S (2013) Serotonin neuron diversity in the dorsal raphe. ACS Chemical Neuroscience 4. 1:22–25.

Andrade R, Huereca D, Lyons JG, Andrade EM, McGregor KM (2015) 5-HT1A Receptor-Mediated Autoinhibition and the Control of Serotonergic Cell Firing. ACS Chemical Neuroscience 6. 7:1110–1115.

Anikeeva P, Andalman AS, Witten I, Warden M, Goshen I, Grosenick L, Gunaydin LA, Frank LM, Deisseroth K (2011) Optetrode: a multichannel readout for optogenetic control in freely moving mice. Nature Neuroscience 15. 1:163–170.

Araragi N, Alenina N, Bader M (2022) Carbon-mixed dental cement for fixing fiber optic ferrules prevents visually triggered locomotive enhancement in mice upon optogenetic stimulation. Heliyon 8. 1:e08692.

Araragi N, Lesch K-P (2013) Serotonin (5-HT) in the regulation of depression-related emotionality: insight from 5-HT transporter and tryptophan hydroxylase-2 knockout mouse models. Current drug targets 14. 5:549–570.

Araragi N, Mlinar B, Baccini G, Gutknecht L, Lesch K-P, Corradetti R (2013) Conservation of 5-HT1A receptor-mediated autoinhibition of serotonin (5-HT) neurons in mice with altered 5-HT homeostasis. Frontiers in Pharmacology 4:97.

Aravanis AM, Wang L-P, Zhang F, Meltzer LA, Mogri MZ, Schneider MB, Deisseroth K (2007) An optical neural interface: in vivo control of rodent motor cortex with integrated fiberoptic and optogenetic technology. Journal of Neural Engineering 4. 3:S143-56.

Asaoka N, Nishitani N, Kinoshita H, Kawai H, Shibui N, Nagayasu K, Shirakawa H, Nakagawa T, Kaneko S (2017) Chronic antidepressant potentiates spontaneous activity of dorsal raphe serotonergic neurons by decreasing GABAB receptor-mediated inhibition of L-type calcium channels. Scientific Reports 7. 1:13609.

Azmitia EC (1981) Bilateral serotonergic projections to the dorsal hippocampus of the rat: simultaneous localization of 3H-5HT and HRP after retrograde transport. The Journal of comparative neurology 203. 4:737–743.

Bacqué-Cazenave J, Bharatiya R, Barrière G, Delbecque J-P, Bouguiyoud N, Di Giovanni G, Cattaert D, Deurwaerdère P de (2020) Serotonin in Animal Cognition and Behavior. International journal of molecular sciences 21. 5:1649.

Balázsfi DG, Zelena D, Farkas L, Demeter K, Barna I, Cserép C, Takács VT, Nyíri G, Gölöncsér F, Sperlágh B, Freund TF, Haller J (2017) Median raphe region stimulation alone generates remote, but not recent fear memory traces. PLOS ONE 12. 7:e0181264.

Barnes NM, Sharp T (1999) A review of central 5-HT receptors and their function. Neuropharmacology 38. 8:1083–1152.

Beck SG, Pan Y-Z, Akanwa AC, Kirby LG (2004) Median and dorsal raphe neurons are not electrophysiologically identical. Journal of Neurophysiology 91. 2:994–1005.

Beecher K, Belmer A, Bartlett SE (2019) Anatomy of the Serotonin Transporter. In: Serotonin, pp 121–133. Elsevier.

Beliveau V, Svarer C, Frokjaer VG, Knudsen GM, Greve DN, Fisher PM (2015) Functional connectivity of the dorsal and median raphe nuclei at rest. NeuroImage 116:187–195.

Belmer A, Klenowski PM, Patkar OL, Bartlett SE (2016) Excitatory/inhibitory balance of serotonergic axon connectivity in the brain. Journal of Neurology & Neuromedicine 1. 9:18–22.

Belmer A, Klenowski PM, Patkar OL, Bartlett SE (2017) Mapping the connectivity of serotonin transporter immunoreactive axons to excitatory and inhibitory neurochemical synapses in the mouse limbic brain. Brain structure & function 222. 3:1297–1314.

Béquet F, Gomez-Merino D, Berthelot M, Guezennec CY (2001) Exercise-induced changes in brain glucose and serotonin revealed by microdialysis in rat hippocampus: effect of glucose supplementation. Acta physiologica Scandinavica 173. 2:223–230.

Bitzenhofer SH, Ahlbeck J, Hanganu-Opatz IL (2017) Methodological Approach for Optogenetic Manipulation of Neonatal Neuronal Networks. Frontiers in Cellular Neuroscience 11:239.

Boldrini M, Santiago AN, Hen R, Dwork AJ, Rosoklija GB, Tamir H, Arango V, John Mann J (2013) Hippocampal granule neuron number and dentate gyrus volume in antidepressant-treated and untreated major depression. Neuropsychopharmacology 38. 6:1068–1077.

Boldrini M, Underwood MD, Hen R, Rosoklija GB, Dwork AJ, John Mann J, Arango V (2009) Antidepressants increase neural progenitor cells in the human hippocampus. Neuropsychopharmacology 34. 11:2376–2389.

Bortolato M, Chen K, Shih JC (2008) Monoamine oxidase inactivation: from pathophysiology to therapeutics. Advanced drug delivery reviews 60. 13-14:1527–1533.

Boyden ES, Zhang F, Bamberg E, Nagel G, Deisseroth K (2005) Millisecond-timescale, genetically targeted optical control of neural activity. Nature Neuroscience 8. 9:1263–1268.

Brezun J, Daszuta A (1999) Depletion in serotonin decreases neurogenesis in the dentate gyrus and the subventricular zone of adult rats. Neuroscience 89. 4:999–1002.

Brezun JM, Daszuta A (2000) Serotonergic reinnervation reverses lesion-induced decreases in PSA-nCAM labeling and proliferation of hippocampal cells in adult rats. Hippocampus 10. 1:37–46.

Brown RE, McKenna JT, Winston S, Basheer R, Yanagawa Y, Thakkar MM, McCarley RW (2008) Characterization of GABAergic neurons in rapid-eye-movement sleep controlling regions of the brainstem reticular formation in GAD67-green fluorescent protein knock-in mice. European Journal of Neuroscience 27. 2:352–363.

Bundgaard C, Larsen F, Jørgensen M, Gabrielsson J (2006) Mechanistic model of acute autoinhibitory feedback action after administration of SSRIs in rats: application to escitalopram-induced effects on brain serotonin levels. European Journal of Pharmaceutical Sciences 29. 5:394–404.

Bunin MA, Wightman RM (1998) Quantitative Evaluation of 5-Hydroxytryptamine (Serotonin) Neuronal Release and Uptake: An Investigation of Extrasynaptic Transmission. Journal of Neuroscience 18. 13:4854–4860.

Burghardt NS, Bauer EP (2013) Acute and chronic effects of selective serotonin reuptake inhibitor treatment on fear conditioning: implications for underlying fear circuits. Neuroscience 247:253–272.

Cao L, Hu R, Xu T, Zhang Z-N, Li W, Lu J (2017) Characterization of Induced Pluripotent Stem Cell-derived Human Serotonergic Neurons. Frontiers in Cellular Neuroscience 11:131.

Cardin JA, Carlén M, Meletis K, Knoblich U, Zhang F, Deisseroth K, Tsai L-H, Moore CI (2010) Targeted optogenetic stimulation and recording of neurons in vivo using cell-type-specific expression of Channelrhodopsin-2. Nature Protocols 5. 2:247–254.

Carey RJ, Müller CP (2013) Serotonin and Behavioral Stimulant Effects of Addictive Drugs. In: Biological Research on Addiction, pp 231–239. Elsevier.

Carlsson A, Davis JN, Kehr W, Lindqvist M, Atack CV (1972) Simultaneous measurement of tyrosine and tryptophan hydroxylase activities in brain in vivo using an inhibitor of the aromatic amino acid decarboxylase. Naunyn-Schmiedeberg's archives of pharmacology 275. 2:153–168.

Castro E, Díaz A, Rodriguez-Gaztelumendi A, Del Olmo E, Pazos A (2008) WAY100635 prevents the changes induced by fluoxetine upon the 5-HT1A receptor functionality. Neuropharmacology 55. 8:1391–1396.

Catavero C, Bao H, Song J (2018) Neural mechanisms underlying GABAergic regulation of adult hippocampal neurogenesis. Cell and Tissue Research 371. 1:33–46.

Chancey JH, Poulsen DJ, Wadiche JI, Overstreet-Wadiche L (2014) Hilar mossy cells provide the first glutamatergic synapses to adult-born dentate granule cells. Journal of Neuroscience 34. 6:2349–2354.

Chow BY, Han X, Dobry AS, Qian X, Chuong AS, Li M, Henninger MA, Belfort GM, Lin Y, Monahan PE, Boyden ES (2010) High-performance genetically targetable optical neural silencing by light-driven proton pumps. Nature 463. 7277:98–102.

Ciranna L (2006) Serotonin as a modulator of glutamate- and GABA-mediated neurotransmission: implications in physiological functions and in pathology. Current neuropharmacology 4. 2:101–114.

Correia PA, Lottem E, Banerjee D, Machado AS, Carey MR, Mainen ZF (2017) Transient inhibition and long-term facilitation of locomotion by phasic optogenetic activation of serotonin neurons. eLife 6:e20975.

Daroff R, Aminoff MJ (2003) Encyclopedia of the neurological sciences. Amsterdam: Elsevier.

Day HEW, Greenwood BN, Hammack SE, Watkins LR, Fleshner M, Maier SF, Campeau S (2004) Differential expression of 5HT-1A, alpha 1b adrenergic, CRF-R1, and CRF-R2 receptor mRNA in serotonergic, gamma-aminobutyric acidergic, and catecholaminergic cells of the rat dorsal raphe nucleus. The Journal of comparative neurology 474. 3:364–378.

Deisseroth K (2004) Excitation-Neurogenesis Coupling in Adult Neural Stem/Progenitor Cells. Neuron 42. 42:535–552.

De-Miguel FF, Leon-Pinzon C, Noguez P, Mendez B (2015) Serotonin release from the neuronal cell body and its long-lasting effects on the nervous system. Philosophical transactions of the Royal Society of London. Series B, Biological sciences 370. 1672.

De-Miguel FF, Trueta C (2005) Synaptic and extrasynaptic secretion of serotonin. Cellular and molecular neurobiology 25. 2:297–312.

Deubner J, Coulon P, Diester I (2019) Optogenetic approaches to study the mammalian brain. Current Opinion in Structural Biology 57:157–163.

Diaz SL, Doly S, Narboux-Nême N, Fernández S, Mazot P, Banas SM, Boutourlinsky K, Moutkine I, Belmer A, Roumier A, Maroteaux L (2012) 5-HT(2B) receptors are required for serotonin-selective antidepressant actions. Molecular Psychiatry 17. 2:154–163.

Diaz SL, Narboux-Nême N, Trowbridge S, Scotto-Lomassese S, Kleine Borgmann FB, Jessberger S, Giros B, Maroteaux L, Deneris E, Gaspar P (2013) Paradoxical increase in survival of newborn neurons in the dentate gyrus of mice with constitutive depletion of serotonin. European Journal of Neuroscience 38. 5:2650–2658.

Dugué GP, Lörincz ML, Lottem E, Audero E, Matias S, Correia PA, Léna C, Mainen ZF (2014) Optogenetic recruitment of dorsal raphe serotonergic neurons acutely decreases mechanosensory responsivity in behaving mice. PLOS ONE 9. 8:e105941.

Encinas JM, Vaahtokari A, Enikolopov G (2006) Fluoxetine targets early progenitor cells in the adult brain. Proceedings of the National Academy of Sciences 103. 21:8233–8238.

Ernst A, Frisén J (2015) Adult neurogenesis in humans- common and unique traits in mammals. PLOS Biology 13. 1:e1002045.

Erofeev A, Gerasimov E, Lavrova A, Bolshakova A, Postnikov E, Bezprozvanny I, Vlasova OL (2019) Light Stimulation Parameters Determine Neuron Dynamic Characteristics. Applied Sciences 9. 18:3673.

Fujita S, Toyoda I, Thamattoor AK, Buckmaster PS (2014) Preictal activity of subicular, CA1, and dentate gyrus principal neurons in the dorsal hippocampus before spontaneous seizures in a rat model of temporal lobe epilepsy. Journal of Neuroscience 34. 50:16671–16687.

Gold C, Henze DA, Koch C, Buzsáki G (2006) On the origin of the extracellular action potential waveform: A modeling study. Journal of Neurophysiology 95. 5:3113–3128.

Gölöncsér F, Baranyi M, Balázsfi D, Demeter K, Haller J, Freund TFF, Zelena D, Sperlágh B (2017) Regulation of Hippocampal 5-HT Release by P2X7 Receptors in Response to Optogenetic Stimulation of Median Raphe Terminals of Mice. Frontiers in Molecular Neuroscience 10:325.

Gomez-Merino D, Béquet F, Berthelot M, Riverain S, Chennaoui M, Guezennec CY (2001) Evidence that the Branched-Chain Amino Acid L-Valine Prevents Exercise-Induced Release of 5-HT in Rat Hippocampus. International Journal of Sports Medicine. 22:317–322.

Gonçalves JT, Schafer ST, Gage FH (2016) Adult Neurogenesis in the Hippocampus: From Stem Cells to Behavior. Cell 167. 4:897–914.

GoodSmith D, Chen X, Wang C, Kim SH, Song H, Burgalossi A, Christian KM, Knierim JJ (2017) Spatial Representations of Granule Cells and Mossy Cells of the Dentate Gyrus. Neuron 93. 3:677-690.e5.

Gradinaru V, Zhang F, Ramakrishnan C, Mattis J, Prakash R, Diester I, Goshen I, Thompson KR, Deisseroth K (2010) Molecular and cellular approaches for diversifying and extending optogenetics. Cell 141. 1:154–165.

Greene J, Banasr M, Lee B, Warner-Schmidt J, Duman RS (2009) Vascular endothelial growth factor signaling is required for the behavioral actions of antidepressant treatment: pharmacological and cellular characterization. Neuropsychopharmacology 34. 11:2459–2468.

Groisman AI, Yang SM, Schinder AF (2020) Differential Coupling of Adult-Born Granule Cells to Parvalbumin and Somatostatin Interneurons. Cell reports 30. 1:202-214.e4.

Guru A, Post RJ, Ho Y-Y, Warden MR (2015) Making Sense of Optogenetics. The international journal of neuropsychopharmacology 18. 11:pyv079.

Gutknecht L, Araragi N, Merker S, Waider J, Sommerlandt FMJ, Mlinar B, Baccini G, Mayer U, Proft F, Hamon M, Schmitt AG, Corradetti R, Lanfumey L, Lesch K-P (2012) Impacts of brain serotonin deficiency following Tph2 inactivation on development and raphe neuron serotonergic specification. PLOS ONE 7. 8:e43157.

Halasy K, Miettinen R, Szabat E, Freund TF (1992) GABAergic Interneurons are the Major Postsynaptic Targets of Median Raphe Afferents in the Rat Dentate Gyrus. European Journal of Neuroscience 4. 2:144–153.

Han X, Boyden ES (2007) Multiple-color optical activation, silencing, and desynchronization of neural activity, with single-spike temporal resolution. PLOS ONE 2. 3:e299.

Han X, Qian X, Bernstein JG, Zhou H, Franzesi GT, Stern P, Bronson RT, Graybiel AM, Desimone R, Boyden ES (2009) Millisecond-timescale optical control of neural dynamics in the nonhuman primate brain. Neuron 62. 2:191–198.

Harmer CJ, Bhagwagar Z, Perrett DI, Völlm BA, Cowen PJ, Goodwin GM (2003) Acute SSRI administration affects the processing of social cues in healthy volunteers. Neuropsychopharmacology 28. 1:148–152.

Hernandez-Lopez S, Garduño J, Mihailescu S (2013) Nicotinic modulation of serotonergic activity in the dorsal raphe nucleus. Reviews in the Neurosciences 24. 5:455–469.

Hernández-Vázquez F, Garduño J, Hernández-López S (2019) GABAergic modulation of serotonergic neurons in the dorsal raphe nucleus. Reviews in the Neurosciences 30. 3:289–303.

Hill DN, Mehta SB, Kleinfeld D (2011) Quality metrics to accompany spike sorting of extracellular signals. Journal of Neuroscience 31. 24:8699–8705.

Hsieh J (2012) Orchestrating transcriptional control of adult neurogenesis. Genes & development 26. 10:1010–1021.

Hu H, Gan J, Jonas P (2014) Interneurons. Fast-spiking, parvalbumin^{+} GABAergic interneurons: from cellular design to microcircuit function. Science 345. 6196:1255263.

Huang G-J, Herbert J (2005) Serotonin modulates the suppressive effects of corticosterone on proliferating progenitor cells in the dentate gyrus of the hippocampus in the adult rat. Neuropsychopharmacology 30. 2:231–241.

Huang KW, Ochandarena NE, Philson AC, Hyun M, Birnbaum JE, Cicconet M, Sabatini BL (2019) Molecular and anatomical organization of the dorsal raphe nucleus. eLife 8:e46464.

Imoto Y, Kira T, Sukeno M, Nishitani N, Nagayasu K, Nakagawa T, Kaneko S, Kobayashi K, Segi-Nishida E (2015) Role of the 5-HT4 receptor in chronic fluoxetine treatment-induced neurogenic activity and granule cell dematuration in the dentate gyrus. Molecular brain 8:29.

Jacobsen JPR, Siesser WB, Sachs BD, Peterson S, Cools MJ, Setola V, Folgering JHA, Flik G, Caron MG (2012) Deficient serotonin neurotransmission and depression-like serotonin biomarker alterations in tryptophan hydroxylase 2 (Tph2) loss-of-function mice. Molecular Psychiatry 17. 7:694–704.

Jessberger S, Gage FH (2014) Adult neurogenesis: bridging the gap between mice and humans. Trends in Cell Biology 24. 10:558–563.

Jha S, Rajendran R, Davda J, Vaidya VA (2006) Selective serotonin depletion does not regulate hippocampal neurogenesis in the adult rat brain: differential effects of p-chlorophenylalanine and 5,7-dihydroxytryptamine. Brain Research 1075. 1:48–59.

Jinde S, Zsiros V, Jiang Z, Nakao K, Pickel J, Kohno K, Belforte JE, Nakazawa K (2012) Hilar mossy cell degeneration causes transient dentate granule cell hyperexcitability and impaired pattern separation. Neuron 76. 6:1189–1200.

Kanno K, Shima S, Ishida Y, Yamanouchi K (2008) Ipsilateral and contralateral serotonergic projections from dorsal and median raphe nuclei to the forebrain in rats: immunofluorescence quantitative analysis. Neuroscience Research 61. 2:207–218.

Karabeg MM, Grauthoff S, Kollert SY, Weidner M, Heiming RS, Jansen F, Popp S, Kaiser S, Lesch K-P, Sachser N, Schmitt AG, Lewejohann L (2013) 5-HTT deficiency affects neuroplasticity and increases stress sensitivity resulting in altered spatial learning performance in the Morris water maze but not in the Barnes maze. PLOS ONE 8. 10:e78238.

Kato HE, Zhang F, Yizhar O, Ramakrishnan C, Nishizawa T, Hirata K, Ito J, Aita Y, Tsukazaki T, Hayashi S, Hegemann P, Maturana AD, Ishitani R, Deisseroth K, Nureki O (2012) Crystal structure of the channelrhodopsin light-gated cation channel. Nature 482. 7385:369–374.

Kaufman DM, Milstein MJ (2013) Chapter 21 - Neurotransmitters and Drug Abuse. In: Kaufman's clinical neurology for psychiatrists (Kaufman DM, Milstein MJ, eds), pp 501–525. London: Saunders.

Keith JR, Wu Y, Epp JR, Sutherland RJ (2007) Fluoxetine and the dentate gyrus: memory, recovery of function, and electrophysiology. Behavioural Pharmacology 18. 5-6:521–531.

Kempermann G, Chesler EJ, Lu L, Williams RW, Gage FH (2006) Natural variation and genetic covariance in adult hippocampal neurogenesis. Proceedings of the National Academy of Sciences 103. 3:780–785.

Kempermann G, Song H, Gage FH (2015) Neurogenesis in the Adult Hippocampus. Cold Spring Harbor Perspectives in Biology 7. 9:a018812.

Kiss JP (2008) Theory of active antidepressants: a nonsynaptic approach to the treatment of depression. Neurochemistry International 52. 1-2:34–39.

Klempin F, Babu H, Pietri Tonelli D de, Alarcon E, Fabel K, Kempermann G (2010) Oppositional effects of serotonin receptors 5-HT1a, 2, and 2c in the regulation of adult hippocampal neurogenesis. Frontiers in Molecular Neuroscience 3.

Klempin F, Beis D, Mosienko V, Kempermann G, Bader M, Alenina N (2013) Serotonin is required for exercise-induced adult hippocampal neurogenesis. Journal of Neuroscience 33. 19:8270–8275.

Klempin F, Mosienko V, Matthes S, Villela DC, Todiras M, Penninger JM, Bader M, Santos RAS, Alenina N (2018) Depletion of angiotensin-converting enzyme 2 reduces brain serotonin and impairs the running-induced neurogenic response. Cellular and Molecular Life Sciences 75. 19:3625–3634.

Kobayashi K, Haneda E, Higuchi M, Suhara T, Suzuki H (2012) Chronic fluoxetine selectively upregulates dopamine D_1-like receptors in the hippocampus. Neuropsychopharmacology 37. 6:1500–1508.

Kobayashi K, Ikeda Y, Sakai A, Yamasaki N, Haneda E, Miyakawa T, Suzuki H (2010) Reversal of hippocampal neuronal maturation by serotonergic antidepressants. Proceedings of the National Academy of Sciences 107. 18:8434–8439.

Kronenberg G, Reuter K, Steiner B, Brandt MD, Jessberger S, Yamaguchi M, Kempermann G (2003) Subpopulations of proliferating cells of the adult hippocampus respond differently to physiologic neurogenic stimuli. The Journal of comparative neurology 467. 4:455–463.

Kulla A, Manahan-Vaughan D (2002) Modulation by serotonin 5-HT(4) receptors of long-term potentiation and depotentiation in the dentate gyrus of freely moving rats. Cerebral Cortex 12. 2:150–162.

Kumamoto N, Gu Y, Wang J, Janoschka S, Takemaru K-I, Levine J, Ge S (2012) A role for primary cilia in glutamatergic synaptic integration of adult-born neurons. Nature Neuroscience 15. 3:399-405, S1.

Lanyi JK (2012) 8.10 Light Capture and Energy Transduction in Bacterial Rhodopsins and Related Proteins. In: Comprehensive biophysics (Egelman EH, ed), pp 206–227. Amsterdam: Elsevier.

Lee JH, Durand R, Gradinaru V, Zhang F, Goshen I, Kim D-S, Fenno LE, Ramakrishnan C, Deisseroth K (2010) Global and local fMRI signals driven by neurons defined optogenetically by type and wiring. Nature 465. 7299:788–792.

Leranth C, Hajszan T (2007) Extrinsic afferent systems to the dentate gyrus. In: Progress in Brain Research : The Dentate Gyrus: A Comprehensive Guide to Structure, Function, and Clinical Implications (Scharfman HE, ed), pp 63–799. Elsevier.

Lesch K-P, Waider J (2012) Serotonin in the modulation of neural plasticity and networks: implications for neurodevelopmental disorders. Neuron 76. 1:175–191.

Levine ES, Jacobs BL (1992) Neurochemical afferents controlling the activity of serotonergic neurons in the dorsal raphe nucleus: microiontophoretic studies in the awake cat. Journal of Neuroscience 12. 10:4037–4044.

Li Y-Q, Li H, Kaneko T, Mizuno N (2001) Morphological features and electrophysiological properties of serotonergic and non-serotonergic projection neurons in the dorsal raphe nucleus. Brain Research 900. 1:110–118.

Lin P, Fang Z, Liu J, Lee JH (2016) Optogenetic Functional MRI. Journal of Visualized Experiments. 110:e53346.

Liu N, Sun S, Wang P, Sun Y, Hu Q, Wang X (2021) The Mechanism of Secretion and Metabolism of Gut-Derived 5-Hydroxytryptamine. International journal of molecular sciences 22. 15:7931.

Liu R-J, van den Pol AN, Aghajanian GK (2002) Hypocretins (Orexins) Regulate Serotonin Neurons in the Dorsal Raphe Nucleus by Excitatory Direct and Inhibitory Indirect Actions. Journal of Neuroscience 22. 21:9453–9464.

Liu Z, Zhou J, Li Y, Hu F, Lu Y, Ma M, Feng Q, Zhang J, Wang D, Zeng J, Bao J, Kim J-Y, Chen Z-F, El Mestikawy S, Luo M (2014) Dorsal raphe neurons signal reward through 5-HT and glutamate. Neuron 81. 6:1360–1374.

Lucas G, Rymar VV, Du J, Mnie-Filali O, Bisgaard C, Manta S, Lambas-Senas L, Wiborg O, Haddjeri N, Piñeyro G, Sadikot AF, Debonnel G (2007) Serotonin(4) (5-HT(4)) receptor agonists are putative antidepressants with a rapid onset of action. Neuron 55. 5:712–725.

Luna VM, Anacker C, Burghardt NS, Khandaker H, Andreu V, Millette A, Leary P, Ravenelle R, Jimenez JC, Mastrodonato A, Denny CA, Fenton AA, Scharfman HE, Hen R (2019) Adult-born hippocampal neurons bidirectionally modulate entorhinal inputs into the dentate gyrus. Science 364. 6440:578–583.

Lyon L (2013) Optogenetics. Materials and Methods 3. 194.

Mahar I, Bambico FR, Mechawar N, Nobrega JN (2014) Stress, serotonin, and hippocampal neurogenesis in relation to depression and antidepressant effects. Neuroscience and Biobehavioral Reviews 38:173–192.

Malberg JE, Eisch AJ, Nestler EJ, Duman RS (2000) Chronic Antidepressant Treatment Increases Neurogenesis in Adult Rat Hippocampus. Journal of Neuroscience 20. 24:9104–9110.

Martínez-Garay I, García-Moreno F, Vasistha N, Marques-Smith A, Molnár Z (2016) In Utero Electroporation Methods in the Study of Cerebral Cortical Development. In: Prenatal and Postnatal Determinants of Development (Walker DW, ed), pp 21–39. New York, NY: Springer New York.

Masiulis I, Yun S, Eisch AJ (2011) The interesting interplay between interneurons and adult hippocampal neurogenesis. Molecular Neurobiology 44. 3:287–302.

Medrihan L, Sagi Y, Inde Z, Krupa O, Daniels C, Peyrache A, Greengard P (2017) Initiation of Behavioral Response to Antidepressants by Cholecystokinin Neurons of the Dentate Gyrus. Neuron 95. 3:564-576.e4.

Meeusen R, Thorré K, Chaouloff F, Sarre S, Meirleir K de, Ebinger G, Michotte Y (1996) Effects of tryptophan and/or acute running on extracellular 5-HT and 5-HIAA levels in the hippocampus of food-deprived rats. Brain Research 740. 1-2:245–252.

Mendez-David I, David DJ, Darcet F, Wu MV, Kerdine-Römer S, Gardier AM, Hen R (2014) Rapid anxiolytic effects of a 5-HT_4 receptor agonist are mediated by a neurogenesis-independent mechanism. Neuropsychopharmacology 39. 6:1366–1378.

Mohammad-Zadeh LF, Moses L, Gwaltney-Brant SM (2008) Serotonin: a review. Journal of Veterinary Pharmacology and Therapeutics 31. 3:187–199.

Mohan M (2017) OPTOGENETICS- A BRIEF REVIEW. IJPSR (2009), Issue 1, Vol. International Journal of Pharmaceutical Sciences and Research 8. 2:440–445.

Mohanty SK, Lakshminarayananan V (2015) Optical Techniques in Optogenetics. Journal of modern optics 62. 12:949–970.

Mokler DJ, Lariviere D, Johnson DW, Theriault NL, Bronzino JD, Dixon M, Morgane PJ (1998) Serotonin neuronal release from dorsal hippocampus following electrical stimulation of the dorsal and median raph nuclei in conscious rats. Hippocampus 8. 3:262–273.

Montagni E, Resta F, Mascaro ALA, Pavone FS (2019) Optogenetics in Brain Research: From a Strategy to Investigate Physiological Function to a Therapeutic Tool. Photonics 6. 3:92.

Moyer JR, Brown TH (1998) Methods for whole-cell recording from visually preselected neurons of perirhinal cortex in brain slices from young and aging rats. Journal of Neuroscience Methods 86. 1:35–54.

Muzerelle A, Scotto-Lomassese S, Bernard JF, Soiza-Reilly M, Gaspar P (2016) Conditional anterograde tracing reveals distinct targeting of individual serotonin cell groups (B5-B9) to the forebrain and brainstem. Brain structure & function 221. 1:535–561.

Nagel G, Szellas T, Huhn W, Kateriya S, Adeishvili N, Berthold P, Ollig D, Hegemann P, Bamberg E (2003) Channelrhodopsin-2, a directly light-gated cation-selective membrane channel. Proceedings of the National Academy of Sciences 100. 24:13940–13945.

Nautiyal KM, Tritschler L, Ahmari SE, David DJ, Gardier AM, Hen R (2016) A Lack of Serotonin 1B Autoreceptors Results in Decreased Anxiety and Depression-Related Behaviors. Neuropsychopharmacology 41. 12:2941–2950.

Newman ME, Shalom G, Ran A, Gur E, van de Kar LD (2004) Chronic fluoxetine-induced desensitization of 5-HT1A and 5-HT1B autoreceptors: regional differences and effects of WAY-100635. European Journal of Pharmacology 486. 1:25–30.

Nichols CD, Sanders-Bush E (2003) Serotonin. In: Encyclopedia of the neurological sciences (Aminoff MJ, ed), pp 245–248. Amsterdam: Acad. Press.

Nozaki K, Kubo R, Furukawa Y (2016) Serotonin modulates the excitatory synaptic transmission in the dentate granule cells. Journal of Neurophysiology 115. 6:2997–3007.

Okuno D, Asaumi M, Muneyuki E (1999) Chloride concentration dependency of the electrogenic activity of halorhodopsin. Biochemistry 38. 17:5422–5429.

Padilla-Coreano N, Canetta S, Mikofsky RM, Alway E, Passecker J, Myroshnychenko MV, Garcia-Garcia AL, Warren R, Teboul E, Blackman DR, Morton MP, Hupalo S, Tye KM, Kellendonk C, Kupferschmidt DA, Gordon JA (2019) Hippocampal-Prefrontal Theta Transmission Regulates Avoidance Behavior. Neuron 104. 3:601-610.e4.

Paez-Gonzalez P, Asrican B, Rodriguez E, Kuo CT (2014) Identification of distinct $ChAT^{+}$ neurons and activity-dependent control of postnatal SVZ neurogenesis. Nature Neuroscience 17. 7:934–942.

Pascual-Brazo J, Castro E, Díaz A, Valdizán EM, Pilar-Cuéllar F, Vidal R, Treceño B, Pazos A (2012) Modulation of neuroplasticity pathways and antidepressant-like behavioural responses following the short-term (3 and 7 days) administration of the $5\text{-}HT_4$ receptor agonist RS67333. The international journal of neuropsychopharmacology 15. 5:631–643.

Pastrana E (2011) Optogenetics: controlling cell function with light. Nature Methods 8. 1:24–25.

Paxinos G, Franklin KBJ (2001) The mouse brain in stereotaxic coordinates. San Diego, Calif.: Acad. Press.

Peck BK, Vanderwolf CH (1991) Effects of raphe stimulation on hippocampal and neocortical activity and behaviour. Brain Research 568. 1-2:244–252.

Pedersen NP, Gross RE (2018) Chapter 35 - Neuromodulation Using Optogenetics and Related Technologies. In: Neuromodulation. Comprehensive Textbook of Principles, Technologies, and Therapies (Krames E, Peckham PH, Rezai AR, eds), pp 487–500. Saint Louis: Elsevier Science.

Pratelli M, Pasqualetti M (2019) Serotonergic neurotransmission manipulation for the understanding of brain development and function: Learning from Tph2 genetic models. Biochimie 161:3–14.
Quentin E, Belmer A, Maroteaux L (2018) Somato-Dendritic Regulation of Raphe Serotonin Neurons; A Key to Antidepressant Action. Frontiers in Neuroscience 12:982.
Ramaswamy S (2015) Exciting times for inhibition: GABAergic synaptic transmission in dentate gyrus interneuron networks. Frontiers in Neural Circuits 9:13.
Repina NA, Rosenbloom A, Mukherjee A, Schaffer DV, Kane RS (2017) At Light Speed: Advances in Optogenetic Systems for Regulating Cell Signaling and Behavior. Annual review of chemical and biomolecular engineering 8:13–39.
Rickgauer JP, Tank DW (2009) Two-photon excitation of channelrhodopsin-2 at saturation. Proceedings of the National Academy of Sciences 106. 35:15025–15030.
Sachs BD, Jacobsen JPR, Thomas TL, Siesser WB, Roberts WL, Caron MG (2013) The effects of congenital brain serotonin deficiency on responses to chronic fluoxetine. Translational Psychiatry 3. 8:e291.
Sagi Y, Medrihan L, George K, Barney M, McCabe KA, Greengard P (2020) Emergence of 5-HT5A signaling in parvalbumin neurons mediates delayed antidepressant action. Molecular Psychiatry 25. 6:1191–1201.
Samuels BA, Anacker C, Hu A, Levinstein MR, Pickenhagen A, Tsetsenis T, Madroñal N, Donaldson ZR, Drew LJ, Dranovsky A, Gross CT, Tanaka KF, Hen R (2015) 5-HT1A receptors on mature dentate gyrus granule cells are critical for the antidepressant response. Nature Neuroscience 18. 11:1606–1616.
Samuels BA, Mendez-David I, Faye C, David SA, Pierz KA, Gardier AM, Hen R, David DJ (2016) Serotonin 1A and Serotonin 4 Receptors: Essential Mediators of the Neurogenic and Behavioral Actions of Antidepressants. The Neuroscientist 22. 1:26–45.
Santarelli L, Saxe M, Gross C, Surget A, Battaglia F, Dulawa S, Weisstaub N, Lee J, Duman R, Arancio O, Belzung C, Hen R (2003) Requirement of hippocampal neurogenesis for the behavioral effects of antidepressants. Science 301. 5634:805–809.
Scharfman HE (2016) The enigmatic mossy cell of the dentate gyrus. Nature Reviews Neuroscience 17. 9:562–575.
Scharfman HE (2018) Advances in understanding hilar mossy cells of the dentate gyrus. Cell and tissue research 373. 3:643–652.
Scharfman HE, Myers CE (2012) Hilar mossy cells of the dentate gyrus: a historical perspective. Frontiers in Neural Circuits 6:106.
Schmitt A, Benninghoff J, Moessner R, Rizzi M, Paizanis E, Doenitz C, Gross S, Hermann M, Gritti A, Lanfumey L, Fritzen S, Reif A, Hamon M, Murphy DL, Vescovi A, Lesch K-P (2007) Adult neurogenesis in serotonin transporter deficient mice. Journal of Neural Transmission 114. 9:1107–1119.
Schmitzer-Torbert N, Jackson J, Henze D, Harris K, Redish AD (2005) Quantitative measures of cluster quality for use in extracellular recordings. Neuroscience 131. 1:1–11.
Segi-Nishida E (2017) The Effect of Serotonin-Targeting Antidepressants on Neurogenesis and Neuronal Maturation of the Hippocampus Mediated via 5-HT1A and 5-HT4 Receptors. Frontiers in Cellular Neuroscience 11:142.
Shih JC, Chen K (2004) Regulation of MAO-A and MAO-B gene expression. Current medicinal chemistry 11. 15:1995–2005.
Skandali N, Rowe JB, Voon V, Deakin JB, Cardinal RN, Cormack F, Passamonti L, Bevan-Jones WR, Regenthal R, Chamberlain SR, Robbins TW, Sahakian BJ (2018) Dissociable effects of acute SSRI (escitalopram) on executive, learning and emotional functions in healthy humans. Neuropsychopharmacology 43. 13:2645–2651.
Soiza-Reilly M, Commons KG (2014) Unraveling the architecture of the dorsal raphe synaptic neuropil using high-resolution neuroanatomy. Frontiers in Neural Circuits 8:105.

Song J, Sun J, Moss J, Wen Z, Sun GJ, Hsu D, Zhong C, Davoudi H, Christian KM, Toni N, Ming G, Song H (2013) Parvalbumin interneurons mediate neuronal circuitry-neurogenesis coupling in the adult hippocampus. Nature Neuroscience 16. 12:1728–1730.
Song N-N, Jia Y-F, Zhang L, Zhang Q, Huang Y, Liu X-Z, Hu L, Lan W, Chen L, Lesch K-P, Chen X, Xu L, Ding Y-Q (2016) Reducing central serotonin in adulthood promotes hippocampal neurogenesis. Scientific Reports 6:20338.
Song N-N, Zhang Q, Huang Y, Chen L, Ding Y-Q, Zhang L (2017) Enhanced dendritic morphogenesis of adult hippocampal newborn neurons in central 5-HT-deficient mice. Stem Cell Research 19:6–11.
Soumier A, Banasr M, Kerkerian-Le Goff L, Daszuta A (2010) Region- and phase-dependent effects of 5-HT(1A) and 5-HT(2C) receptor activation on adult neurogenesis. European Neuropsychopharmacology 20. 5:336–345.
Stark E, Koos T, Buzsáki G (2012) Diode probes for spatiotemporal optical control of multiple neurons in freely moving animals. Journal of Neurophysiology 108. 1:349–363.
Stewart CA, Reid IC (2000) Repeated ECS and fluoxetine administration have equivalent effects on hippocampal synaptic plasticity. Psychopharmacology 148. 3:217–223.
Stuart G (2001) Patch-pipet recording in brain slices. Current Protocols in Neuroscience Chapter 6:Unit 6.7.
Teixeira CM, Rosen ZB, Suri D, Sun Q, Hersh M, Sargin D, Dincheva I, Morgan AA, Spivack S, Krok AC, Hirschfeld-Stoler T, Lambe EK, Siegelbaum SA, Ansorge MS (2018) Hippocampal 5-HT Input Regulates Memory Formation and Schaffer Collateral Excitation. Neuron 98. 5:992-1004.e4.
Ting JT, Feng G (2013) Development of transgenic animals for optogenetic manipulation of mammalian nervous system function: progress and prospects for behavioral neuroscience. Behavioural Brain Research 255:3–18.
Ting JT, Feng G (2014) Recombineering strategies for developing next generation BAC transgenic tools for optogenetics and beyond. Frontiers in Behavioral Neuroscience 8:111.
Tischler RC, Morin L (2003) Reciprocal serotonergic connections between the hamster median and dorsal raphe nuclei. Brain Research 981. 1-2:126–132.
Turcotte-Cardin V, Vahid-Ansari F, Luckhart C, Daigle M, Geddes SD, Tanaka KF, Hen R, James J, Merali Z, Béïque J-C, Albert PR (2019) Loss of Adult 5-HT1A Autoreceptors Results in a Paradoxical Anxiogenic Response to Antidepressant Treatment. Journal of Neuroscience 39. 8:1334–1346.
Tye KM, Deisseroth K (2012) Optogenetic investigation of neural circuits underlying brain disease in animal models. Nature Reviews Neuroscience 13. 4:251–266.
Ueda S, Sakakibara S, Yoshimoto K (2005) Effect of long-lasting serotonin depletion on environmental enrichment-induced neurogenesis in adult rat hippocampus and spatial learning. Neuroscience 135. 2:395–402.
Umschweif G, Greengard P, Sagi Y (2019) The dentate gyrus in depression. European Journal of Neuroscience. doi:10.1111/ejn.14640.
Ung K, Arenkiel BR (2012) Fiber-optic implantation for chronic optogenetic stimulation of brain tissue. Journal of Visualized Experiments. 68:e50004.
Valiulahi P, Vidyawan V, Puspita L, Oh Y, Juwono VB, Sittipo P, Friedlander G, Yahalomi D, Sohn J-W, Lee YK, Yoon JK, Shim J (2021) Generation of caudal-type serotonin neurons and hindbrain-fate organoids from hPSCs. Stem Cell Reports 16. 8:1938–1952.
van Praag H, Christie BR, Sejnowski TJ, Gage FH (1999a) Running enhances neurogenesis, learning, and long-term potentiation in mice. Proceedings of the National Academy of Sciences 96. 23:13427–13431.
van Praag H, Kempermann G, Gage FH (1999b) Running increases cell proliferation and neurogenesis in the adult mouse dentate gyrus. Nature Neuroscience 2. 3:266–270.

Vandermaelen CP, Aghajanian GK (1983) Electrophysiological and pharmacological characterization of serotonergic dorsal raphe neurons recorded extracellularly and intracellularly in rat brain slices. Brain Research 289. 1-2:109–119.

Vivar C, Potter MC, Choi J, Lee J-Y, Stringer TP, Callaway EM, Gage FH, Suh H, van Praag H (2012) Monosynaptic inputs to new neurons in the dentate gyrus. Nature Communications 3. 1:1107.

Waller DG, Sampson AP (2018) Neurotransmission and the peripheral autonomic nervous system. In: Medical Pharmacology and Therapeutics, pp 73–90. Elsevier.

Wang DV, Yau H-J, Broker CJ, Tsou J-H, Bonci A, Ikemoto S (2015) Mesopontine median raphe regulates hippocampal ripple oscillation and memory consolidation. Nature Neuroscience 18. 5:728–735.

Wang J, Wagner F, Borton DA, Zhang J, Ozden I, Burwell RD, Nurmikko AV, van Wagenen R, Diester I, Deisseroth K (2012) Integrated device for combined optical neuromodulation and electrical recording for chronic in vivo applications. Journal of Neural Engineering 9. 1:16001.

Wang M, Yu Y, Shao J, Heng BC, Ye H (2017) Engineering synthetic optogenetic networks for biomedical applications. Quantitative Biology 5. 2:111–123.

Warden MR, Selimbeyoglu A, Mirzabekov JJ, Lo M, Thompson KR, Kim S-Y, Adhikari A, Tye KM, Frank LM, Deisseroth K (2012) A prefrontal cortex-brainstem neuronal projection that controls response to behavioural challenge. Nature 492. 7429:428–432.

Waselus M, Valentino RJ, van Bockstaele EJ (2011) Collateralized dorsal raphe nucleus projections: a mechanism for the integration of diverse functions during stress. Journal of Chemical Neuroanatomy 41. 4:266–280.

Watling KJ (2006) The Sigma-RBI handbook of receptor classification and signal transduction. Natick, Ma.: Sigma-RBI.

Watson TC, Becker N, Apps R, Jones MW (2014) Back to front: cerebellar connections and interactions with the prefrontal cortex. Frontiers in Systems Neuroscience 8:4.

Wietek J, Beltramo R, Scanziani M, Hegemann P, Oertner TG, Wiegert JS (2015) An improved chloride-conducting channelrhodopsin for light-induced inhibition of neuronal activity in vivo. Scientific Reports 5. 1:14807.

Wietek J, Wiegert JS, Adeishvili N, Schneider F, Watanabe H, Tsunoda SP, Vogt A, Elstner M, Oertner TG, Hegemann P (2014) Conversion of channelrhodopsin into a light-gated chloride channel. Science 344. 6182:409–412.

Wong AM, Rozovsky I, Arimoto JM, Du Y, Wei M, Morgan TE, Finch CE (2009) Progesterone influence on neurite outgrowth involves microglia. Endocrinology 150. 1:324–332.

Wyler SC, Lord CC, Lee S, Elmquist JK, Liu C (2017) Serotonergic Control of Metabolic Homeostasis. Frontiers in Cellular Neuroscience 11:277.

Yan W, Wilson CC, Haring JH (1997) 5-HT1a receptors mediate the neurotrophic effect of serotonin on developing dentate granule cells. Developmental Brain Research 98. 2:185–190.

Yeh C-Y, Asrican B, Moss J, Quintanilla LJ, He T, Mao X, Cassé F, Gebara E, Bao H, Lu W, Toni N, Song J (2018) Mossy Cells Control Adult Neural Stem Cell Quiescence and Maintenance through a Dynamic Balance between Direct and Indirect Pathways. Neuron 99. 3:493-510.e4.

Yi Y, Song Y, Lu Y (2020) Parvalbumin Interneuron Activation-Dependent Adult Hippocampal Neurogenesis Is Required for Treadmill Running to Reverse Schizophrenia-Like Phenotypes. Frontiers in Cell and Developmental Biology 8:24.

Yizhar O, Fenno LE, Davidson TJ, Mogri M, Deisseroth K (2011) Optogenetics in neural systems. Neuron 71. 1:9–34.

Yoshida K, Drew MR, Mimura M, Tanaka KF (2019) Serotonin-mediated inhibition of ventral hippocampus is required for sustained goal-directed behavior. Nature Neuroscience 22. 5:770–777.

Zemelman BV, Lee GA, Ng M, Miesenböck G (2002) Selective Photostimulation of Genetically ChARGed Neurons. Neuron 33. 1:15–22.

Zhang F, Gradinaru V, Adamantidis AR, Durand R, Airan RD, Lecea L de, Deisseroth K (2010) Optogenetic interrogation of neural circuits: technology for probing mammalian brain structures. Nature Protocols 5. 3:439–456.

Zhang F, Prigge M, Beyrière F, Tsunoda SP, Mattis J, Yizhar O, Hegemann P, Deisseroth K (2008) Red-shifted optogenetic excitation: a tool for fast neural control derived from Volvox carteri. Nature Neuroscience 11. 6:631–633.

Zhang F, Wang L-P, Brauner M, Liewald JF, Kay K, Watzke N, Wood PG, Bamberg E, Nagel G, Gottschalk A, Deisseroth K (2007) Multimodal fast optical interrogation of neural circuitry. Nature 446. 7136:633–639.

Zhang G-W, Shen L, Zhong W, Xiong Y, Zhang LI, Tao HW (2018) Transforming Sensory Cues into Aversive Emotion via Septal-Habenular Pathway. Neuron 99. 5:1016-1028.e5.

Zhao S, Ting JT, Atallah HE, Li Qiu, Tan J, Gloss B, Augustine GJ, Deisseroth K, Luo M, Graybiel AM, Feng G (2011) Cell type–specific channelrhodopsin-2 transgenic mice for optogenetic dissection of neural circuitry function. Nature Methods 8. 9:745–752.

Zoli M, Torri C, Ferrari R, Jansson A, Zini I, Fuxe K, Agnati LF (1998) The emergence of the volume transmission concept. Brain Research Reviews 26. 2-3:136–147.

Statutory Declaration

I, Dr. Naozumi Araragi, by personally signing this document in lieu of an oath, hereby affirm that I prepared the submitted dissertation on the topic "Acute optogenetic stimulation of serotonergic neurons in raphe nuclei reduces cell proliferation in the dentate gyrus of the mouse (Akute optogenetische Stimulation von serotonergen Neuronen in Raphe-Kernen reduziert Zellproliferation im Gyrus dentatus der Maus)", independently and without the support of third parties, and that I used no other sources and aids than those stated.

All parts which are based on the publications or presentations of other authors, either in letter or in spirit, are specified as such in accordance with the citing guidelines. The sections on methodology (in particular regarding practical work, laboratory regulations, statistical processing) and results (in particular regarding Figures, charts and tables) are exclusively my responsibility.

Furthermore, I declare that I have correctly marked all of the data, the analyses, and the conclusions generated from data obtained in collaboration with other persons, and that I have correctly marked my own contribution and the contributions of other persons (cf. declaration of contribution). I have correctly marked all texts or parts of texts that were generated in collaboration with other persons.

My contributions to any publications to this dissertation correspond to those stated in the below joint declaration made together with the supervisor. All publications created within the scope of the dissertation comply with the guidelines of the ICMJE (International Committee of Medical Journal Editors; www.icmje.org) on authorship. In addition, I declare that I shall comply with the regulations of Charité – Universitätsmedizin Berlin on ensuring good scientific practice.

I declare that I have not yet submitted this dissertation in identical or similar form to another Faculty.

The significance of this statutory declaration and the consequences of a false statutory declaration under criminal law (Sections 156, 161 of the German Criminal Code) are known to me."

Date Signature

Naozumi Araragi contributed to the following publication:

Araragi N, Alenina N, Bader M (2022) Carbon-mixed dental cement for fixing fiber optic ferrules prevents visually triggered locomotive enhancement in mice upon optogenetic stimulation. Heliyon 8. 1:e08692.

Contribution:
Naozumi Araragi conceived and designed the experiments, performed all the experiments, analyzed and interpreted all the data, created all figures and tables, and wrote the paper manuscript in close consultation with co-authors.

Natalia Alenina and Michael Bader conceived and designed the experiments, contributed reagents, materials, and analysis tools for data.

_____

Signature, date and stamp of first supervising university professor / lecturer

_____

Signature of doctoral candidate

Curriculum vitae

Mein Lebenslauf wird aus datenschutzrechtlichen Gründen in der elektronischen Version meiner Arbeit nicht veröffentlicht.

Mein Lebenslauf wird aus datenschutzrechtlichen Gründen in der elektronischen Version meiner Arbeit nicht veröffentlicht.

List of Publications

Araragi N, Petermann M, Suzuki M, Larkum M, Mosienko V, Bader M, Alenina N, Klempin F (in preparation) Acute optogenetic stimulation of serotonin raphe neurons reduces cell proliferation in the dentate gyrus of mice.

Araragi N, Alenina N, Bader M (2022) Carbon-mixed dental cement for fixing fiber optic ferrules prevents visually triggered locomotive enhancement in mice upon optogenetic stimulation. Heliyon 8. 1:e08692

Waider J, Popp S, Mlinar B, Montalbano A, Bonfiglio F, Aboagye B, Thuy E, Kern R, Thiel C, **Araragi N**, Svirin E, Schmitt-Böhrer AG, Corradetti R, Lowry CA, Lesch KP (2019) Serotonin Deficiency Increases Context-Dependent Fear Learning Through Modulation of Hippocampal Activity. Frontiers in Neuroscience 13, 245

Araragi N, Mlinar B, Baccini G, Gutknecht L, Lesch KP, Corradetti R (2013) Conservation of 5-HT1A receptor-mediated autoinhibition of serotonin (5-HT) neurons in mice with altered 5-HT homeostasis. Frontiers in Pharmacology. Aug 2; 4:97

Araragi N, Lesch KP (2013) Serotonin (5-HT) in the regulation of depression-related emotionality: insight from 5-HT transporter and tryptophan hydroxylase-2 knockout mouse models. Current Drug Targets. May 1; 14(5):549-70

Gutknecht L, **Araragi N**, Merker S, Waider J, Sommerlandt FM, Mlinar B, Baccini G, Mayer U, Proft F, Hamon M, Schmitt AG, Corradetti R, Lanfumey L, Lesch KP (2012) Impacts of Brain Serotonin Deficiency following Tph2 Inactivation on Development and Raphe Neuron Serotonergic Specification. PLoS One 7(8):e43157

Lesch KP, **Araragi N**, Waider J, van den Hove D, Gutknecht L (2012) Targeting brain serotonin synthesis: insights into neurodevelopmental disorders with long-term outcomes related to negative emotionality, aggression and antisocial behaviour. Philosophical Transactions of the Royal Society of London. Series B, Biological Sciences 367:2426-2443

Waider J, **Araragi N**, Gutknecht L, Lesch KP (2011) Tryptophan hydroxylase-2 (TPH2) in disorders of cognitive control and emotion regulation: a perspective. Psychoneuroendocrinology. Apr; 36(3):393-405

Goto H, Watanabe K, **Araragi N**, Kageyama R, Tanaka K, Kuroki Y, Toyoda A, Hattori M, Sakaki Y, Fujiyama A, Fukumaki Y, Shibata H (2009) The identification and functional implications of human-specific "fixed" amino acid substitutions in the glutamate receptor family. BMC Evolutionary Biology. Sep 8; 9:224

Acknowledgements

First, I would like to express my gratitude to my principal supervisor, Prof. Michael Bader for his supervision on this MD thesis. His profound knowledge in the molecular biology of the serotoninergic system guided the direction of the whole study. In particular, I feel indebted for the opportunity to engage myself with this project with the new methodology, despite the limited availability as a medical student. I would also like to thank my second supervisor Prof. Matthew E. Larkum for his expertise in optogenetics and electrophysiology. His scientific inputs were helpful in establishing the methodology needed for the whole study. I would also like to thank Dr. Natalia Alenina for sharing her knowledge in the serotonergic system and arrangement of animals for experiments. I am also grateful to Dr. Markus Petermann and PD Dr. Friederike Klempin for their cooperation and scientific ideas in the study of cell proliferation, in particular, BrdU injection and processing of BrdU-stained brain slices.

I would also like to express my gratitude to the scientists in the laboratory of Prof. Larkum in NeuroCure, Charité. Especially, I would like to thank Dr. Mototaka Suzuki for his technical advice on optogenetic and electrophysiological methods. I am also thankful to Prof. Mihail Todiras for his guidance on operation and anesthesia with animals. I am grateful to Dr. Fatimunnisa Qadri for her guidance in histological processing of brain slices and use of a fluorescent microscope. I would like to also thank Susanne da Costa Goncalves and Madeleine Skorna-Nussbeck for their excellent technical assistance, especially in genotyping of mice, histological preparation of brain slices, and conduction of HPLC analysis.

I am also thankful to all the members in the laboratory of Prof. Bader. It was a great pleasure to work in such a friendly and familiar atmosphere. I enjoyed not only scientific exchanges but also occasional social activities in the laboratory. I would also like to take this opportunity to thank all the good friends I met during my medical study at Charité. It is encouraging to have friends with whom I can share joy and difficulties during six years of study. For administrative matters of my MD thesis, I am thankful to all the staff of the Office for Doctoral Studies at Charité.

Last but not least, I would like to thank my parents and sister in Japan, who supported me and allowed me to pursue my interests in life. I know that I made them feel uneasy by not coming back to my home country for such a long time and continuing to study till now. I hope I can finally do something good for them and other people by contributing to the progress of medicine and science.

Confirmation by a Statistician

CHARITÉ

CharitéCentrum für Human- und Gesundheitswissenschaften

Charité | Campus Charité Mitte | 10117 Berlin

Institut für Biometrie und Klinische Epidemiologie (iBikE)

Direktor: Prof. Dr. Geraldine Rauch

Postanschrift:
Charitéplatz 1 | 10117 Berlin
Besucheranschrift:
Reinhardtstr. 58 | 10117 Berlin

Tel. +49 (0)30 450 562171
geraldine.rauch@charite.de
https://biometrie.charite.de/

Name, Vorname: Araragi, Naozumi

Emailadresse: naozumi.araragi@charite.de

Matrikelnummer: 219373

PromotionsbetreuerIn: Prof. Michael Bader

Promotionsinstitution/Klinik: Max-Delbrück-Centrum für Molekulare Medizin

Bescheinigung

Hiermit bescheinige ich, dass Herr Naozumi Araragi innerhalb der Service Unit Biometrie des Instituts für Biometrie und Klinische Epidemiologie (iBikE) bei mir eine statistische Beratung zu einem Promotionsvorhaben wahrgenommen hat. Folgende Beratungstermine wurden wahrgenommen:

- *27.12.2021*

Folgende wesentliche Ratschläge hinsichtlich einer sinnvollen Auswertung und Interpretation der Daten wurden während der Beratung erteilt:

- Verwendung von Konfidenzintervallen zur Quantifizierung der Größe von Messunterschieden.
- Angabe aller relevanten Parameter, inkl. der verwendeten Fallzahl in jeder Auswertung.

Diese Bescheinigung garantiert nicht die richtige Umsetzung der in der Beratung gemachten Vorschläge, die korrekte Durchführung der empfohlenen statistischen Verfahren und die richtige Darstellung und Interpretation der Ergebnisse. Die Verantwortung hierfür obliegt allein dem Promovierenden. Das Institut für Biometrie und Klinische Epidemiologie übernimmt hierfür keine Haftung.

Datum: 27.12.2021 Name des Beraters: Dario Zocholl

[redacted]

CHARITÉ
UNIVERSITÄTSMEDIZIN BERLIN
Institut für Biometrie und Klinische Epidemiologie
Campus Charité Mitte
Charitéplatz 1 | D-10117 Berlin
Sitz: Reinhardtstr. 58

Unterschrift BeraterIn, Institutsstempel